Thermal behaviour of lithium-ion batteries and the implications on submarine system design

N.H.D. Gartner

SDPO.20.038.m

TU Delft

Defensie Materieel Organisatie
Ministerie van Defensie

Defensie Materieel Organisatie
Ministerie van Defensie

Thermal behaviour of lithium-ion batteries and the implications on submarine system design

by

N.H.D. Gartner

To obtain the degree of Master of Science
at the Delft University of Technology.

To be defended publicly on Thursday March 25, 2021 at 14:30.

Student number: 4371003

Thesis committee:		
	Rear-Admiral (ret.) Ir. K. Visser	TU Delft, chairman
	Dr. ir. P. de Vos	TU Delft, supervisor
	Dr. E.M. Kelder	TU Delft
	Dr. ir H. Polinder	TU Delft
	LTZ2OC (TD) R.J. van de Mheen, MSc	Defensie Materieel Organisatie (DMO)

TU Delft

Abstract

Submarines face an ongoing (technical) battle to improve the operational effectiveness by increasing the submerged endurance and range. Installing lithium-ion batteries on new or refitted diesel-electric submarines has become increasingly interesting based on their relatively high energy density and specific energy. The characteristics compared to the currently implemented lead-acid batteries are known, meaning that the implementation of lithium-ion batteries on submarines can increase the submerged range and endurance based on their better specifications. Additionally, lithium-ion batteries require less maintenance and provide a relatively longer life expectancy compared to lead-acid batteries.

However, lithium-ion batteries can develop a thermal runaway: a process which exponentially generates heat, leading to the risk of an explosion and fire. A thermal runaway can be initiated based on internal failure mechanisms and external causes, such as exceeding critical temperature limits. Understanding of the thermal behaviour of lithium-ion batteries is essential to reduce the probability of a thermal runaway. The probability of initiating a thermal runaway can be further reduced by auxiliary systems such as a cooling system and a battery management system. The main objective of this research is therefore to investigate the implications on preliminary submarine system design based on the thermal behaviour of lithium-ion batteries and to quantify the thermal behaviour and design implications. The relevance is that by quantifying the thermal behaviour, the cell temperatures can be estimated. As a consequence, awareness of the risk of a thermal runaway is established, while at the same time input for the dimensioning of a cooling system is provided.

An analysis has been performed concerning the safety of lithium-ion batteries. The causes, the characteristics and the prevention methods regarding a thermal runaway have been studied in this research. The four stages of a thermal runaway are discussed, as well as the generation of toxic and flammable gasses. Moreover, the sources of heat generation in a lithium-ion cell have been described. The heat generation typically consists of reversible and irreversible heat components, of which the relative contributions have been described based on the charge or discharge rate.

To support preliminary submarine design, a thermal model of a lithium-ion battery module has been created. The first model that has been created describes the electric behaviour of a lithium-ion battery cell that is typically implemented in marine applications. EST-Floattech has provided technical specifications of the lithium-ion pouch cell that is implemented in their modules. The second model determines the generated heat based on the electrical model and cell specific properties. The third model simulates a lithium-ion battery module, where heat is generated by multiple cells and heat transfer rates with the surroundings are modelled. A lumped thermal capacity approach has been implemented and cooling is modelled to provide insight in typical cooling rates regarding thermal management.

Conclusions have been drawn regarding the temperatures of the cells in the module based on three operational profiles. Based on a submerged sprint, C-rates up to 1.0C can be sustained without cooling while remaining below the critical temperature limit of 55°C. For consecutive cycles during a covert transit or covert surveillance, cooling is typically necessary. Only at C-rates below 0.3C a covert transit can be sustained. Typical cooling rates vary between 60 W and 185 W, where the effects of cooling are most significant for covert transit and covert surveillance. Module optimisation provides increased cooling rates while increasing the energy density and specific energy. This results in a decreased mass and volume of the module, resulting in a significant amount of extra space in the entire battery system on board of a submarine. The largest improvement in thermal management can be realised by choosing the right conductive filler. Moreover, the cooling capacity has a significant influence on the cell temperatures. Cell temperatures remain relatively constant after the fourth cell in a row, meaning that modules are typically not limited by the number of cells.

Preface

This thesis indicates the final phase to conclude the Master of Science program Marine Technology at the Technical University Delft. The research has been conducted for the Defence Materiel Organisation and the TU Delft. The document functions as a graduation project on the thermal behaviour of lithium-ion batteries to be implemented on diesel-electric submarines.

I am very thankful for the support I have received from my daily supervisor Jordy van de Mheen. Jordy always knew to keep me inspired during the entire period of my master thesis. Based on his knowledge and enthusiasm for submarines, he always provided interesting discussions and thorough feedback on my report. Even during the Covid pandemic he provided me with regular discussions and lively conversations. I would like to thank Kees Posthumus for offering detailed feedback. Based on his expertise on lead-acid batteries he knew how to provide me with critical thinking and writing.

I would like to thank Peter de Vos and Klaas Visser for helping me set up my research project. Both have provided me with clear and constructive feedback, making me aware to focus on the right subjects. Feedback has been discussed with me with clear reasoning and lots of enthusiasm which gave direction to my research.

Many thanks to EST-Floattech for sharing their information and knowledge with respect to their battery modules. A special thanks to Walter van der Pennen for providing interesting discussions and showing me the actual stages of assembling a lithium-ion battery module.

Finally, my gratitude goes out to my family and friends. I appreciated the time everyone took to listen to my questions and discussions. Their support has helped me to keep me focused on the right subjects of my research and allowed me to enjoy my time as a student.

N.H.D. Gartner
Alphen aan den Rijn, March 2021

Contents

List of Figures

List of Tables

Nomenclature

Abbreviations

BESS	Battery Energy Storage System
BMS	Battery Management System
CAFS	Compressed Air Foam System
CFD	Computational Fluid Dynamics
CID	Current Interrupt Device
DOD	Degree of Discharge
EMF	Electromotive Force
FEM	Finite Element Method
IDLH	Immediately Dangerous to Life or Health
IR	Indiscretion Ratio
ISC	Internal Short Circuit
LCO	Lithium Cobalt Oxide
LFP	Lithium Iron Phosphate
Li-ion	Lithium-ion
LMO	Lithium Manganese Oxide
LTO	Lithium Titanate Oxide
MAPE	Mean Absolute Percentage Error
NCA	Lithium Nickel Cobalt Aluminum Oxide
NiCd	Nickel Cadmium
NiMH	Nickel Metal Hydride
NMC	Lithium Nickel Manganese Cobalt Oxide
OCV	Open Circuit Voltage
PE	Polyethylene
PP	Polypropylene
PTC	Positive Temperature Coefficient
SEI	Solid Electrolyte Interface
SOC	State of Charge
SOH	State of Health
TRL	Technology Readiness Level

List of Symbols

β	Volumetric coefficient of expansion	$1/K$
ΔG	Gibbs free energy	J
ΔH	Enthalpy change	J
ΔS	Entropy change	J/K
ΔU	Change in internal energy	J
$\dot{Q}$	Transferred heat	W
$\dot{Q}_v$	Generated heat	
$\dot{Q}_{cond}$	Conductive heat flow	W
$\dot{Q}_{conv}$	Convective heat flow	W
$\dot{Q}_{irr}$	Irreversible heat	W
$\dot{Q}_{rad}$	Radiative heat flow	W
$\dot{Q}_{rev}$	Reversible heat	W
$\dot{Q}_{tot}$	Total heat	W
ϵ	Emissivity	$-$
η	Polarization	V
η_{act}	Activation polarization	V
η_{con}	Concentration polarization	V
ν	Kinematic viscosity	m^2/s
Ψ	Pandtl number function	$-$
ρ	Density	kg/m^3
σ	Stefan-Boltzmann constant	$5.67 \cdot 10^{-8}\ W/(m^2K^4)$
${}_aM$	Reactive material anode	$-$
${}_cM$	Reactive material cathode	$-$
A	Area	m^2
A	Exponential zone amplitude	V
B	Exponential zone time constant inverse	$1/Ah$
Bi	Biot number	$-$
C	C-rate	$1/h$
c	Specific heat capacity	$J/(kg\ K)$
c_p	Specific heat capacity (constant pressure)	$J/(kg\ K)$
F	Faraday's constant	$96484\ C/mol$
F_{12}	Shape factor	$-$
g	Gravitational acceleration	$9.81\ m/s^2$
Gr	Grashof number	$-$
h	Heat transfer coefficient	$W/(m^2K)$
I	Current	A
i_{curve}	Current of (dis)charge curve	A
it	Discharged capacity	Ah

K	Polarization constant	V/Ah
k	Thermal conductivity	$W/(m\ K)$
L	Length	m
n	Number of data points	$-$
n	Number of electrons	$-$
Nu	Nusselt number	$-$
Pr	Prandtl number	$-$
Q	Battery capacity	Ah or Wh
Q_{exp}	Capacity exponential zone	Ah
Q_{nom}	Capacity nominal zone	Ah
Q_{rev}	Reversible heat	J
R	Battery internal resistance	Ω
R	Thermal resistance	K/W
R_{in}	Cell internal resistance	Ω
R_{tot}	Total cell resistance	Ω
Ra	Raleigh number	$-$
T	Temperature	K
U_{OCV}	Open Circuit Voltage (OCV)	V
V	Battery terminal voltage	V
V	Volume	m^3
V_0	Constant voltage	V
V_{data}	Voltage from data	V
V_{exp}	Voltage exponential zone	V
V_{full}	Voltage at maximum capacity	V
V_{nom}	Voltage nominal zone	V
W	Work done	J

1 Introduction

Lithium-ion batteries are increasingly making their way into our everyday lives. The batteries were commercialised in 1991 by Sony [9]. Due to their high energy density and specific energy, lithium-ion batteries increased their popularity compared to alternative batteries such as lead-acid batteries. Throughout the years, lithium-ion batteries increased their market share due to the growth in electronic devices. Lithium-ion batteries started to be implemented in mobile phones, other handheld electronics and laptops. From an environmental perspective, lithium-ion batteries in combination with sustainable energy sources have the potential to serve as an alternative to fossil fuels. Instead of burning fuel, lithium-ion batteries can provide electrical power to the automotive and marine industry. The first fully electric vehicle implementing lithium-ion batteries was the Tesla Roadster, released in 2008 [23]. Hybrid vehicles utilising lithium-ion batteries followed shortly after with the Mitsubishi i-MiEV and the Mercedes-Benz S400 BlueHybrid in 2009 [17]. Besides the automotive industry, the marine industry has also started developing hybrid vessels. Hybrid diesel-electric ferries have been build, such as the MV Hallaig in 2013 and the fully electric ferry MV Ampere in 2014 [19]. Additionally, hybrid fishing vessels and cruise ships have been designed and developed, as well as the design for fully electric autonomous container vessels [114]. Diesel-electric submarines have been sailing for over 100 years, where typically lead-acid batteries provided the electrical energy while being submerged. This is typically the case for the Walrus Class submarines of the Royal Netherlands Navy (shown on the front and back cover [70] [71]). However, the time has come for diesel-electric submarines to switch to lithium-ion batteries as well.

1.1. Motivation

The motivation for this thesis is the increased interest to install lithium-ion batteries on new or refitted diesel-electric submarines. Research has already been conducted with regards to the lithium-ion batteries itself and the comparison with conventional lead-acid batteries has been made. The characteristics compared to lead-acid batteries are known, meaning that the implementation of lithium-ion batteries on submarines can increase the submerged range and endurance based on their better specifications. Additional advantages are less maintenance and a relatively longer life expectancy. Besides better specifications, knowledge has also increased in terms of the failure modes present at lithium-ion batteries. The most significant failure mode of a lithium-ion battery is a thermal runaway: a process which exponentially generates heat, leading to the risk of an explosion and fire. Additionally, the gasses formed in the thermal runaway process are toxic, corrosive and flammable. A thermal runaway can be initiated based on internal failure mechanisms and external causes, such as exceeding critical temperature limits. Depending on the chemistry of the battery and its associated auxiliary systems (a cooling system and battery management system (BMS) for example) the probability of such an event can be reduced. With the implementation of lithium-ion batteries on diesel-electric submarines, large numbers of battery cells are expected. With a 25+ year lifetime of the submarines, the batteries are expected to be replaced several times. The chance that a failure occurs in one of the cells during the lifetime of the submarine is statistically inevitable. For that reason, navies have to take into account that a thermal runaway event might occur during the fleet lifetime. The failure of a single lithium-ion cell can

have serious consequences if the thermal runaway is not identified in time and preventive measures are taken accordingly.

Nowadays, the diversity of lithium-ion batteries is large. Cells with different chemistries, shapes and sizes are available. Certain chemistries such as LTO cells are claimed to be safer than others, by having a higher thermal runaway threshold temperature. Additionally, cells can have build-in safety features, such as a venting mechanism in cylindrical cells. However, currently all lithium-ion batteries have a chance of a thermal runaway. Solid state lithium-ion batteries are claimed not to go into thermal runaway. However, this technology is currently under development. Therefore it has a low Technology Readiness Level (TRL). It is not expected that similar technologies are mature enough to be implemented in submarines within the next 10 to 15 years. Therefore, research has to be performed towards the batteries that are currently available.

1.2. Research objective

The main objective of this research is to investigate the thermal behaviour of lithium-ion batteries. Based on the thermal characteristics and failure mechanisms, recommendations can be made on the system design. Due to the limited amount of space in a diesel-electric submarine implications on the system design have to be well understood. The main thesis question is:

What are the implications on preliminary submarine system design based on the thermal behaviour of lithium-ion batteries and how can the thermal behaviour and design implications be quantified?

The implementation of lithium-ion batteries is always accompanied by a risk. A risk can be defined as the probability multiplied by the consequence. The consequences can be severe for a submarine. Therefore the probability of an event that can cause such consequences should be minimised as much as possible. Defining risk acceptation criteria is beyond the scope of this thesis. Understanding should be created on the properties of relevant lithium-ion chemistries and how heat is generated in lithium-ion batteries in general. The implications that are associated with the implementation of lithium-ion batteries is of importance for submarine system design. Additionally, battery system design is of importance to limit electrical and physical abuse, as well as limiting critical temperatures that can initiate a thermal runaway. To safely implement lithium-ion batteries on a submarine, understanding should include why a thermal runaway happens, what it exactly is, and how it can be prevented. For the reasons mentioned in this paragraph, the main research question of the literature study is:

What are the risks involved with the implementation of lithium-ion batteries in general?

Based on the literature research question, sub-questions are formulated:

- *What are the causes of a thermal runaway?*
- *What are the characteristics of a thermal runaway?*
- *How can a thermal runaway be prevented?*
- *What are the sources of heat generation?*

Based on the literature study several research gaps have been found, as described in chapter 6. The first research gap is the absence of a comparative analysis between different lithium-ion chemistries based on their thermal behaviour. Thorough research in a specific chemistry has been done, however the comparison between chemistries is missing. A second research gap has occurred within the uncertainty in temperature indications during the event of a thermal runaway. The stages of a thermal runaway are well understood, but the temperature range of onset temperatures is large, meaning that distinctive temperatures are hard to define. A third research gap can be concluded based on the thermal behaviour on a module regarding relatively low C-rates. Research commonly focuses on the thermal behaviour of single cells. The analysis of the effects of the module geometry and the required cooling rates for a specific application have been analysed to a minimal extend.

Based on the literature gap concluded from the analysed literature the research objective is established of the follow-up research. The follow-up research will fill the gap based on the limited knowledge regarding the thermal behaviour of battery modules. The follow-up research focuses on the thermal behaviour of a lithium-ion battery module that has the potential to be implemented on diesel-electric submarines. The relevance of this research is that it serves as an estimation of the heat generation profile of a lithium-ion battery module. Additionally, it can serve as a tool for initial dimensioning of the cooling system of a lithium-ion battery energy storage system (BESS). First of all, the battery system cannot simply burn out on a submarine as is the case for surface vessels or electric cars, because toxic gasses and hot air cannot be blown out of the vessel easily when submerged. Secondly, due to the fact of being submerged, cooling systems are more expensive and need to be well designed to fit in the allocated spaces. Therefore exact numbers are needed since over-sizing is expensive and the amount of space is not unlimited. The third point of relevance is that on a submarine the response time is limited. This means that during the event of a thermal runaway an indication of the response time is critical to prevent propagation to other modules. Therefore the objective of the follow-up research is formulated as:

Develop a thermal model of a lithium-ion battery module to support preliminary submarine design.

Based on the objective, sub-questions are formulated:

- *What are the thermal characteristics of the selected battery?*
- *What are the operational implications of implementing lithium-ion batteries?*
- *What cooling rates are expected?*
- *Can the response time of a thermal runaway be quantified?*

The approach for the follow-up research will start by modelling the electrical behaviour of a single cell. A lithium-ion battery cell with the potential to be implemented on a diesel-electric submarine will be selected. EST-Floatech has provided the technical specifications of the lithium-ion cell that is implemented in their modules. The cell voltage will be based on the specific cell properties, and should include temperature dependence and current dependence. The second model will determine the heat generation behaviour of single cell based on the previously determined electrical model. Based on literature, multiple sources of heat will be modelled. Finally, a thermal model will be created of a lithium-ion battery module. A typical module geometry will be formulated, for which heat transfers are calculated based on conduction, convection and radiation. Recommendations can be made on the needed cooling rates and the consequences of a typical thermal runaway can be analysed.

1.3. Thesis structure

This thesis functions as a graduation project on the thermal behaviour of lithium-ion batteries to be implemented on diesel-electric submarines. The graduation project is a collaboration between the Delft University of Technology and Defence Materiel Organisation (DMO) and delivers a contribution to safer usage of lithium-ion batteries. Part I contains chapters 2 to 6 concerning the literature study. Chapter 2 discusses the working principle of a battery in general, typical characteristics and provides an overview of the most relevant battery chemistries. Chapter 3 analyzes different lithium-ion chemistries, promising future chemistries which are currently under development and different cell designs. Chapter 4 discusses the safety of lithium-ion batteries, based on thermal runaway causes, thermal runaway stages, gas generation and thermal runaway prevention. Chapter 5 analyzes the sources of heat generation and state of the art thermal modelling of lithium-ion batteries as well as performed experimental studies. Chapter 6 provides a conclusion of the reviewed literature and the research gap is defined. Part II contains chapters 7 to 12 concerning the follow-up research. Chapter 7 analyzes the various modelling options. Chapter 8 discussed the methodology of modelling the electrical behaviour of a single cell, including results of (dis)charge and temperature behaviour. Chapter 9 determines the heat generation of the single cell model based on reversible and irreversible heat. Chapter 10 describes the methodology of creating the thermal model of the battery module, including the module geometry and

heat transfers coefficients of conduction, convection and radiation. Chapter 11 discusses the results obtained with the thermal model of the battery module based on three operational profiles. Cell temperatures are analysed, as well as typical cooling rates. Finally a thermal runaway scenario has been simulated in the battery module. Chapter 12 provides the conclusion and recommendations.

I

Literature review

2

Battery principles

Batteries are divided in two main categories. These are primary and secondary batteries. Primary batteries can only be used once, because the chemical reaction is irreversible. High-energy materials are chemically changed to low-energy materials. A secondary battery can be used multiple times because the chemical reactions can take place in both ways. Secondary batteries can be charged by applying a source of electrical energy to them [101]. Only secondary batteries will be discussed in in the following sections.

2.1. Battery working principle

Batteries work according to the principle of storing chemical energy inside a battery cell. This chemical energy is transformed into electrical energy which is used by the consumer. A single cell is the most basic battery form. A cell is a single unit, while a battery can consist of multiple cells, connected either in series or in parallel. A battery cell consists of three main components. Those components are the anode (negative electrode), cathode (positive electrode) and the electrolyte. A representation of a basic cell during discharge can be seen in figure 2.1. During charge and discharge of the battery, a reversible reduction-oxidation (redox) reaction takes place inside the cell. During discharge, an oxidation reaction occurs at the anode, releasing electrons that pass through the external circuit. The oxidation reaction is presented in equation 2.1, where ${}_aM$ is the reactive material at the anode (a). Energy is provided for the user by the electrons, after which the electrons pass on to the cathode. The cathode acts as a sink for the electrons: this is where the reduction reaction takes place. The reduction reaction is presented in equation 2.2. The reactive material at the cathode is ${}_cM$. Reactions 2.1 and 2.2 are half reactions, and together form the cell reaction, equation 2.3 [101]. To maintain a neutral charge balance at the anode, not only negatively charged electrons but also positively charged ions are produced. These are released in the electrolyte. The electrolyte functions as a medium for the ions to travel through. At the same time at the cathode, positively charged ions are received to maintain a neutral balance as well. Alternatively, negatively charged ions can be produced at the cathode and accepted at the anode as well to provide a neutral balance at the electrodes. If the battery cell needs to be recharged, the redox reactions will be reversed by supplying electrical power to the cell.

$$anode: \quad {}_aM_{red} \rightarrow {}_aM_{ox} + ne^- \tag{2.1}$$

$$cathode: \quad {}_cM_{ox} + ne^- \rightarrow {}_cM_{red} \tag{2.2}$$

$$cell: \quad {}_aM_{red} + {}_cM_{ox} \rightarrow {}_aM_{ox} + {}_cM_{red} \tag{2.3}$$

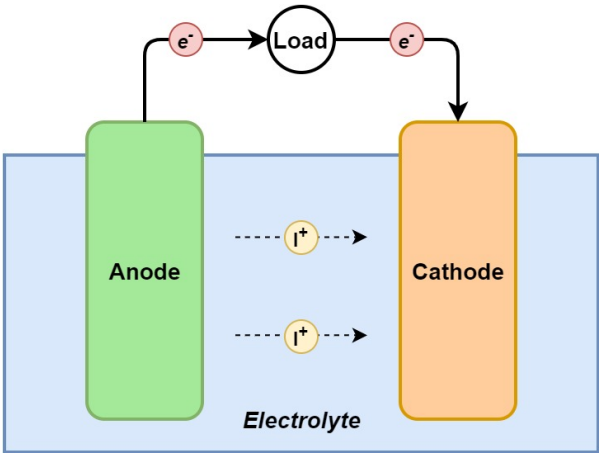

Figure 2.1: Schematic diagram of a battery cell during discharge

2.1.1. Capacity

The capacity is the amount of energy that is stored inside the battery that can be used. The variable for the battery capacity is typically Q. The most common units to measure the capacity is either in Ampere-hours [Ah] or Watt-hours [Wh]. This is either equal to the current that can be delivered for one hour (Ah) or the amount of power (Watt) that a battery can deliver in one hour (1 kWh = 3.6 MJ). By multiplying the ampere-hour capacity by the nominal voltage of the battery, the Watt-hour capacity is obtained. The capacity can be related to the volume called *energy density* [Wh/L], or the capacity can be related to the mass called *specific energy* [Wh/kg] [97]. The capacity is influenced by the chemistry of the cell and the amount of energy that can be stored in the electrodes. The specific energy consequently depends on the densities of the materials, such as using lead in the electrodes. The energy density depends on the volume of the battery as well. For instance the spacing between cells and the entire battery casing can reduce the energy density drastically. With large capacity battery systems, consisting of large amounts of cells, the amount of auxiliary systems needed to run the battery increases. For example a battery management system (BMS) and a cooling system are needed to safely operate the battery system. This increases the total volume of the battery system, therefore decreasing the energy density. This inherently also decreases the specific energy. The energy density is most important for a diesel-electric submarine, since space is usually the limiting factor instead of the weight.

Generally speaking, the capacity of the battery decreases over time due to cycling and temperature variations, called degradation of the battery. The initial capacity is called the nominal capacity. The degraded capacity is indicated by the State Of Health (SOH). The SOH is the percentage of the nominal capacity and indicates the amount of energy that can still effectively be used. The State Of Charge (SOC) indicates the amount of energy stored in the battery at a specific time. This is defined as a percentage of the SOH, as can be seen in figure 2.2.

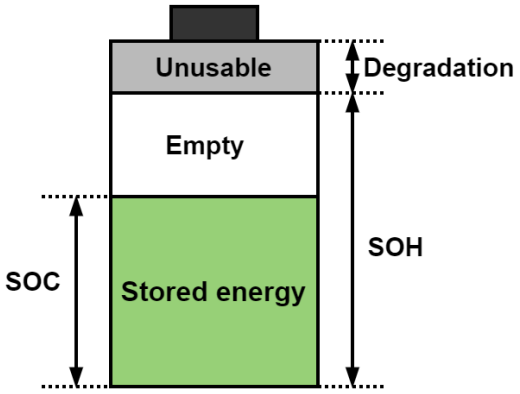

Figure 2.2: Graphic representation of SOC, SOH and degradation

The theoretical capacity of a battery cell can be determined by the change in the Gibbs free energy. The change in the Gibbs free energy ($\Delta G\ [J]$) is related to the enthalpy change of the cell reaction (ΔH) and the entropy change of the cell reaction (ΔS) multiplied by the absolute temperature (T). The Gibbs free energy describes the spontaneity of a system, and is defined by equation 2.4 under constant pressure and temperature. If the change in Gibbs free energy is negative, a process will proceed spontaneously. However, depending on the sign of ΔH and ΔS, a process will not proceed spontaneously. Also the temperature can influence whether a process will proceed spontaneously. In the case of a battery, the process describes a battery discharging itself, converting chemical energy into electrical energy. The change in Gibbs free energy can be related as well to the electromotive force (EMF). ΔG is related to the number of electrons (n) multiplied by Faraday's constant ($F = 96484$ C/mol) and the electromotive force, also referred to as the Open Circuit Voltage (OCV), formulated in equations as $U_{OCV}\ [V]$. This is the cell voltage when the cell is at chemical equilibrium [83]. The formula is shown in equation 2.5. The Gibbs free energy is used to calculate the maximum amount of reversible work that can be extracted from the closed system (the battery cell). This is the theoretical value, meaning that the maximum amount of reversible work is always lower in reality due to losses.

$$\Delta G = \Delta H - T\Delta S \tag{2.4}$$

$$\Delta G = -nFU_{OCV} \tag{2.5}$$

2.1.2. Power

The power of a battery determines how quickly the capacity can be discharged or charged and is measured in Watts. Similar to the capacity, the power can be measured in power density [W/L] or specific power [W/kg]. A high power means that the chemical reaction rate is relatively high. A high chemical reaction rate can be achieved by increasing the surface area of the electrodes and making sure the reactions have as little resistance as possible. The speed of charging and discharging is described by the C-rate. As shown in equation 2.6, the C-rate is equal to the charge or discharge current (I) divided by the battery capacity (Q). A C-rate of 1C means that a battery is charged in 1 hour. A C-rate of 2C means a battery is charged or discharged in half an hour. For example, a 1 kWh battery being discharged with a rate of 0.5 C will provide 0.5 kW of power for 2 hours [58]. The C-rate values can be different for the charging and discharging process of a specific battery type. Certain battery types are capable of delivering a very high discharge rate, while charging can only be performed at a low charge rate. For example: A smartphone has to last all-day, while the battery desirably is charged within hours. A battery with a high discharge rate and low charge rate is for example a handheld drill.

$$\text{C-rate} = \frac{I}{Q} \tag{2.6}$$

2.1.3. Battery life

The lifetime of a battery depends strongly on the implemented chemistry. Additional influencing factor are the operating temperature, the charge and discharge C-rate and the cycling profile. Certain battery types can last years with limited maintenance, while others, depending on their operational profile, last much shorter. The battery lifetime is determined by two major characteristics:

- Calendar life
- Cycle life

The calendar life results from the degradation of the battery over a specific period of time. This depends on for instance the temperature at which the battery is stored and the state of charge at which the battery is kept. The cycle life of a battery describes the amount of cycles a battery can perform before the SoH has decreased to 80%. However, the definition of a ”cycle” is very broad. An important property of a cycle is the Depth Of Discharge (DOD), presented as a percentage of the SOH. Batteries with a low DOD will usually last longer than with a high DOD. The rate of charging also has an effect on the cycle life, while usually the number of cycles is defined by the depth of discharge.

2.1.4. Operating temperature

Batteries can operate in a wide temperature range. Colder temperatures slow down the reaction rate within batteries, and can drastically reduce the ability to charge. The internal resistance usually increases at lower temperatures with most battery types, meaning that energy is delivered less efficiently. Also the charge transfer resistance increases at lower temperatures [104]. Low temperatures can increase the viscosity of the electrolyte, as is the case with lithium-ion batteries. This decreases the ionic conductivity and thus the reaction rate [64]. With lead-acid batteries, the aqueous electrolyte can even freeze with a decreased concentration of sulfuric acid in the solution. At higher temperatures, the reaction rate increases in batteries, but the cycle life usually decreases. In lead-acid batteries the corrosion rate increases with an increase in temperature, as well as an increased self-discharge rate [94]. Temperatures above the recommended upper temperature limit can even cause permanent damage and failure of the battery, such as a thermal runaway in lithium-ion batteries. Certain battery types have a higher performance at higher temperatures. For instance dry solid polymer batteries require a temperature between 60-100°C to become conductive so ions can flow [104]. Other battery types such as sodium-sulphur batteries require sodium in liquid form, meaning that the battery can only operate above the melting point of sodium at 98°C [27].

2.1.5. Safety

Safety is a very important aspect for implementing a battery. The safety of a battery cell depends on the chemistry, the cell design and for instance possible venting mechanisms. The electrode and electrolyte chemistry lay down the basis for safety, since the chemicals inside the cell determine the possible reactions that can occur at a certain temperature. Similarly, the toxicity of a battery can decrease the level of safety. lead-acid batteries implement for example sulphuric acid as an electrolyte, which is highly corrosive and harmful for the environment and humans. Similarly, lithium-ion batteries can release toxic gasses in the event of venting. The safety of lithium-ion batteries can have a correlation with the operating temperature. Note that the safety of the battery is based on a cell level, since supporting systems such as a Battery Management System (BMS) and short circuit protection increase the overall system safety.

2.1.6. Costs

The costs of a battery can be divided in three components: The material costs, the manufacturing costs and the operational costs. The battery costs are most commonly indicated by the price per kWh. The material costs make up the biggest share in the total battery costs to roughly 60%, depending on the battery type [86]. For instance the costs of cobalt as cathode in lithium-ion batteries play an important role, where only the raw materials before processing make up a large portion of the costs, as can be seen in figure 2.3. The manufacturing costs are usually low for most batteries, since factories can mass-produce batteries, and thus reducing the costs per product. The operational costs depend strongly on the battery chemistry due to maintenance or replacement. A lithium-ion battery needs hardly any maintenance, while a lead-acid battery needs cleaning and refilling of the electrolyte depending on the type [105]. This is caused by hydrogen and oxygen being formed during charging. The costs in table 2.1 represent the total costs for the consumer. This is an indication since the costs highly depend on the application.

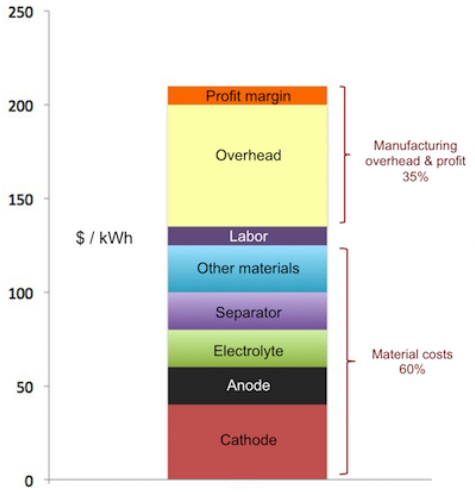

Figure 2.3: Indicative cost components of a lithium-ion battery [86]

2.2. Main battery types

During the years many different battery types have been created based on different chemistries and the electrode potentials of different metals. Based on those chemistries a large variety of materials have been tested to use as electrodes and electrolyte. Each new battery composition has resulted in different characteristics based on capacity, power and cycle life. Research in batteries resulted in four major battery types, which are lead-acid based batteries, nickel-cadmium, nickel-metal-hydride and lithium-ion batteries. An overview of the battery characteristics is given in table 2.1. High temperature batteries are excluded since those are harder to implement successfully and efficiently on a diesel-electric submarine, where high internal temperatures are not desired.

2.2.1. Lead-acid battery

The first rechargeable battery was a lead-acid battery, invented by Gaston Planté in 1859 [12]. lead-acid batteries are widely used in the automotive industry and in stationary applications. They have a high popularity due to their low cost, robustness and low self-discharge. Unfavourable is their low energy density and their negative environmental impact [11]. Lead-acid batteries consist of a lead metal anode and a lead dioxide cathode. The electrolyte is made up of sulfuric acid. As the battery discharges, both electrodes react into lead sulphate and the sulphuric acid reacts into water. During charging hydrogen and oxygen gas is released due to the electrolysis of water, which is vented out through the openings at the top of the battery. This means that lead-acid batteries have to be refilled, which requires regular maintenance. In response valve regulated lead-acid (VRLA) batteries have been designed, where the electrolyte is replaced by a gel. However, this type of battery is designed with a low over voltage potential to prevent gas generation during charging. Due to corrosion of the cathode a lead-acid battery is capable of 200-300 cycles [105].

2.2.2. Nickel-cadmium battery

Nickel-cadmium (NiCd) batteries have been invented in 1899. The battery uses a nickel-oxide-hydroxide cathode and a cadmium anode. As an electrolyte a potassium hydroxide solution is used. NiCd batteries have a relatively long cycle life, and if properly maintained over a 1000 cycles can be obtained. However, a memory effect is present if not fully discharged periodically. If a full discharge is not performed periodically, crystals will form internally decreasing its performance. Another downside is a relatively high self discharge of around 40% in three months time, and a relatively low specific energy compared to newer technologies [102].

2.2.3. Nickel-metal-hydride battery

Research on the Nickel-metal-hydride (NiMH) battery started in the 1970s. A NiMH battery has a similar chemical reaction at the positive electrode as a NiCd cell where nickel-oxide-hydroxide reacts. The reaction at the negative electrode is different, where the negative electrode uses a hydrogen absorbing alloy instead of cadmium. The NiMH cell has a higher energy density compared to NiCd, but its self-discharge rate significantly increased as well.

2.2.4. Lithium-ion battery

The first lithium-ion (Li-ion) batteries have been developed around the 1970s and commercialised in the 1990s by Sony [9]. Lithium is the lightest metal of all metals and it has one of the highest electrode potentials of –3.0401 V [106]. In Li-ion batteries, positively charged lithium ions (Li^+) move from anode to the cathode during discharge. These characteristics provide the largest energy density in terms of weight. Lithium-ion batteries have a low degree of maintenance. No scheduled cycling is needed to maintain the desired battery life, and no memory effect is present. Self-discharge is less than 50% compared to nickel-cadmium batteries [11]. Ageing does occur in Li-ion batteries, resulting in deterioration of the battery capacity [97]. A very large drawback of a lithium-ion battery is the possibility of a thermal runaway. This process can happen when exothermic chemical reactions are triggered due to physical abuse or electrical abuse such as a short circuit, external heating or over(dis)charging. The results of a thermal runaway are high temperatures, formation of toxic gasses, risk of explosion and fire [105].

Table 2.1: Overview of battery characteristics [103][11][74][26]

	Li-ion	Lead-acid	NiCd	NiMH
Specific energy [Wh/kg]	100-300	30-50	45-80	60-120
Energy density [Wh/L]	125-600	50-90	50-70	160-420
Specific power [W/kg]	500-5000	50-180	100-150	100-500
Cycle life (to 80% of SoH)	2000-4000	500-800	300-1000	500-1000
C-rates [h^{-1}]	1-10	0.2	1	0.5
Operating temperature [°C]	-20 to 60	-20 to 60	-40 to 60	-20 to 60
Costs [€/kWh]	300-1000	100-200	300-600	300-600

2.3. Conclusion

In this chapter, the working principles of a battery cell have been explained. A comparison has been made between different battery chemistries. Based on the selection criteria such as specific energy, energy density and cycle life, it can be concluded that lithium-ion batteries are superior compared to the alternatives on the market such as lead-acid, nickel-cadmium and nickel-metal-hydride. As can be seen in table 2.1, lithium-ion batteries have a much higher specific energy and energy density. Also the specific power is much higher compared to other types. Another important criterion is the cycle life, which increases the longevity up to four times with respect to other major chemistries. The costs are still relatively high at the moment, but costs are likely to be reduced as the technology is implemented more in electric vehicles and battery electric storage systems. However, lithium-ion batteries have a large drawback, which is a thermal runaway. This has to be well understood before the batteries can be implemented in diesel-electric submarines. The safety aspects of lithium-ion batteries will be further explained in chapter 4.

3

Lithium-ion batteries

Based on table 2.1 it can be seen that lithium-ion batteries have the highest potential to be installed on submarines. Due to their high capacity and their relatively long cycle-life, Li-ion batteries are a more appropriate choice compared to conventional lead-acid and nickel based batteries. However, implementing lithium-ion batteries can be accompanied with a lower level of safety, having the chance of a thermal runaway. Selecting a lithium-ion battery does not give a single option. Many different combinations of Li-ion cells are available nowadays where each has its own specific properties. The most common chemistries are shown in table 3.1.

3.1. Lithium-ion working principle

A lithium-ion battery cell consists of six main components. The components are the anode, cathode, separator, electrolyte and two current collectors. A schematic representation of a lithium-ion battery cell is presented in figure 3.1. A lithium-ion battery delivers electricity according to redox reactions that take place at the anode and cathode. Positively charged lithium ions (Li^+) are transported between the anode and the cathode through the electrolyte. During discharge of the battery, an oxidation reaction occurs at the anode, releasing ions and electrons that were stored inside the material. This process is called deintercalation. The lithium ions move with the use of the electrolyte through the separator towards the cathode. At the cathode the second reactions takes place, the reduction reaction. Here, the lithium ions and electrons react again and are included in the material to form new compounds, called intercalation [15]. The positively charged lithium ions travel through the separator. As the word suggests, it separates the cathode and the anode. This barrier only allows lithium ions to pass through while electrons are rejected. Therefore, the electrons have to travel through an external circuit. The electrons that are generated in the electrodes are collected by the current collectors. The anode typically contains a copper current collector, whereas the cathode typically contains an aluminium current collector. Copper is used since it is stable at lower potentials up to 3 V, but starts oxidising at higher voltages with lithium ions. Aluminium is used as a cathode current collector since it reacts with lithium at a lower potential around 0.6V, but is stable above 1 V [79].

During the first discharge of a lithium-ion battery, a formation process occurs where the organic electrolyte reacts with the carbon anode. A carbon anode is usually implemented in a lithium-ion cell, except for an LTO cell, as will be elaborated in section 3.1.1. The result of this reaction is a layer on the anode surface called the Solid Electrolyte Interface (SEI), as can be seen in figure 3.1. After cell assembly the battery cell is slowly charged to produce a uniform and stable layer on the anode [75]. The SEI allows the transport of lithium ions and blocks electrons to prevent electrolyte decomposition by reactions with the anode. After repeated cycles, the SEI layer can still grow, limiting the ionic conductance of the cell [108].

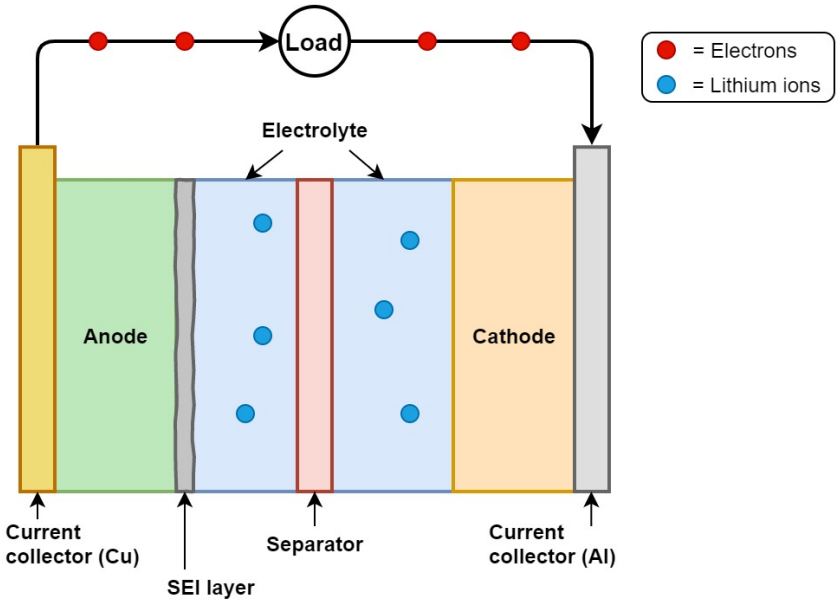

Figure 3.1: Schematic diagram of a lithium-ion battery during discharge

3.1.1. Current chemistries

The main Li-ion battery types are realised by changing either the anode, the cathode or the electrolyte, or a combination of one of the three. The most common form of a Li-ion cell consists of a graphite anode. The cathode usually consists of a lithium metal oxide and the electrolyte is made of of a lithium salt in an organic solvent. Water is not used, since lithium is highly reactive with water. As can be seen in table 3.1, most lithium cells use a graphite anode, while the chemical composition of the cathode is different. The values for specific energy and energy density all are within the same magnitude, where each chemistry has its own advantages and disadvantages, such as higher power, higher energy or a longer cycle life. The values are indicative, since improvements in current researches can improve the values stated in the table. The operating temperature is the same for all types ranging from -20°C to 60°C, except for the LTO cell, ranging from -30°C to 75°C [74]. This is because an LTO cell is claimed to not have a thermal runaway potential. This is however not entirely true. Due to the absence of a carbon anode, an SEI layer is not formed. This means that SEI decomposition will not occur. However, a conventional cathode, either LMO or NMC, is still present. This means that an exothermic reaction can still be triggered above a temperature of 180°C [105] [59]. The stages of a thermal runaway will be further discussed in section 4.2. The downside of a LTO cell is that the costs are much higher compared to alternative Li-ion cells.

Table 3.1: Lithium-ion battery characteristics [76][74]

	Anode	Cathode	Specific energy [Wh/kg]	Energy density [Wh/L]	Cycle life (100% DOD)	Thermal runaway onset [°C]
LCO	Graphite	$LiCoO_2$	175-240	400-640	500	150
LMO	Graphite	$LiMn_2O_4$	150-240	240-360	1000	250
NMC	Graphite	$LiNi_xMn_yCo_zO_2$	100-200	150-400	1500	210
LFP	Graphite	$LiFePO_4$	70-150	100-300	2000	270
NCA	Graphite	$LiNiCoAlO_2$	130-240	490-670	500	150
LTO	$Li_4Ti_5O_{12}$	LMO or NMC	90-130	170-230	12000	N.A.

3.1.2. Chemistries under development

Research still continues on improving and testing the current lithium-ion batteries. Most of them have already proven itself of being able to function in smartphones, electric cars, but also some fully or hybrid electric ships. Research is also still ongoing with new lithium based batteries, such as lithium-air, lithium-sulphur and solid-state lithium. Unfortunately, the technology readiness level is not high enough to be safely implemented in diesel-electric submarines.

Lithium-air Lithium-air batteries work according to the oxidation and reduction reactions of lithium with oxygen. The oxygen is taken from the surrounding air around the battery. The theoretical specific energy is up to ten times higher compared to the current Li-ion batteries, at a value of 1910 Wh/kg [45]. However, currently only an energy density twice as high has been realised. The challenge is to extract oxygen from the air, because N_2, CO_2 and water will react with lithium. Current methods to extract O_2 from the air are still too energy consuming to be implemented [53]. This reduced the energy density of the entire system.

Lithium-sulphur Lithium-sulphur batteries have a theoretical specific energy of 2500 Wh/kg. Its drawback is the formation of Lithium dendrites which can cause short circuits and explosion hazards. Methods for improvement have been tested, leading to a cycle life of 500 cycles. This indicates that the lithium-sulphur technology is already more mature than Lithium-air [53].

Solid-state Solid-state lithium batteries have a solid electrolyte instead of a liquid. This allows one layer of the cell to be much thinner compared to conventional methods, increasing the energy density. A solid electrolyte is stated to have a higher cycle life, and the absence of a liquid electrolyte increases its safety (Conventional organic liquid electrolytes are flammable). However, there are still several challenges, such as insufficient conductivity of the solid electrolyte and insufficient fundamental understanding of the charge and discharge process [92].

3.2. Cell design

Not only the chemistry but also the design is of importance for the characteristics of the battery cell. Only cell designs of lithium-ion cells will be considered, due to their better performance based on table 2.1. A battery system has a modular structure. Multiple cells are connected in series and in parallel and form a module. Dependent on the requirements of the entire system, a desired current and voltage can be obtained in this way. Next the modules can be connected in series to form a rack, increasing the voltage. Finally, the racks can be connected in parallel, delivering the required power for the system. Figure 3.2 depicts the modular structure from cell, to module, to rack, to system.

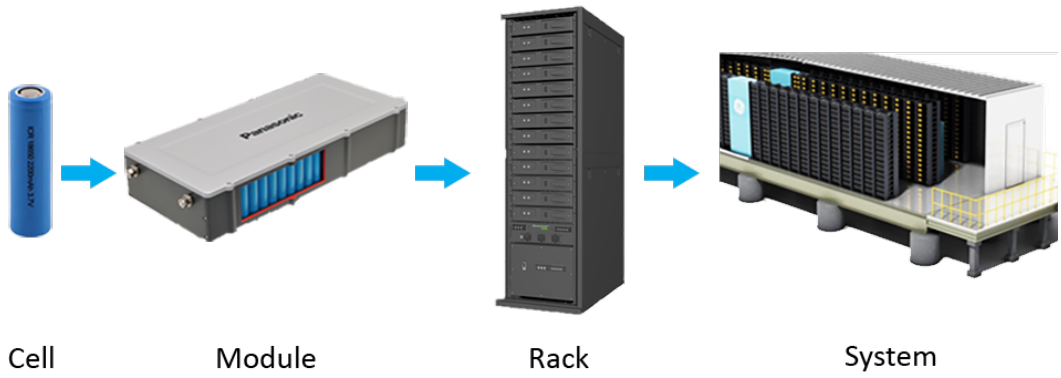

Figure 3.2: Modular structure of a battery system [7] [46] [84] [95]

Cylindrical The most common cell design is the cylindrical battery cell, such as the widely used ”AA battery” format implemented for both primary and secondary batteries. Cylindrical cells used for Li-ion batteries are popular because they are easy and cheap to manufacture and due to their geometry they have a high strength. Two dimensions are commonly used. The 18650 cell, which measures 18 mm in diameter and 65 mm in length. The other is the 26650 cell, having a diameter of 26 mm and a length of 65 mm. Most cylindrical cells include a venting mechanism to release excess gas, increasing its safety. The packing density is low, but the cavities can be used for (air) cooling.

Button Button cells are a very compact design, mainly used for small electronic devices such as watches and handheld calculators. They are unfavourable for larger applications due to their limited capacity and lack of safety vent. To reach a similar capacity to a cylindrical cell, more material is needed due to the separate casings of each cell. Most commercial button cells are known to be non-rechargeable [11]. Due to its limited capacity, button cells will not further be discussed.

Prismatic Prismatic cells are usually packed in a rectangular metal casing. This casing increases robustness and humidity protection but needs slightly more material compared to cylindrical cells. A venting mechanism can also be build into the casing. There are no universal dimensions for a prismatic cell. The prismatic cell design is therefore popular to be used in electronic devices since they can be manufactured according to the wishes of the customer. Larger formats are also used for electric vehicles. Packing multiple prismatic cells is usually more efficient than cylindrical cells due to the form factor [74].

Pouch Pouch cells are characterised by their electrode stack which is packed in a plastic-aluminium foil. Since the packing foil is thin and made of aluminium, it offers good heat transfer, and makes excellent use of space and weight. Pouch cells have therefore the highest energy density and highest specific energy in general. To increase robustness pouch cells are often stacked in a module that provides the necessary level of strength. The pouch is sealed, only leaving an opening for the positive and negative terminals. Due to this seal, the battery will swell if excess gasses are formed due to the first stage of a thermal runaway, as explained in section 4.3. If a cell is unable to swell, venting can occur. If for instance a module is sealed, released gas can accumulate increasing the risk of an explosion. This reduces the level of safety. Pouch cells are commonly implemented in smartphones. Similar to prismatic cells, dimensions are not universal. Based on the application pouch cells can reach an capacity of 240 Ah [48].

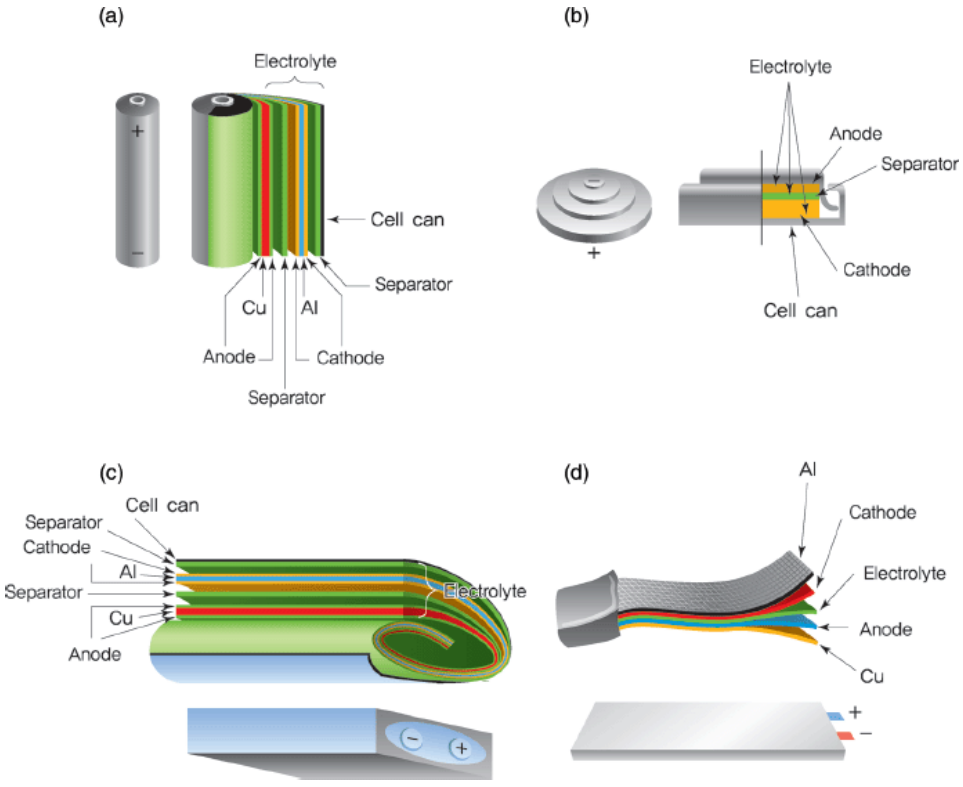

Figure 3.3: Different cell designs: cylindrical (a), button (b), prismatic (c), pouch (d) [85]

3.3. Conclusion

This chapter described the working principle of a lithium-ion battery cell. Commonly a graphite anode is implemented in a cell, whereas the cathode material is varied. Generally speaking, six main chemistries are available that have a high enough TRL. The highest specific energies and energy densities can be achieved with LCO, LMO and NCA cells. LTO cells are supposed to have the highest cycle life, although the costs are generally higher. The onset temperature for a thermal runaway varies between 150°C and 270°C, although this can vary significantly between various researches. For a specific chemistry to be implemented on a diesel-electric submarine, a balance has to be found between the specific energy, the energy density, the cycle life, safety, costs and TRL. The market availability plays an important role as well.

Based on the cell design, cylindrical cells and prismatic cells have the highest potentials to be implemented independently, offering a relatively high strength due to their geometry. Pouch cells have a rather low strength, although the energy density and specific energy is relatively high. For large BESS applications, such as a diesel-electric submarine, pouch cells are effective. The module casing can provide the increased robustness of the cells. By implementing cells with a higher capacity, less cells are needed to reach the desired capacity. A smaller number of cells can reduce the chance of a failure mechanism statistically.

4

Safety of lithium-ion batteries

Generally speaking, a thermal runaway occurs when exothermic reactions inside the cell start to generate significant amounts of heat. As the battery temperature rises, the reaction rate inside the cell increases. From a temperature above roughly 80°C, the heating results in positive feedback, meaning that the reaction rate will further increase due to self created heat [59]. Other side reactions can be triggered as well that are exothermic, further increasing the self-heating process. The high temperatures and chemical reactions cause the formation of toxic and flammable gasses, and can cause fire and explosive danger [20]. A thermal runaway occurring in a single cell is a minor threat. The threat increases once the generated heat starts to propagate to adjacent cells, causing them to go into a thermal runaway as well. This exponential increase can cause a fire in the entire battery system, which is very hard to extinguish and cool down. Figure 4.1 shows the causes of a thermal runaway, the prevention measures, the propagation prevention measures and the fire suppression measures. If those measures are still inadequate, a fire can occur in the entire battery system. Figure 4.1 will be illustrated in the following sections.

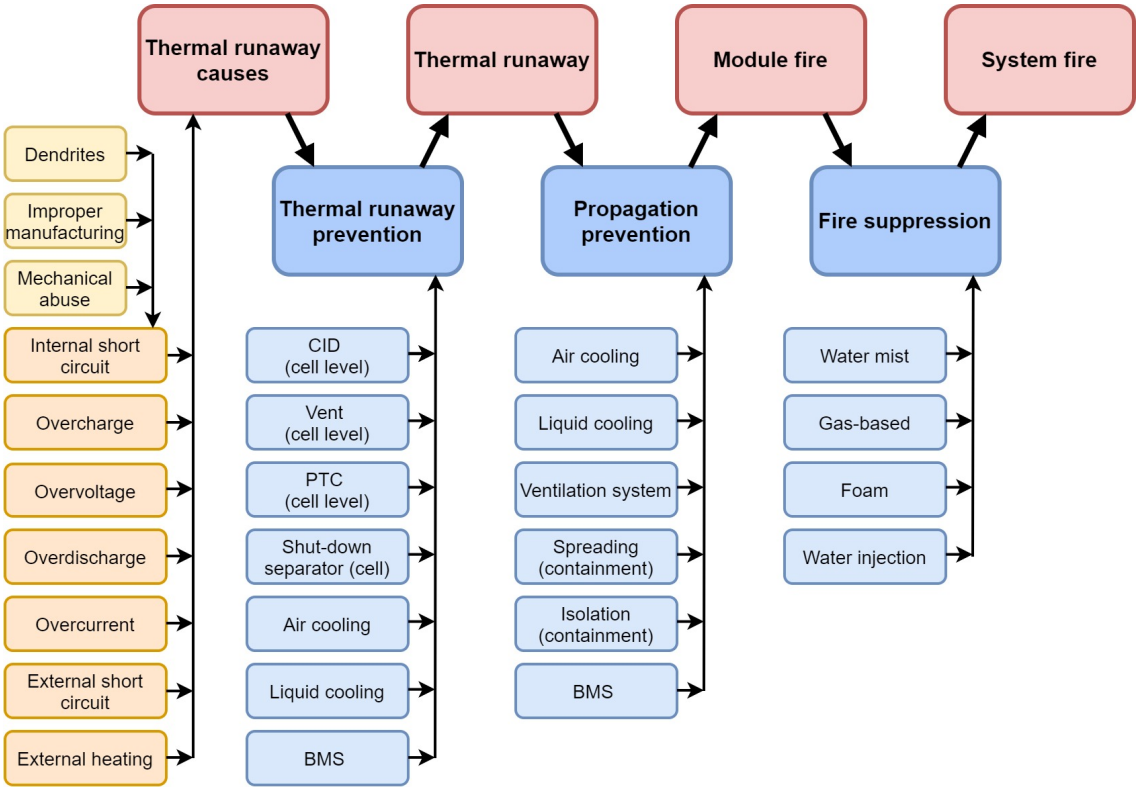

Figure 4.1: Causes and prevention methods of a thermal runaway

4.1. Causes of a thermal runaway

A thermal runaway usually starts from an abuse mechanism that causes the internal temperature to rise sufficiently to start generating heat independently. If a battery is operated and stored within the limits recommended by the manufacturer, the failure rate is estimated to only be 1 in 40 million [110]. A proper Battery Management System (BMS) contributes to a limited failure rate, protecting electrical abuse. A BMS monitors the temperature as well and acts accordingly. A thermal runaway can be initiated due to several causes. For instance mechanical abuse or overcharging a battery can cause a thermal runaway. Several causes that can lead to a thermal runaway are listed below. Note that external heating will not be discussed in depth, since no specific reactions or mechanisms are in that case causing the initiation of a thermal runaway.

4.1.1. Internal short circuit

Internal Short Circuits (ISC) are caused by an electrical connection between the anode and cathode inside a battery cell. Depending on the cell design, up to 70% of the energy of the cell can be released in less than 60 seconds, leading to significant self-heating. High electrical current (10A-15A) causes localised heating, which in turn can cause a thermal runaway [66]. Failure modes such as the formation of dendrites, improper manufacturing, and mechanical abuse can cause a short circuit, but are independent of the operational profile of the battery. This means that with a battery management system these failure modes can still occur. An internal short circuit can also be initiated by overdischarge and overcurrent. However, those failure modes are external factors meaning they can be measured better and thus be better predicted.

Dendrites

Dendrite growth is one of the failure modes leading to an ISC. Inconsistencies on the anode surface may cause the chemical potential to be more positive. This imperfection causes lithium to plate and grow into a dendrite. If the dendrite continues to grow in the electrolyte, eventually it may penetrate through the separator. This causes direct contact between the anode and cathode, and thus a short circuit inside the cell [111]. Charging the battery at higher currents can also stimulate the growth of dendrites. The deposit rate of lithium onto the electrode will be faster than the diffusion rate, resulting in a buildup of lithium [59].

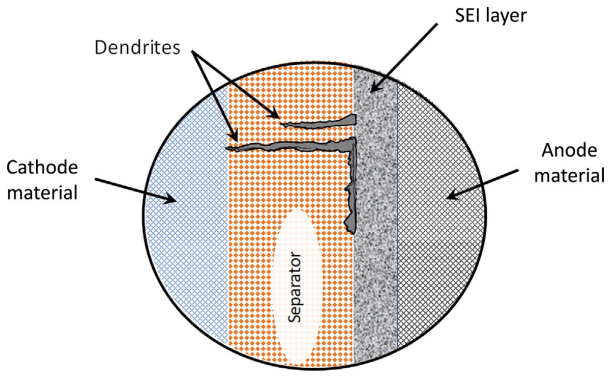

Figure 4.2: Dendrite growth causing a short circuit [111]

Improper manufacturing

During the manufacturing process, debris could get into the cell. Particles can penetrate the separator causing a short circuit. The main cause of debris getting into a cell are assembly rooms that are not clean or dry enough. Another cause of battery failure is improper assembly, for instance electrode misalignment. This caused stresses leading to battery failure [111]. Improper manufacturing is a large threat since the BMS is unable to detect it. Often these failures come to light after the cells have been used in products such as laptops and smartphones. For instance Sony recalled batteries from laptops due to metallic particles inside the cell [113]. Samsung has recalled their Note 7 smartphones due to the very thin separator being easily damaged by outside pressure and the electrodes being bend in the corners of their batteries. This led to a short circuit causing smoke and fire and in certain cases a thermal runaway [61].

Mechanical abuse
Mechanical abuse can result from damage to the entire battery pack. If a battery is dropped, dents can form in the casing, causing the electrodes to come into contact with each other which results in a short circuit. The same holds when a battery gets pierced or crushed. For instance a car crash with an electric vehicle can cause a thermal runaway due to one of these failure modes, as has happened throughout the years with a variety of electric vehicles [93]. Intentional mechanical abuse in the form of nail tests is conducted to investigate the internal short circuit in lithium-ion battery cells [110]. The heat generation rate due to the short circuit is also related to the position where the nail penetrated the battery cell. Mao et al. [68] concluded that the thermal runaway reaction is more severe when damage occurred at the center of the battery due to faster propagation.

4.1.2. Overcharge
Overcharge of a battery cell can be caused by a battery management system that has not been designed properly. In a battery system where many cells are connected in parallel and in series, the chance exists that certain batteries have a higher or lower internal resistance than others due to inconsistent manufacturing. This causes certain cells to be overcharged while other cells are still within the SOC limits [111]. Overcharging occurs when a cell charged above 100% SOC. Overcharging a lithium-ion cell above 100% SOC typically requires voltages over 5 V according to Lyness et al. [63]. The effect of overcharging a battery also increases its impedance, thus increasing the property gap to other cells [52]. The impact to the temperature depends on the voltage difference and the duration of overcharge. A small amount of overcharging will have a minimal effect on the performance and lifetime of the battery. Continuous overcharging will force all lithium ions from the cathode to the anode, which is an irreversible reaction [111]. Overcharge also leads to an oxidation reaction of the electrolyte, causing the release of CO_2, CO and H_2 and heat [55] [38]. The generated heat is caused by Ohmic heating as well, as described in section 5.1.3 [110]. Continued overcharge can cause the cathode material to decompose accompanied by a large release of heat [63].

4.1.3. Overvoltage
Overvoltage is a specific case of overcharge, where the voltage exceeds the required charge voltage. However, for overvoltage the state of charge of the battery does not have to be exceeded. This means delithiation of the cathode does not occur. Therefore overvoltage is less harmful than overcharging the battery. During overvoltage when enough current is applied, certain reactions can be activated, such as the decomposition of the electrolyte and other side reactions resulting in the generation of heat. Again Ohmic heating is also a source of heat related to overvoltage. Excessive gas formation is also related to overvoltage due to the electrolyte decomposition [63].

4.1.4. Overdischarge
Overdischarge can occur to cells which are connected in series, similarly to overcharge. Due to inconsistencies in a cell, the SOC can differ from other cells after numerous cycles. A malfunctioning or absent BMS can be the cause of this. The cell may be forced to continue discharging, meaning that current is continuously pushed through the cell while it is already completely discharged. Overdischarging occurs when the battery cell operates below its voltage range [111]. Overdischarge of a lithium-ion battery cell leads to deintercalation of lithium ions at the anode, and intercalation of ions at the cathode. The voltage potential of the anode increases, which causes oxidation at the copper current collector [39]. The copper can dissolve and form dendrites, which can occur at an anode potential above 3.4V [39]. Once these dendrites penetrate the separator they can cause an internal short circuit. At the same time, the SEI layer can also start to decompose during overdischarge. However, Lai et al. [52] stated that the chances of overdischarge leading to a thermal runaway are smaller compared to overcharge.

4.1.5. Overcurrent
Overcurrent is another failure mechanism of a lithium-ion battery. Due to an excessive current flowing through the cell, heat is generated at a faster rate than can be dissipated by the battery. Usually, a mismatch between the battery pack and the consumer causes overcurrent. If the battery is charged or discharged with too much power the current can increase outside its limits. Overcurrent causes heat generation in the form of Ohmic heating. Ohmic heat is based on Ohm's law, which is a function

of the voltage, current and the cell resistance. This will be explained in detail in chapter 5. When the resistance decreases, the current will increase. An incorrect cell design can also contribute to an increase in current and heat generation. For instance the current collectors or internal welds can cause an increase in temperature due to inconsistencies [63].

4.1.6. External short circuit

An external short circuit is a mechanism that can have similar consequences compared to an internal short circuit. In an external short circuit a connection is created between the battery terminals with a very low resistance. The resistance of the external short circuit may vary considerably in several orders of magnitude, meaning the short circuit current can vary significantly too. The electrical energy is dissipated in the form of Ohmic heating [51]. Experiments have shown that during tests the cells reached temperatures slightly higher than 100°C and caused gas formation and rupturing of the cells [51]. However, the tested cells did not go into thermal runaway immediately due to the short circuit, but this could happen at a later stage due to the excessive heat generation. However, this is also strongly dependent on the SOC of the battery [111]. If the current due to a external short circuit is too high, it can result in the cell wiring fusing together internally and stop the current flowing, resulting in a minimal release of heat. Thus a short circuit with a higher resistance and a lower current can result in more heat generation in specific cases [63].

4.2. Thermal runaway stages

A thermal runaway is typically initiated due to overheating of the battery cell. At a certain temperature, the first phase of a thermal runaway will initiate. Note that the exact temperature depends mostly on the composition of the anode, cathode and electrolyte. The four stages described below do not have to follow the exact order, but can also occur simultaneously. Figure 4.3 shows the locations where the four stages of a thermal runaway occur.

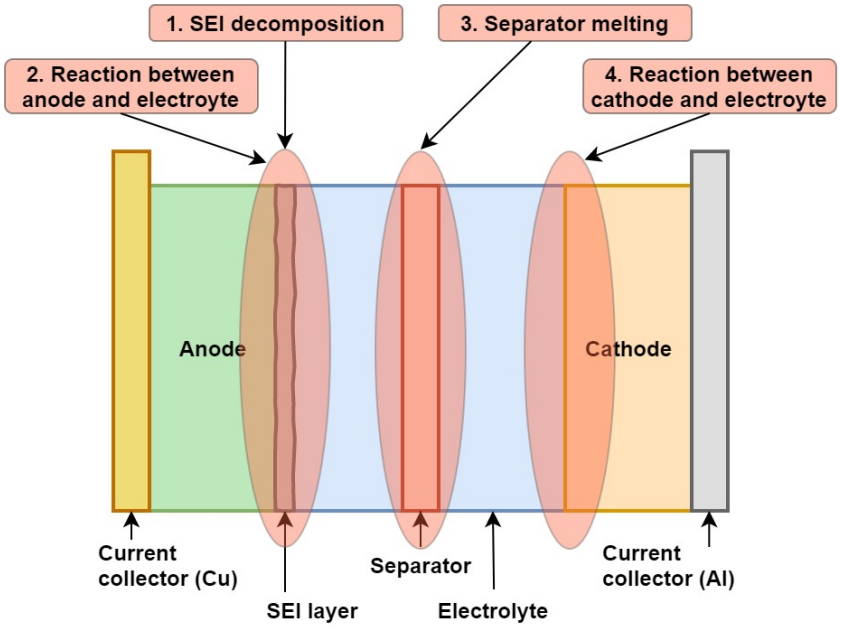

Figure 4.3: The four stages initiating during a thermal runaway

1. SEI decomposition

The first phase of a thermal runaway usually starts with the breakdown of the solid-electrolyte interface. The SEI layer that was initially formed during the first discharge of the battery cell. The SEI allows the transport of lithium ions and blocks electrons to prevent electrolyte decomposition. The SEI consists of both stable and metastable components. The metastable components such as polymers will start to decompose exothermically at a temperature roughly above 90°C [59]. However, this temperature can be lower, as has been shown by Wang et al. [109], where the SEI of a LFP cell started to decompose at a

temperature of 57°C. During the decomposition of the SEI, flammable gasses and oxygen are released. At this point the battery is still functional, but will deviate strongly from its original specifications. Since the SEI is (partially) consumed, it no longer functions as a barrier between the anode and electrolyte.

2. Reaction between anode and electrolyte

Subsequently, the intercalated lithium in the anode starts to react with the organic solvents in the electrolyte. This exothermic reaction initiated at a temperature between 100°C and 120°C [111]. This reaction mostly occurs after the decomposition of the SEI layer, because it no longer offers protection to the anode [110]. Flammable gasses such as ethane and methane are released in this exothermic reaction, increasing the temperature even more.

3. Separator melting

Around a temperature of 130°C, the separator starts to melt. The separator is usually composed of polyethylene (PE) or polypropylene (PP) [59]. Wang et al. [110] stated that PE and PP start to melt at 135°C and 166°C respectively. The decrease in size of the separator causes the cell to self-discharge. Eventually, the absence of a separator causes the anode and cathode to come into contact with each other, causing an internal short circuit. Note that the chemical energy stored inside the cell is released in the form of heat during the self-discharge and short circuiting. Wang et al. [110] stated that in the case of an LCO cell, the reaction creates a heat flow of 87.8 W per gram battery.

4. Reaction between cathode and electrolyte

In the final phase, the cathode reacts with the electrolyte in an exothermic reaction due to the decomposition of the cathode material. This can occur at a temperature above 180°C [59]. During this highly exothermic reaction, oxygen is released. Due to the high temperatures reached in stages three and four, combustion of the electrolyte starts [59] [111]. As oxygen is released during the decomposition of the cathode material, the fire becomes self sustaining until all fuel has been used within the cell. This phase characterises the thermal runaway, since the temperature increase and heat release rates are the largest. Due to the build up of gasses within the cell, venting may occur, which is the release of gasses. This can happen through a safety valve which is build in to the cell. If this feature is not present or not functioning, the cell could rupture or explode [111]. Whether this takes place depends on the cell design, and can happen either at stage three or four depending on the conditions.

4.3. Gas generation

A thermal runaway is always accompanied by the generation of gasses. This can be attributed to the electrochemical side reactions that occur during the process of a thermal runaway. The release of a large amount of gasses increases the internal pressure of a cell, which leads to venting of the gasses. Venting occurs either through a safety valve or cracks in the cell casing if a safety valve is malfunctioning or absent [55]. The gas release strongly depends on the cell design. In certain cell designs the pressure increase can lead to rupture of the cell. The accumulated gasses consist of flammable gasses, which can ignite by the high temperature of the battery. A large accumulation of gasses can lead to an explosion on ignition [67].

During a thermal runaway, the main gasses that are generated are H_2, CO_2 and CO, CH_4, C_2H_4 and C_2H_6. The flammable hydrocarbons are usually related to the electrolyte. Another group of gasses that are generated during a thermal runaway is hydrogen fluoride (HF), which is highly toxic [50]. Fluoride originates from the electrolyte, that can contain fluoride in the form of hexafluorophosphate (PF_6^-). Measurements have been performed on multiple thermal runaway tests by Golubkov et al. [38], where a thermal runaway was initiated by external heating. The tested chemistries are LFP, NMC, and a combination of LFP and NMC. The main components found during the off-gassing are H_2 and CO_2, as can be seen in figure 4.4. Most gasses are flammable and can be toxic due to CO being present.

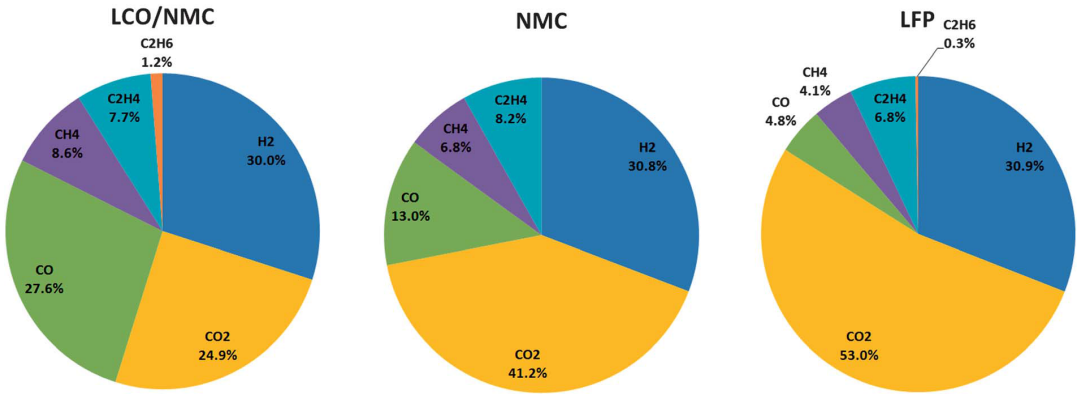

Figure 4.4: Gas composition during a thermal runaway (mol%) [38]

Off-gas measurements have been performed as well by DNV GL [20], and also gas contents before a thermal runaway have been measured by means of external overheating or overcharging of an NMC cell. Hydrogen is not measured in pre-runaway tests, and concluded is that it is only produced after the onset of the thermal runaway, which is in line with observations from Kong et al. [50]. CO present for the longest period of time before and during a thermal runaway. Since the gas is formed in an early stage where a complete thermal runaway can still be prevented, CO is considered important for early stage detection [20]. It is not uncommon for lithium-ion battery fires to consume all oxygen available. For that reason oxygen that is released from the cathode will rapidly be consumed in other exothermal reactions releasing CO and CO_2 [38]. Regarding toxicity, the most dangerous gasses are CO, NO2 and HCL and HF. HF can pose a serious threat, especially for larger battery installation and confined spaces. In general, [20] stated that a lithium-ion battery fire is comparable to a plastic fire in terms of toxicity. Results from fire tests from Larsson et al. [54] indicate that between 20 and 200 mg/Wh of HF is released. DNV GL [20] stated that an amount of 0.0962 L/Ah of HF gas is released. This is equal to roughly 33.5 mg/Ah of HF gas. The IDLH (Immediately Dangerous to Life or Health) value for HF is stated at 30 ppm. Therefore a thermal runaway of a lithium ion battery can pose threats in terms of toxicity.

4.4. Thermal management

A thermal runaway can be prevented in several ways. Certain causes as described in section 4.1 can lead to heat generation. First of all, the initiation of a thermal runaway should be prevented. Thermal runaway prevention can be implemented on a cell level and module level. On a cell level features can be implemented that provide cooling to the cells and protect the cells from excessive currents. On a module level, excessive currents and over(dis)charging can be monitored and prevented by the battery management system. If a battery module develops heat, liquid or air cooling can be used for thermal management. However, if these measures happened to be not sufficient, a thermal runaway can occur in a cell. Thermal runaway propagation prevention is needed at this stage to prevent other cells from initiating a thermal runaway as well. This will usually be in the form of increased cooling rates, off-gas management and containment. If, however, multiple cells develop a thermal runaway, a fire occurs in the module. In that scenario fire suppression is needed to limit the fire in the module. Typically fire suppression methods can extinguish the flames but are insufficient to cool down the temperatures of the affected cells, having the consequence that the reactions proceed and flammable gasses continue to be released. Therefore a combination of systems is likely needed. If those measures are still inadequate, a fire can occur in the entire battery system. The steps described are illustrated by figure 4.1. Note that specific measures can be applied on multiple levels. The measures in the figure are placed in the most applicable stages, as will be further explained in this section.

4.4.1. Thermal runaway prevention

In order to minimize the chances of the initiation of a thermal runaway, the chance that one of the causes described in section 4.1 occurs should be minimised. Most important is a proper battery management system. This system protects the battery system in terms of voltage, temperature and current,

and balances the SOC of the cells within a serial connection [19]. It can monitor and isolate the affected battery module in the cases of overcharge, overdischarge, overcurrent and overheating. Battery modules may contain a basic BMS that checks voltage, current, temperature and balance the SOC of the cells. A rack BMS and a system BMS can control the interactions between the modules and racks, controlling the battery system on a larger scale while still measuring currents between modules. Therefore sensors can be installed on cell level, module level or rack level. On a cell level, safety measures can be build in depending on the cell design. Cell level features are:

- **Current Interrupt Device (CID):** This functions as a fuse, interrupting the current once a threshold value is reached. This is usually implemented in cylindrical and prismatic cells, not in pouch cells.
- **Vent:** Due to the formation of gasses, overpressure can escape through a vent. This prevents rupture of the cell. A safety vent can be implemented in cylindrical and prismatic cells. Pouch cells will burst open as a consequence of overpressure.
- **Positive Temperature Coefficient (PTC):** The resistance of a PTC resistor increases with temperature, which will decrease the current flowing through the cell. This reduces heat generation and stabilizes the temperature.
- **Shut-down separator:** The separator allows the transport for lithium ions. However, when the cell temperature increases, the separator melts and blocks the ions. This stops the current from flowing, minimising heat generation in the cell.

4.4.2. Methods of cooling

Besides the cell level safety features and the battery management system, the module can still develop heat under normal operating conditions during charging and discharging. Therefore a cooling system is needed, often either in the form of air cooling or liquid cooling. Liquid cooling is effective in removing larger amounts of heat with low flow rates because the heat capacity is much higher compared to air cooling. However, liquid cooling has drawbacks such as potential leaks, higher weight, and increased complexity. For air cooling to achieve a similar performance, a much higher air flow is required due to the lower heat capacity of air. On the other hand, air cooling is much simpler, lighter and easier to maintain [40]. Air cooling requires typically more space compared to liquid cooling. However, ventilation is needed to prevent the accumulation of gasses due to unexpected gas generation from battery cells, as discussed in section 4.3. Ventilation reduces the toxic hazard as well. The degree of ventilation depends on the amount of cells and the expected rate of gas generation [20]. For that reason liquid cooling systems need to have additional ventilation. Both liquid cooling and air cooling can be applied on a module level and cell level. On a module level, cooling can be applied to the casings of the module. On a cell level, liquid cooling can be applied in the form of cooling plates between the cells, although this increases the complexity and thus costs of the cooling system. In the case of air cooling on cell level, air can be blown through the cavities inside the module. A more state of the art cooling system is immersion cooling, where the battery cells are submerged in a liquid coolant. This cooling technique has previously been used in high-performance computing and grid power systems. The system enables superior thermal contact and homogeneity and the flame-retardant nature of the fluid acts as a safety feature, suppressing thermal runaway events before propagation [24]. Currently XING Mobility is offering immersion-cooled battery packs for the electric automotive market as an alternative to the air and fluid cooled methods [78].

4.4.3. Thermal runaway propagation prevention

If the thermal runaway prevention measures described above are not sufficient to prevent the generation of heat, a thermal runaway can be initiated in a single cell. To prevent propagation of the single-cell thermal runaway to other cells, other safety measures can be implemented. First of all, an inherent safe design of a battery module should prevent thermal runaway propagation to other cells. Secondly, air cooling and liquid cooling as described in the previous section can be scaled up to deliver a higher rate of cooling. This can keep the adjacent cells cooler, and extract heat from the overheating cell. In terms of off-gas management, a ventilation system is needed to extract toxic, corrosive and flammable gasses. This is more important at this stage, since gas generation increases with multiple cells generating gasses.

Containment is another form of propagation prevention. The goal is to limit the amount of fuel that can be added, meaning that the amount of cells should be limited. However, a certain storage capacity is needed. Therefore, limiting the amount of cells is not possible, but the amount of cells clustered at one location is. By spreading the cells on module or rack level, the chance and consequences of thermal runaway propagation will decrease [21]. Instead of spreading modules or racks to minimize propagation, isolating battery modules can offer a solution to propagation. By implementing a module casing that is fire retardant, propagation can be contained to the module. The module can be completely sealed off although this can increase explosive risks, but limits propagation if it does not occur. By completely sealing the module, toxic gasses will also not be harmful for humans in the periphery of the off-gassing battery. By isolating battery modules, one module is sacrificed, while others remain unharmed [21]. Isolation of battery modules can be implemented on different levels, either on module level or rack level, depending on design preferences.

4.4.4. Fire suppression

The situation can occur where the preventive measures of a thermal runaway have been ineffective, and a single cell or multiple cells catch fire. A lithium-ion battery fire is extremely difficult to extinguish, since multiple types of fire occur simultaneously, such as metallic and chemical fires. Moreover, the reactions are highly exothermic and can produce its own oxygen, being independent of using surrounding air [20] [110]. The goal of fire suppression is to limit the heat transfer to neighbouring modules and absorb heat, preventing the propagation of the thermal runaway to the entire battery installation. Module-to-module propagation should be prevented and multiple battery module fire suppression should be realised [19]. Note that the systems discussed below are strongly dependent on the stage of the thermal runaway,

Water is most widely used as an extinguishing agent and is the cheapest option available. Unfortunately, water can react with the electrolyte, releasing large amounts of HF which is toxic. Lithium can also react with water, generating hydrogen which is highly flammable [110]. Finally, water is also conductive which can therefore create external short circuits in the battery system. On the other hand, water has a great heat capacity, being able to absorb large amounts of energy from a fire. CO_2 is ineffective to use as a fire suppression agent, because the gas is unable to cool down the battery to a great enough [110]. Secondly, the mechanism of extracting oxygen away from the fire is ineffective, since a lithium fire can generate its own oxygen.

- **Water mist:** Water mist is a common method for fire extinguishing and fire suppression. Increasing the surface area of the water droplets by creating mist improves its effectiveness compared to a regular spray of water. Large volumes of water can be supplied increasing its cooling capacities. Experiments by Liu et al. [60] have been performed, concluding that adding gaseous extinguishing agents such as NOVEC 1230 ($C_6F_{12}O$) in water mist increases the cooling effect.
- **Gas-based suppression:** Specific gas-based fire suppression can also be used, of which Novec 1230 is an example. The working principle is to cool down burning chemicals below their ignition temperature and constrain the fuel source [19]. The room needs to be sealed for effective suppression.
- **Compressed Air Foam System (CAFS):** Compressed air foam systems can be deployed to be injected directly into the battery modules. Tests by DNV GL [20] report a significant improvement over suppression media that are applied outside the module. The reason for this is that internally the cell fire remains ongoing since it is not affected directly.
- **Direct injection:** Direct injection of water is considered the most effective suppression medium. This is however a last resort option since the affected module will be completely lost. Depending on the severity of the thermal runaway the battery module could be lost already, meaning it is the last resort option. This option is not recommended for high voltage applications due to the risk of short circuit and hydrogen generation, as described previously.

4.5. Conclusion

This chapter described the safety of lithium-ion batteries regarding a thermal runaway. The causes, the characteristics and the prevention methods of a thermal runaway have been described. Based on literature, the causes of a thermal runaway are well understood. However, the exact contribution to the generation of heat and the severity of each of the causes has not been fully understood or mapped. The thermal runaway stages are also understood in general. Only the specific initiation temperatures of the four phases are globally defined. The exact temperatures are not known, but those have a correlation with the chemistry and cell design. Most importantly is the absence of an exact indication when the SEI layer starts to decompose, since this helps in defining the point where permanent damage occurs. Gas generation can play in important role in identifying a thermal runaway. Especially CO is useful in early stage detection since it is formed in an early stage and present for the longest period of time compared to other gasses. Finally, prevention methods have been described, where both cell-level safety features can be implemented, but also on module or rack level. Important to note is that the safety features (such as air or liquid cooling and fire suppression methods) each have their own advantages and disadvantages. Not a single solution is most effective, but likely a combination of systems will provide the highest level of safety. In terms of module cooling, either air cooling or liquid cooling can be implemented. Liquid cooling is effective in removing larger amounts of heat with low flow rates, but has drawbacks such as potential leaks and increased complexity. Air cooling required much higher air flow rates and more space to achieve a similar performance, but a relatively lower complexity is achieved.

5

Heat generation in batteries

5.1. Sources of heat generation

Heat generation in lithium-ion batteries is commonly divided in two categories. These are reversible heat and irreversible heat. The reversible heat generation process is known as entropic heat. The irreversible heat generation process accounts for multiple heat generation sources such as Ohmic heating, concentration polarization and activation polarization. Heat of mixing and enthalpy heat have been mentioned in literature as well, although to a minimal extend. The sources of heat generation can be found in figure 5.1. The main contributors to the heat generation in lithium-ion batteries are entropic heat and Ohmic heat. The amount of heat that is released in each of the heat sources is mainly dependent on factors such as the state of charge, the charge or discharge current, the operating temperature, the capacity of the cell and the cell chemistry.

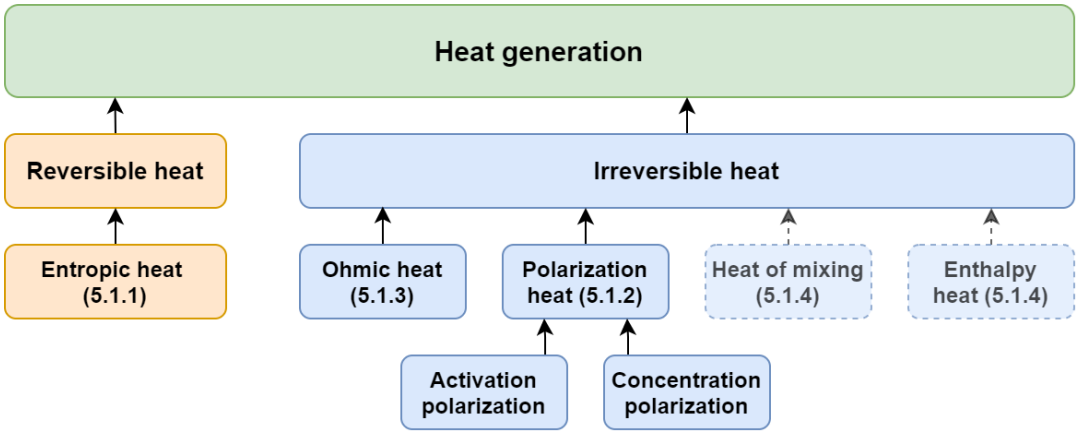

Figure 5.1: Heat generation sources in a lithium-ion battery

5.1.1. Entropic heat

Entropic heat originates from the process of the change in entropy. Alternative formulations for entropic heat are reversible heat or reaction heat. As described in section 2.1.1, the theoretical capacity of a battery cell can be determined by the Gibbs free energy. As seen in equation 2.4, the change in Gibbs free energy is related to the change in enthalpy and the change in entropy multiplied by the absolute temperature. Consider the battery cell as a purely reversible process, where energy is stored and released without losses. For a reversible process that reversibly exchanges a quantity of heat with the surroundings, the entropy change is defined as being equal to the reversible heat divided by the temperature, as shown in equation 5.1 [56]. The change in entropy can be related to the temperature coefficient of the OCV as shown in equation 5.2 [101]. Since the number of electrons (n) multiplied by Faraday's constant (F) is equal to the charge in Coulombs, the final formulation of entropic heat is

given by equation 5.3 [115]. I is the battery current, defined positive when discharged. T the battery temperature [K] and U_{OCV} the open circuit voltage when the cell is at equilibrium.

$$\Delta S = \frac{Q_{rev}}{T} \tag{5.1}$$

$$\frac{\partial U_{OCV}}{\partial T} = \frac{\Delta S}{nF} \tag{5.2}$$

$$\dot{Q}_{rev} = -I \cdot T \cdot \frac{\partial U_{OCV}}{\partial T} \tag{5.3}$$

Entropic heat is related to the change in entropy of the battery cell. The entropy change occurs within the electrochemical reactions in the battery cell. Lithium ions are intercalated and deintercalated in the electrodes of the cell. In the process of intercalation lithium ions are included in the layered lattice of the electrode material [5]. The chemical reactions that take place internally change the accompanied entropy in a reversible process. Due to the complexity of multiple reactions taking place internally, the entropy change is not constant, and can either be positive or negative. The SOC of the battery and the specific chemistry influences the entropy change. Since it is assumed that for a reversible process no losses occur, the entropic heat is the same but opposite in sign during charge and discharge respectively.

To calculate the entropic heat for a battery cell, the temperature derivative of the OCV has to be determined. This can be done through several measurements of the OCV at specific temperature intervals and specific SOCs. The slope of the OCV versus the temperature determines the temperature derivative of the OCV for a specific SOC [5]. A higher temperature derivative of the the OCV correlates with a higher entropy change, which leads to more reversible heat generation. Nazari and Farhad [80] described that LCO cells have a negative derivative, resulting in an exothermic discharge and endothermic charge, based on entropic heat. LFP and LMO cells have a positive derivative, meaning an endothermic discharge and exothermic charge. However, Forgez et al. [35] concluded that the temperature derivative can be both negative and positive (based on an LFP cell). Zhao et al. [119] researched the significance of entropic heat in an LMO cell. Charging or discharging at low C-rates can produce a significant amount of entropic heat compared to the total amount of heat produced. At higher C-rates, its contribution decreases due to an increase of Ohmic heat, which is explained in section 5.1.3. Zhao et al. [119] stated that entropic heat should be taken into account at C-rates below 10 C.

5.1.2. Polarization heat

Polarization heat is based on the difference between the open circuit voltage and the closed circuit voltage. The OCV is obtained when the battery is at rest, based on the SOC of the battery and the temperature. When the battery is being charged or discharged, the closed circuit voltage is obtained. The difference between the two voltages is called overpotential or polarization, given by the symbol η [V]. The contributions to the total polarization can be classified in Ohmic and non-Ohmic effects [83]. Activation polarization and concentration polarization are non-Ohmic terms, and will be discussed in this section. Ohmic overpotential will be discussed in section 5.1.3. The total polarization is defined by equation 5.4, and the heat generated due to the total polarization is given in equation 5.5. Where the Ohmic overpotential follows Ohm's law, activation and concentration polarization can have an uneven contribution based on the charge or discharge current. A graphic representation of a typical contribution to the overpotential is given in figure 5.2.

$$\eta = U_{OCV} - V = \eta_{act} + \eta_{con} + \eta_{ohm} \tag{5.4}$$

$$\dot{Q}_{irr} = I \cdot \eta \tag{5.5}$$

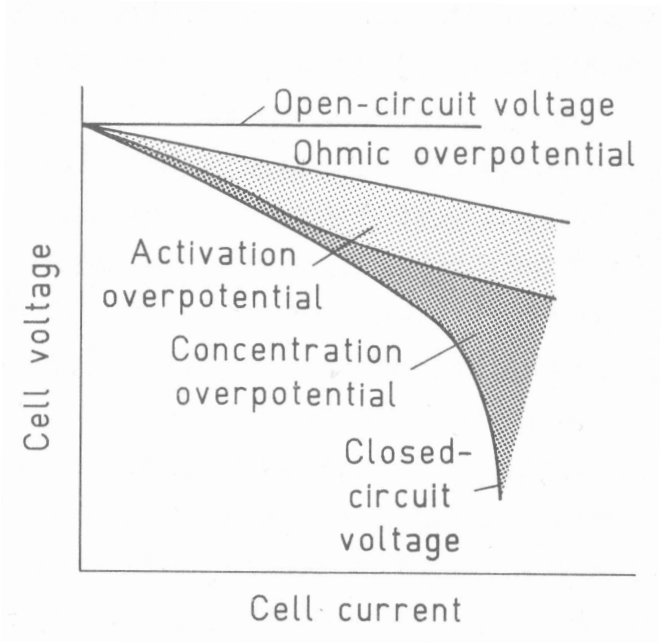

Figure 5.2: Contributions of various types of polarization to voltage loss, shown schematically [101]

Activation polarization
Activation polarization is caused by the activation energy required to start chemical reactions at the electrode and electrolyte interfaces. The excess energy needed to start the reactions is released in the form of heat [3]. The activation polarization is mainly related to the charge transfer process and follows the dynamics of the Butler-Volmer equation [83]. The activation energy barrier that has to be overcome is associated with the slowest reaction that limits the overall reaction rate within the cell.

Concentration polarization
Concentration polarization occurs due to differences in concentration between the reactants in the interface of the electrodes and the electrolyte and the electrolyte itself. This is caused by the mass transfer limitations due to the diffusion of lithium ions. Concentration polarization occurs during a higher consumption of reactants compared to the rate at which they can diffuse in the electrode particles [83]. The transport of lithium ions will be driven by the concentration gradient in the electrolyte. The concentration polarization depends on the applied current, the temperature, the particle size and the structure of the material [83]. Polarization heat has been discussed in several research studies, by Balasundaram et al. [5], Amiribavandpour et al. [3] and Nazari and Farhad [80] and Ovejas and Cuadras [83]. However, the degree of heating by the polarization heat related to the total amount of heat generation has not consistently been concluded. Ovejas and Cuadras [83] related the activation and concentration polarization with respect to overpotential instead of generated heat. They stated that concentration polarization starts to dominate at low C-rates. Generally, concentration polarization increases as the SOC of the cell reaches below 25%. Activation polarization has a much smaller, but generally more constant contribution based on the state of charge according to Ovejas and Cuadras [83]. It increases with higher discharge rates, but remains to have a smaller contribution than concentration polarization. The temperature influence on the concentration and activation polarization is not discussed in literature.

5.1.3. Ohmic heat

Ohmic heating, also known as Joule heating and resistive heating, occurs when current flows through the battery cell. Resistance to the flow of electrons and resistance to the ionic flow in the electrolyte form the internal resistance of the cell responsible for Ohmic heat, as described by Esmaeili and Jannesari [30]. Additionally the interfaces between electrodes and current collectors and electrical tabs contribute to the internal resistance [83]. The internal resistance is not constant, but subject to temperature, state of charge and ageing processes. The internal resistance causes an overpotential, also called polarization. The voltage drop can be expressed by Ohm's law in equation 5.6. R_{in} equals the total

internal resistance of the battery cell and I the charge or discharge current of the cell. Equation 5.7 shows the Ohmic heat generated due to the internal resistance, where the generated heat follows a quadratic relationship with the battery current.

$$\eta_{ohm} = IR_{in} \tag{5.6}$$

$$\dot{Q}_{ohm} = I \cdot \eta_{ohm} = I^2 R_{in} \tag{5.7}$$

This irreversible heating process occurs both at charging and discharging. As described by Ma et al. [64], the Ohmic heating process occurs in both the electrode and electrolyte. The internal resistance causes a voltage drop during charging, meaning a higher voltage needs to be applied to overcome the resistance, called overpotential. The same holds for discharge, resulting in a lower output voltage.

5.1.4. Other forms of heat

Heat of mixing

Heat of mixing, also called enthalpy of mixing, is based on the nonuniform distribution of the ions in the battery cell. When a cell is being charged or discharged, the ion distribution becomes in-homogeneous for a period of time. This results in mixing of ions and heat is generated [64]. The ion concentrations are not consistent, so the SOC is different as well at every location. This means that the equilibrium potential is different compared to the average SOC of the battery [115]. Forgez et al. [35] stated that the heat of mixing occurs specifically in the electrolyte and the materials of the electrodes. The heat of mixing can either be positive or negative, based on the enthalpy being released or absorbed in the process of mixing. Yan et al. [116] concluded that the heat of mixing in lithium-ion battery cells is significantly lower than other heat sources, due to the relative high diffusivity of lithium ions. In modelling the term is deliberately neglected in several instances. If the charge or discharge current is zero, the heat of mixing can still generate heat due to the levelling of the ion distributions, also named as heat of relaxation [98]. In the case of an LMO cell, the heat generation continued for up to 60 seconds after a discharge rate of 7C was interrupted [115].

Enthalpy heat

Enthalpy heat is caused by the heat released during the chemical reactions taking place in the electrodes. The diffusion of lithium ions in the electrode material causes a phase change, which is responsible for this form of heating [64] [30]. Enthalpy can be thought of as the total amount of energy stored in the battery. For a process at constant pressure, the enthalpy change is equal to absorbed or released heat. As enthalpy decreases, the energy is released in the form of heat. In literature, the contribution of enthalpy heating is 55% to 70% according to Xiao and Choe [115] (LMO cell). However, according to Esmaeili and Jannesari [30], ignoring the enthalpy heating (and heat of mixing) only results in an error between 8.7% and 9.8% regarding cell temperature (LMO cell). The contribution of enthalpy heat to the total generated heat is therefore not consistent.

5.2. Modelling of heat generation

Thermal modelling of lithium-ion batteries has been performed in a variety of ways. To model the thermal behaviour, several ways of modelling are mentioned throughout literature. A lumped thermal model is used to describe the heat generation based on the assumption of a uniform temperature distribution in the cell. Similarly two or three dimensional methods have been described to model heat with the use of FEM and CFD software, assuming temperature gradients in the cell. For more accurate thermal modelling, physical modelling in the form of electrochemical models is implemented. Mathematical modelling is implemented to model electrical behaviour based on formulated equations. Alternative, abstract modelling in the form of an equivalent electrical circuit is used to mimic cell behaviour. The heat sources which are taken into account in the studied literature have been analysed as well. This is presented in table 5.1.

Lumped thermal model

Modelling of heat generation has already been done in 1984 by Bernardi, Pawlikowski and Newman [8], who determined an energy balance for a lithium-aluminium, iron sulfide battery. The temperature

Table 5.1: Sources of heat generation in literature

				Source of heating				
Year	Research	Chemistry	Cell design	Entropic	Ohmic	Polarization	Mixing	Other
1984	Bernardi et al. [8]	LiAl	-	X	X		X	phase changes
1999	Al Hallaj et al. [2]	LCO	cylindrical (18650)	X	X			
2003	Thomas and Newman [98]	LCO	coin	X			X	
2004	Chen et al. [14]	-	prismatic	X	X			
2010	Forgez et al. [35]	LFP	cylindrical (26650)	X	X		X	
2012	Feng et al. [33]	LCO	cylindrical (18650)	X	X			
2013	Liu et al. [58]	LMO	prismatic	X	X			
2013	Xiao and Choe [115]	LMO	pouch	X	X			enthalpy
2013	Yan et al. [116]	LCO	-	X	X		X	reaction heat
2014	Saw et al. [88]	LFP	cylindrical (18650)	X	X			
2014	Lin et al. [57]	LFP	cylindrical	X				
2014	Zhao et al. [119]	LMO	prismatic	X	X			reaction heat
2015	Amiribavandpour et al. [3]	LFP	cylindrical (26650)	X	X	X		
2015	Zhao et al. [120]	LMO	prismatic	X	X			
2015	Damay et al. [18]	LFP	prismatic	X	X			
2016	Brodsky [10]	NCA & LFP	cylindrical (18650 & 26650)		X	X		
2016	Ye et al. [117]	LCO & NMC	prismatic	X	X			side reactions
2016	Balasundaram et al. [5]	LFP	cylindrical (18650)	X	X	X		
2016	Zhao et al. [121]	LCO	prismatic	X	X			
2017	Esmaeili and Jannesari [30]	LMO	-	X	X		X	enthalpy
2017	Nazari and Farhad [80]	LFP, LMO, LCO	-	X	X	X		
2018	Ma et al. [64]	LFP	cylindrical (18650)	X	X	X	X	enthalpy
2019	Yoo and Kim [118]	LCO	cylindrical (18650)	X	X			
2019	Geifes et al. [37]	LCO	-	X	X			
2019	Ovejas and Cuadras [83]	LCO & NMC	cylindrical (18650)		X	X		

within the cell was assumed to be uniform, and entropic heat, Ohmic heat, phase changes, mixing effects and changes in the heat capacity of the system have been investigated. Based on similar research by John Newman and others, similar models have been created with uniform temperature distributions. Forgez et al. [35] developed a lumped parameter thermal model for a cylindrical 26650 LFP cell. Ohmic heating and entropic heat are modelled, while heat of mixing and heat produced by side reactions due to ageing are neglected. This is because heat by side reactions is stated to be slow enough to be neglected, and heat of mixing is neglected because concentration gradients are small enough in LFP cells. Similarly, Liu et al. [58] and Lin et al. [57] developed a lumped thermal model to calculate temperature variation during the charge/discharge process. Al Hallaj et al. [2] developed a one-dimensional thermal model in radial direction to simulate temperature profiles of a 18650 cell. An internal temperature gradient was only significant at higher cooling rates. At lower cooling rates the cell behaves as a lumped system with uniform temperature. Esmaeili and Jannesari [30] created a one-dimensional model including the thermal-physical behaviour based on porous media theory and concentrated solution theory. They derived a relation to scale from cell level to pack level, where heat source terms were based on relations between current density, time and temperature as an input for each cell.

3-dimensional thermal model

Instead of a lumped thermal model, simulations have also been performed based on three-dimensional models. Chen et al. [14] created a more detailed three-dimensional model of an LCO cell, while only focusing on entropic heat and Ohmic heat. This model is compared to a simplified one-dimensional model, where a maximum error of 0.54°C was measured, indicating minimal differences between their methodologies. Similarly, Yoo and Kim [118] modelled a full scale battery pack through CFD simulations. Nazari and Farhad [80] modelled with the use of Comsol Multiphysics, performing a comparative analysis for LFP, LMO and LCO cells regarding Ohmic heat, as well as activation and concentration polarization. Zhao et al. [121] modelled the heat generation as well with the use of Comsol. Zhao et al. [119] constructed a 1-D electrochemical model and a 3-D thermal model.

Electrochemical model

The cell behaviour based on input parameters such as the voltage, current and the state of charge has to be known to be able to determine the heat generation rate. An electrochemical model on cell level can be created to model the cell behaviour, as has been done by Brodsky [10]. In this research, a thermal model of a Samsung 18650 NCA battery cell was developed, based on an electrochemical model developed by Marcicki et al. [69]. The model is constructed from a diffusion based electrochemical model of a single cell. Based on the behaviour of the electrochemical model both ohmic heat and

activation and concentration polarization have been modelled. An electrochemical model has also been made by Xiao and Choe [115], Amiribavandpour et al. [3] and Zhao et al. [120]. The equations for the model of Xiao and Choe [115] are solved in longitudinal and radial directions, after which a thermal model is created based on the electrochemical model. Their thermal model of an LMO cell includes not only Ohmic heat and entropic heat, but heat of mixing and enthalpy heating as well. The model is validated under different discharge rates at 22°C.

Equivalent electrical circuit
Instead of using an electrochemical model, Damay et al. [18], Lin et al. [57] and Balasundaram et al. [5] used an equivalent electrical circuit to model the electrical behaviour of an lithium-ion battery. An equivalent electrical circuit model has the advantage that it is simple enough to be used for fast computations in for instance battery management systems. In the study of Damay et al. [18] also the heat generation is modelled in the form of an electrical circuit, similar to the study of Amiribavandpour et al. [3]. Damay et al. [18] only focus on entropic heat and electrical losses. Heat of mixing is neglected based on their conclusions, since its contribution is minor compared to electrical losses. Feng et al. [33] developed a simplified equivalent circuit composed of two resistances, being able to model heat development based on internal resistance changes and entropic heat. Results deviated slightly from expected values at high discharge currents and extreme temperatures, but overall performed well. Based on the operational profile of a diesel-electric submarine, low(er) discharge currents and moderate temperatures could stay within the capabilities of such a model. Madani et al. [65] build an equivalent electrical circuit model as well, only to determine the battery behaviour itself of a LTO cell, where an extensive lookup table has been created for the relationship between C-rate, OCV and SOC (at 30°C). Geifes et al. [37] used an electric equivalent circuit to determine the entropic coefficient of an LCO cell.

Mathematical model
Alternative to an equivalent electrical circuit, mathematical models can be implemented to determine the electrical behaviour of lithium-ion battery cells. Similar to an equivalent electrical circuit, the computational complexity can be low for implementation into battery management systems. The models can be based on existing equations that have been verified in literature. Examples of mathematical models are for instance the Nernst model and the Unnewehr model [44]. Another mathematical model that has been implemented consistently is the Shepherd's model from C.M. Shepherd [90]. The original model has been extended by Tremblay et al. [100] and modified for instance by Hemi et al. [42] and Verstraete et al. [107].

5.3. Experiments

The models described in the previous section need validation to see whether the model outcomes are correct. This is done in the form of experiments where additional cell properties can be measured besides the generated heat. Liu et al. [58] have determined the battery cell internal resistance for a LMO prismatic cell of 8 Ah. The internal resistance has been determined for the SOC of the battery at 5°C, 25 °C and 45 °C for both aged and new cells. Additionally, the entropic heat coefficient has been determined. Ye et al. [117] studied the dynamic overcharge behaviour in LCO and NMC cells and different overcharge regimes. The implemented prismatic cells were overcharged with 0.2C under adiabatic conditions at a starting temperature of 25°C. Balasundaram et al. [5] performed measurements on a cylindrical 18650 LFP cell at 35°C. The specific heat capacity, internal resistance and heat generation rate have been determined. Their calculated heat generation was purely based on Ohmic heating and entropic heat. They concluded that the heat release at charging is higher than at discharging. Irreversible heat is higher than reversible heat at rates of 1C and more. Entropic heat dominates at lower C-rates, and is therefore important to consider at relatively low-current applications such as a submarine. Experiments by Thomas and Newman [98] have been performed to purely calculate the heat of mixing for a LCO coin cell. They concluded that the heat of mixing is generally small, whereas both entropic heat and Ohmic heat are significant and in the same order of magnitude. Ovejas and Cuadras [83] experimentally determined the Ohmic overpotential and activation and concentration polarizations from voltage and impedance measurements for a LCO and NMC cell. Besides experimental studies aiming at internal heat generation, Zhao et al. [121] performed external short circuit experiments and nail penetration tests on a LCO cell. Hereby the effects from two external factors were evaluated in terms of heat generation.

5.4. Conclusion

Extensive research has been performed on the thermal behaviour of lithium-ion batteries. Research has been done on a large variety of chemistries, such as LCO, LMO, NCA and LFP cells. Cell design has also varied, from the widely used cylindrical 18650 cell and the 26650 cell, to pouch and prismatic cells. Battery behaviour has either been simulated through electrochemical modelling or by mathematical models or equivalent electrical circuits. Thermal models have either been constructed as lumped models or three-dimensional models, where heat generation is based on separate cell components. Experimental studies have obtained heat generation rates, as well as internal resistances of cells and entropic coefficients. Modelling has mostly been performed on a cell level. Limited research has been performed on a module level.

The main consensus that can be seen in literature is the contribution of reversible and irreversible heat. At a discharge rate of 1 C, roughly 25% of the total heat can be accounted to reversible heat, and 75% to irreversible heat. With increasing C-rates, reversible heat decreases and irreversible heat increases [5]. Liu et al. [58] roughly confirmed this relationship, stating that Ohmic heat is between 2 to 3 times as much as entropic heat, increasing the difference with increased C-rates. In addition, Nazari and Farhad [80] concluded that the reversible heat remained generally constant for an increasing C-rate (based on LFP, LMO and LCO chemistries). However, the irreversible heat increased with an increase in C-rate. The distribution of roughly 25% reversible to 75% irreversible at 1 C has been confirmed as well. Yan et al. [116] claimed that reversible heat can even be ignored at high discharge rates, although this statement is inconsistent within other researches.

Based on irreversible heat, several sources of heat are mentioned in literature. Only Ohmic heat is discussed with nearly every decomposition of heat generation. Based on heat of mixing, Forgez et al. [35] and Yan et al. [116] concluded that the contribution is minimal and can be neglected due to the relatively high diffusivity of lithium ions in the electrolyte. Polarization heat is alternatively generalised as Ohmic heat, contributing to the total overpotential. Similarly, enthalpy heating has been mentioned in literature without consistence regarding its exact source and contribution to the total generation of heat. Therefore the total heat generation is most consistently based on Entropic heat, Ohmic heat and concentration and activation polarization.

6

Conclusion

Conclusions can be made based on the literature review. Based on table 2.1 in chapter 2, it can be concluded that lithium-ion batteries have much better specifications compared to alternatives on the market such as lead-acid, nickel-cadmium and nickel metal hydride. Lithium-ion batteries have a relatively higher specific energy and energy density. However, the main drawback is the chance of a thermal runaway. Generally speaking, six main chemistries are available that have a high enough TRL, as described in chapter 3. The highest specific energies and energy densities can be achieved by implementing either LCO, LMO or NCA cells. The LTO chemistry is has a higher level of safety compared to the alternative li-ion chemistries. Additionally, a significantly higher cycle life is realised, although at higher costs compared to other li-ion chemistries. However, the specific energy and energy density are generally lower, meaning a minimal improvement compared to lead-acid batteries. The onset temperature for a thermal runaway for various chemistries varies between 150°C and 270°C, although this can vary significantly between researches. Therefore no distinctive conclusion can be drawn yet for selecting a lithium-ion chemistry in terms of the risk of a thermal runaway. A more precise indication temperature is needed based on the chemistry. Based on the cell geometry, pouch cells are most suitable for a diesel-electric submarine. Pouch cells offer the highest energy density and specific energy, although the strength is relatively low. The implication on module design is that the casing has to provide the increased robustness of the cells on board of a submarine. Additional safety features can be applied on module, rack and system level.

Chapter 4 described the safety of lithium-ion batteries regarding a thermal runaway. The first three sub-questions of the literature review are answered in this chapter. The causes, the characteristics and the prevention methods of a thermal runaway have been described. The mechanisms and the characteristics of a thermal runaway are generally well understood. Most importantly is the absence of an exact indication when the SEI layer starts to decompose, since this helps in defining the point where permanent damage occurs. Gas generation can play in important role in identifying a thermal runaway. Prevention methods have been discussed, where safety features can be implemented on cell level, module level and rack level. It can be concluded that not a single method is most effective, but likely a combination of systems will provide the highest level of safety.

Chapter 5 described the sources of heat generation in a lithium-ion cell. The thermal behaviour is of importance since it can cause a cell to initiate a thermal runaway. Research has been done on a large variety of chemistries, as well as several geometries. Heat generation consists of reversible and irreversible heat. Reversible heat is called entropic heat, caused by the change in entropy in the cell. Irreversible heat is mainly caused by activation polarization, concentration polarization and Ohmic heating, although heat of mixing and enthalpy heating have been mentioned in literature as well. The main consensus that can be seen in literature is the contribution of reversible and irreversible heat. At a discharge rate of 1 C, roughly 25% of the total heat can be accounted to reversible heat, and 75% to irreversible heat. With increasing C-rates, reversible heat decreases and irreversible heat increases. For low C-rate applications such as a diesel-electric submarine, reversible heat delivers a significant contribution besides irreversible heat.

6.1. Research gap

Based on the analysed literature, three main research gaps can be concluded. The first research gap is the absence of a comparative analysis between different lithium-ion chemistries based on their thermal behaviour. Research is often very specific, providing an in-depth analysis of for instance overcharging a battery or nail penetration tests. Similarly, contributions of various sources of heat have been analysed in depth. However, most of these researches are based upon a specific chemistry or a specific cell design. This means that obtained results are only valid for that specific experimental setup and cell, not necessarily for other temperatures, chemistries or cell designs. This leaves the engineer with a large amount of information, while the decision-making of the battery type and the consequences in terms of safety still have to be investigated.

A second research gap occurs within the uncertainty in temperature indications during the event of a thermal runaway. As described in chapter 4, modelling has been done and experiments have been performed regarding a thermal runaway, such as external short circuit tests [121], overcharging experiments [117] and overdischarge-induced internal short circuit tests [52]. However, no clear conclusions can be drawn based on the thermal runaway behaviour for different chemistries and cell designs. For instance the range of onset temperatures of a thermal runaway is relatively large, meaning that distinctive temperatures are hard to define for lithium-ion cells. The various stages of a thermal runaway are understood, but the exact temperature points are not. For instance: The SEI decomposition starts roughly above 90°C [59], while a temperature of 57°C has been mentioned as well [109]. A precise indication is of importance for the engineer.

A third research gap can be formulated based on the thermal behaviour on a module regarding relatively low C-rates. Thermal behaviour has mostly been modelled based on individual cells. The analysis of thermal behaviour of battery modules has mostly been limited to low capacity cells such as typical cylindrical cells. Moreover, the effect of cooling on the module temperature has been discussed on a minimal level. Understanding of temperature variations between the cells is important to ensure safe implementation. For a diesel-electric submarine it is essential to know the heat generation rates to dimension the cooling systems to prevent temperatures from exceeding the allowable range. The influence of the module geometry and the cooling rates that are needed to maintain desirable temperatures is limited in the analysed literature. Therefore the thermal behaviour of a battery module and the implications of system design is the third research gap.

6.2. Research objective

Based on the previously stated research gaps, the research objective is established of the follow-up research. The follow up research will fill the gap based on the limited knowledge regarding the thermal behaviour of battery modules. The follow-up research focuses on the thermal behaviour of a lithium-ion battery module that has the potential to be implemented on diesel-electric submarines. Therefore the TRL of the selected battery chemistry needs to be high enough. The relevance of this research is that it serves as an estimation of the heat generation profile of a lithium-ion battery module. Additionally, it can serve as a tool for initial dimensioning of the cooling system of a lithium-ion battery energy storage system (BESS). First of all, the battery system cannot simply burn out on a submarine as is the case for surface vessels or electric cars. Secondly, toxic gasses and hot air cannot be blown out of the vessel easily when submerged. Thirdly, due to the fact of being submerged, cooling systems are more expensive and need to be well designed to fit in the allocated spaces. Therefore exact numbers are needed since over-sizing is expensive and the amount of space is not unlimited. The fourth point of relevance is that on a submarine the response time is limited. This means that during the event of a thermal runaway an indication of the response time is critical to prevent propagation to other modules. Therefore the objective of the follow-up research is formulated as:

Develop a thermal model of a lithium-ion battery module to support preliminary submarine design.

Based on the objective, sub-questions are formulated:

- *What are the thermal characteristics of the selected battery?*
- *What are the operational implications of implementing lithium-ion batteries*
- *What cooling rates are needed?*
- *Can the response time of a thermal runaway be quantified?*

The approach for the follow-up research will start by modelling the electrical behaviour of a single cell. A lithium-ion battery cell with the potential to be implemented on a diesel-electric submarine will be selected. The electrical behaviour of a lithium-ion cell is related to the heat generation rate. The electrical model will therefore simulate the cell voltage based on specific cell properties. Additionally, temperature dependence and current dependence should be included. The second model will determine the heat generation behaviour of single cell based on the previously determined electrical model. Additionally cell related and chemistry related properties will be included in the heat generation model. Based on chapter 5, multiple sources of heat will be modelled. Finally, a thermal model will be created of a lithium-ion battery module consisting of multiple cells. Each cell is modelled based on the electrical model and heat generation model. A typical module geometry will be formulated, for which heat transfers are calculated based on conduction, convection and radiation. The thermal model will be simulated for typical charge and discharge currents that can be expected on a diesel-electric submarine. Recommendations can be made on the needed cooling rates for the battery module to maintain a desired temperature. Finally the event of a thermal runaway can be modelled, where the consequences for the adjacent cells in the module can be analysed.

II

Modelling

7

Model structure & Battery selection

7.1. Model structure

In part II of this thesis, the modelling methodology is described and results and conclusion are discussed. As a result, a thermal model of a lithium-ion battery module is developed. The model consists of three separate models as presented in figure 7.1. The electrical model and heat generation model are based on a cell level. The heat generation model is based on a module level.

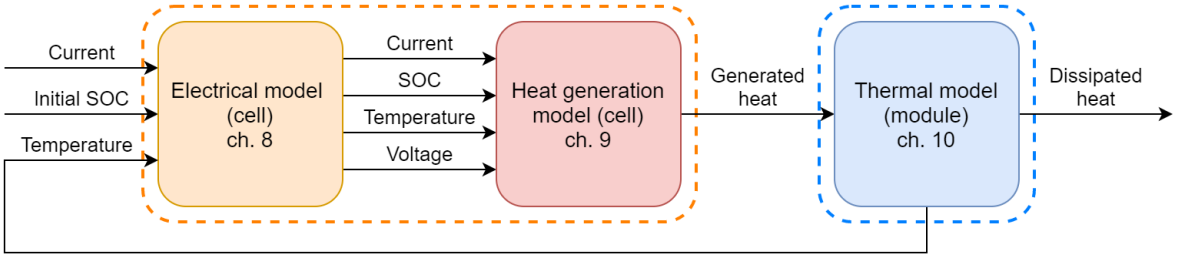

Figure 7.1: Schematic overview of the three implemented models

- The electrical model is discussed in chapter 8. The electrical behaviour of a lithium-ion battery cell is modelled on a cell level based on input parameters such as the current, the initial SOC and the cell temperature. The output of the model is the battery voltage and the remaining SOC. The electrical model thus includes temperature dependence and (dis)charge current dependence.
- The heat generation model is discussed in chapter 9. The input for the heat generation model is the voltage and SOC from the electrical model as well as the current and the cell temperature of the cell. Additionally, the model is based on cell-specific properties such as the OCV and entropic coefficients. The output of the model is the generated heat during operation of the cell.
- The thermal model is discussed in chapter 10. The input of the thermal model is the heat generated by multiple cells. Heat is dissipated based on the module geometry, the selected form of cooling and various temperatures such as the cells and the surroundings. Based on the generated and dissipated heat, the change in temperature of each cell can be determined. This results in the temperature input for the electrical and heat generation model.

7.2. Battery selection

A lithium-ion battery cell has to be selected to be implemented in the models. The cell needs to have a TRL high enough to be implemented on a diesel-electric submarine. To select a lithium-ion cell, a market analysis will be performed on lithium-ion battery modules that are currently available and have the potential to be implemented on a submarine. Various battery modules can be compared based on their specifications such as the specific energy, the energy density, the cell capacity and cell chemistry.

Six battery modules from various companies have been selected. The selected modules are presented in table 7.1. What can be concluded is that most often pouch cells are implemented in a module, which could be explained by the relatively higher energy density and specific capacity of the cell design (discussed in section 3.2). Moreover, relatively high capacity cells are implemented where the NMC chemistry seems most common. EST-Floattech implements the largest cells with a capacity of 200 Ah. The EASy Marine Module from EAS Batteries has the lowest specific energy and energy density. However, the module is stated to offer a high level of safety due to liquid cooling. The module from Samsung offers the highest energy density. However, the module is typically used for residential energy storage solutions.

Table 7.1: Overview of commercial modules

		Cell			Module		
Company	**Module**	**Design**	**Chemistry**	**Capacity** [Ah]	**Capacity** [kWh]	**Energy density** [Wh/L]	**Specific energy** [Wh/kg]
EAS Batteries [6]	EASy Marine	Cylindrical	LFP	40	3.1	66	50
Samsung [89]	E3-M088	Prismatic	NMC	100	8.8	233	144
XALT Energy [29]	XMOD 111E	Pouch	NMC	126	11.1	207	173
EST-Floattech [31]	Green Orca 1050	Pouch	NMC	200	10.5	118	140
Kokam [49]	Kol Series	Pouch	NMC	103	15.1	145	119
Lechlanché [91]	Energy M2 (4s8p)	Pouch	NMC	55	6.1	200	127

The module that has been selected is the *Green Orca 1050* module from EST-Floattech. This module has widely been adopted in the maritime industry. The module consists of 14 cells. The cells that have been implemented in this module are 200 Ah pouch cells manufactured by Kokam. EST-Floattech has been willing to provide the technical specifications of the cells, as well as charge and discharge curves. The cell specifications can be seen in table 7.2. The cells are based on an NMC chemistry, having a graphite anode and a $LiNi_xMn_yCo_zO_2$ cathode. Additional specifications of the cell can be found in appendix A.

Table 7.2: Kokam SLPB140460330 specifications [32]

Kokam SLPB140460330	
Nominal capacity (at 23 °C & 0.2C)	200 Ah
Nominal voltage	3.7 V
Charging voltage	4.2 V
AC impedance	0.45 mΩ
Discharge current (max)	400 A (2C)
Charge current (max)	200 A (1C)
Thickness	13.7 mm
Width	464 mm
Height	327 mm
Weight	4.2 ± 0.1 kg
Volumetric energy density	356 Wh/L
Gravimetric energy density	176 Wh/kg

7.3. Modelling options

To model the thermal behaviour of a lithium-ion battery module, three separate models are required that interact with each other. First of all, an electrical model should be formulated to model the electrical behaviour of a cell. The dynamics are usually based on the state of charge, the operating temperature, and the charge or discharge current. As a result the voltage can be modelled. The second model determines the heat generation of the cell, which is inherently connected with the electrical model and properties of the cell. The third model is the thermal model of a battery module. This is based on the heat generation model of multiple single cells and the heat transfer with the module casing and the surroundings.

The modelling options mostly concern the selection for the electrical model. The modelling options can be applied to the heat generation model and the thermal model as well, although the main focus is on the electrical model. The electrical battery models currently described in literature can be classified in four different groups. Those are physical models, mathematical models, abstract models and mixed models [87]. The electrical models have been evaluated according to four criteria, as can be seen in table 7.3. Those criteria are accuracy, computational complexity, configuration effort and analytical insight:

- **Accuracy:** Defines how closely the predicted values correlate with the experimental values.
- **Computational complexity:** Defines the time it takes to compute the simulation.
- **Configuration effort:** Relates the amount of parameters that have to be inserted and the amount of parameters that can be estimated by the model.
- **Analytical insight:** Describes how well the model can be understood based on the implemented equations.

Table 7.3: Overview of battery modelling techniques [87]

Model	Accuracy	Computational complexity	Configuration effort	Analytical insight
Physical	Very high	High	Very high	Low
Mathematical	Medium	Low	Low	Low
Abstract	Medium	Medium	Medium	Medium
Mixed	High	Medium	Low	High

7.3.1. Physical models

Physical models are the most accurate way to model the behaviour of a battery and to optimize physical parameters [87]. Physical models represent a battery cell based on a physical basis. This physical basis involves the electrochemical reactions that take place inside the cell. These models are generally very complex, requiring a large amount of input parameters and extensive knowledge of the chemical composition of the battery. Simulations can require more than 50 parameters regarding the chemical composition, structure, temperature, capacity and other factors [87]. A very high accuracy can be reached at the expense of intense computational power [81]. Due to their complexity the models are hard to configure because of the large amount of parameters that are involved and have to be adjusted. The large amount of parameters provides limited analytical insight. Examples of physical models is for instance the diffusion-based electrochemical model by Marcicki et al. [69] and the three-dimensional electrochemical model by Xiao and Choe [115].

7.3.2. Mathematical models

Mathematical models have a very simple basis, with low requirements in computational terms. These models can also be referred to as empirical or analytical models. Mathematical models are easy to configure, but less accurate as well. The formula's that are implemented can be based on existing literature verified by experiments, as is the case in for instance various forms of heat transfer. Sometimes, based on the application, the implemented formula's have no physical meaning, leading to hardly any analytical insight [87]. In the case of modelling the electrical behaviour of batteries, charge and discharge curves are typically fitted from experimental data from researches or the manufacturer [44]. Examples of mathematical models are: a Weibull fit model based on statistical methods and the Nernst model, implementing curve fitting. More well known is the Shepherd's model, where a single equation describes the discharge behaviour of a battery cell [90].

7.3.3. Abstract models

Abstract models attempt to provide an equivalent representation of a battery. The number of parameters that have to be used for a functioning model is not large, although lookup tables are often required. The accuracy of abstract models is relatively high and computational complexity is low. However, abstract models do not have any analytical expressions as is the case for physical models. The main downside of abstract models is the large amount of input data needed to accurately represent the behaviour [81]. Equivalent electrical circuits models are widely used nowadays, where the battery voltage behaviour

is represented based on capacitors and resistors in parallel and series. An example is the model from Damay et al. [18] which is simple enough for fast computations. Another example is the circuit from Madani et al. [65] who determined the battery behaviour of a cell of which an extensive lookup table has been created to describe the relationship between C-rate, OCV and SOC.

7.3.4. Mixed models

Mixed models use a combination of the previous modelling techniques stated. Often mixed models use simplified physical processes and implement them with experimental data. Other mixed models can for instance be neural networks, with low insight and high computational requirements. However they do require a large amount of input parameters [81]. Alternatively a combination can be made between a mathematical model implemented in an equivalent electrical circuit, which results in better analytical insight. Similarly a curve fitting model has been implemented by Gao et al. [36], which utilizes lookup tables to scale discharge curves based on discharge rates and temperature influences. Mixed models generally have a higher accuracy and high analytical insight [87].

7.4. Conclusion

This chapter has described the selection procedure for a lithium-ion battery module that has the potential to be installed on a diesel-electric submarine. The lithium-ion battery module that has been selected is a 10.5 kWh module from EST-Floattech. The technical specifications of the module and the cells have been provided by EST-Floattech. The module implements 200 Ah NMC pouch cells manufactured by Kokam. The pouch cells will be implemented in the electrical model (chapter 8) and the heat generation model (chapter 9).

Additionally, this chapter has discussed the available modelling techniques for the electrical model of a lithium-ion battery cell. Based on the four modelling techniques, mixed modelling has been chosen to model the electrical behaviour of a battery cell. Based on table 7.3, this technique is chosen based on the high level of analytical insight and accuracy. Based on the accuracy a physical model could be chosen. However, a physical model requires a large configuration effort. The goal is to provide electrical behaviour of a lithium-ion cell at a preliminary design phase for a diesel-electric submarine. Therefore analytical insight is important at this stage and a low configuration effort is desired. At a later design stage a high fidelity physical model could be preferred once a specific cell has been selected. The model that will be utilised to model the electrical behaviour is the Shepherd's model. This model is a physical model on its own. However, additional parameter estimation and curve fitting will be implemented to increase accuracy, which categorises the model as a mixed model. The model will be discussed in chapter 8.

The heat generation model discussed in chapter 9 is based on a mathematical basis. The model consists of equations describing the reversible and irreversible heat that have been discussed in chapter 5. The model implements the output from the electrical model discussed in chapter 8, as well as experimental data from previous research.

The thermal model of the battery module discussed in chapter 10 is based on a mixed model basis. The model is based on a lumped thermal capacity approach implementing an electrical analogy for the transfer of heat. Physical modelling is not desired at a preliminary design stage due to the high configuration effort in case of design changes. Design changes could imply a different chemistry or cell geometry. Heat transfer coefficients have been based on existing literature. The basis of the heat transfer coefficients can often be found in experimental results that have been fitted. Therefore the thermal modelling has a mixed model basis.

The results of the thermal model of the battery module are discussed in chapter 11. The cell temperatures and typical cooling rates are analysed based on three operational profiles. The operational implications based on the thermal behaviour are discussed, providing the relevance of the model. Finally a thermal runaway scenario has been simulated in the battery module.

8

Electrical model - Cell

This chapter describes the process of modelling the electrical behaviour of a lithium-ion battery cell. The voltage of the battery will be modelled according to the charge and discharge current, the state of charge of the battery and the operating temperature. This results in the schematic overview of the electrical model visualised in figure 8.1. First the implemented model will be described, followed by the data extraction and parameter optimisation. Next the methodology and the results of the discharge model, the charge model and the temperature dependency are discussed.

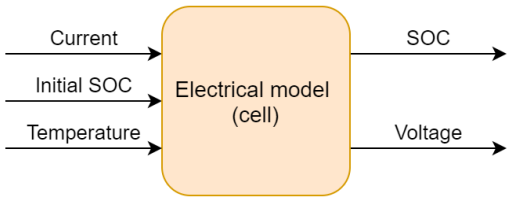

Figure 8.1: Schematic overview of the electrical model - cell

8.1. Shepherd's model

A very common battery model is the Shepherd's model. The original Shepherd's model has been developed in 1965, and its basis is still found in current literature. The model is based on a single equation that gives the cell potential as a function of the discharge current, time, and other parameters [90]. The model needs five data points from a battery discharge curve to be able to estimate the remaining parameters. Shepherd's original formula is shown in equation 8.1:

$$V = V_0 - K\left(\frac{Q}{Q - it}\right)i - R \cdot i + Ae^{(-B \cdot it)} \tag{8.1}$$

where:

- V = battery terminal voltage [V]
- V_0 = constant voltage [V]
- Q = battery capacity [Ah]
- i = battery current [A]
- it = discharged capacity [Ah]
- R = battery internal resistance [Ω]
- K = polarization constant [V/Ah]
- A = exponential zone amplitude [V]
- B = exponential zone time constant inverse [Ah^{-1}]

Note that the term it equals the current integrated over time. This means that when the battery is completely charged, the term it is equal to zero. As the battery is being discharged it increases until it reaches the value of the fully charged capacity Q. The formula for the discharged capacity it is given in equation 8.2:

$$it = \int i\,dt \tag{8.2}$$

The original shepherd's model is popular due to its simplicity and its relatively high accuracy. However, only constant current discharge is considered in the model. For that reason the original Shepherd's model has been extended by Tremblay and Dessaint [99]. The original formula is extended as shown in equation 8.3, where an extra term is added. The modified version of Shepherd's model is widely used in literature [41] [43] [81] [99] [100]. The modified Shepherd's model is also implemented in Simscape by the name "Generic battery model" in Matlab-Simulink [73].

$$V = V_0 - K\left(\frac{Q}{Q-it}\right)it - K\left(\frac{Q}{Q-it}\right)i - R\cdot i + Ae^{(-B\cdot it)} \tag{8.3}$$

The extra term involves the polarization constant multiplied by it as shown in red in equation 8.3. In the original Shepherd's model, the voltage is dependent on the current and the actual charge. This means that when no current is flowing, and the battery is almost completely discharged, the voltage will return to V_0. As soon as a current is applied again, the voltage drops drastically. This behaviour is not completely realistic. By adding the extra term shown in red, a memory effect is incorporated. When no current is flowing, the voltage will return to its open circuit voltage instead of the constant voltage V_0. The OCV is dependent on the SOC, and decreases with a decrease in the SOC. The equation provides a better fit with the added term, particularly at a low SOC. More reliable behaviour is realised with the added term, especially for strong voltage reductions when the battery is almost completely discharged.

The modified Shepherd's model accounts for both charging and discharging. For charging a different model is used, shown in equation 8.4. With a positive current the battery is discharged while with a negative current the battery is charged. The factor of 0.1 is determined by Tremblay and Dessaint [99]. When a lithium-ion battery reaches full capacity, the voltage increases rapidly when it reaches towards 0. According to Tremblay the polarization resistance is shifted by 10% based on experimental results, accounting for the value 0.10.

$$V = V_0 - K\left(\frac{Q}{Q-it}\right)it - K\left(\frac{Q}{it+0.1Q}\right)i - R\cdot i + Ae^{(-B\cdot it)} \tag{8.4}$$

8.2. Parameter estimation

The modified Shepherd's model is well known due to the minimal amount of parameters needed for configuration. The parameters that are needed can be extracted from a typical battery discharge curve, as can be seen in figure 8.2. From this curve five points can be extracted. Those are the voltage at maximum capacity (V_{full}), the data points where the exponential zone ends (Q_{exp} and V_{exp}) and the data points where the nominal zone ends (Q_{nom} and V_{nom}).

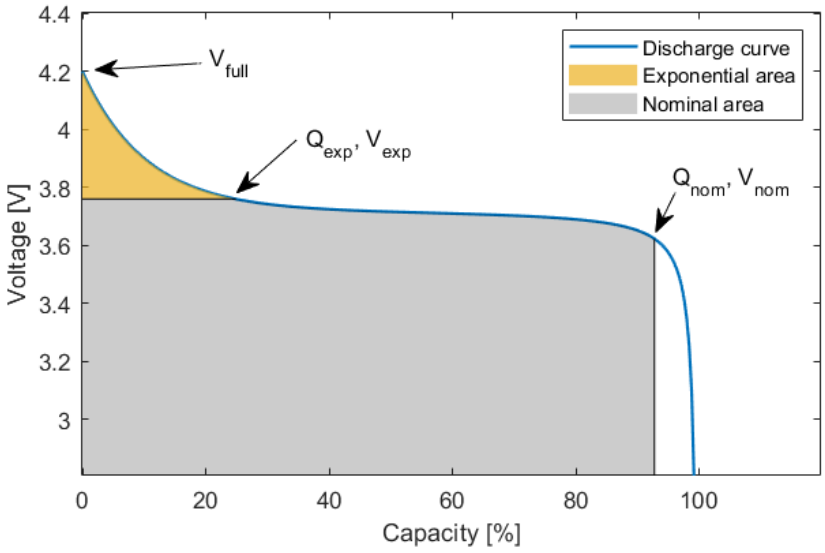

Figure 8.2: A typical lithium-ion discharge curve

Based on those five data points, other battery parameters can be calculated that are needed for the main equation. Based on research done by Tremblay et al. [100], equations have been formulated and parameters have been estimated. The parameters that have to be estimated to fit the model are R, K, A, B and V_0. The parameters can be estimated by the five equations below. A sensitivity analysis on the influence of varying the parameter values is described in section 8.3.2. Results are shown in appendix B.

$$A = V_{full} - V_{exp} \tag{8.5}$$

$$B = \frac{3}{Q_{exp}} \tag{8.6}$$

$$R = V_{nom} \cdot \frac{1 - \eta}{0.2\ Q_{nom}} \tag{8.7}$$

$$K = \left[V_{full} - V_{nom} + A\left(e^{(-B \cdot Q_{nom})} - 1\right)\right] \cdot \frac{Q - Q_{nom}}{Q_{nom}} \tag{8.8}$$

$$V_0 = V_{full} + K + R \cdot i_{curve} - A \tag{8.9}$$

- The curve fitting coefficient A indicates the amplitude of the exponential zone, which is the difference between the fully charged voltage and the voltage where the exponential zone ends (V_{exp}).
- The second coefficient, B, uses a factor 3. This value has been chosen by Tremblay and Dessaint [99] since the energy stored in the exponential area reduces to nearly zero after three time constants.
- The internal resistance of the battery, R, is usually given by the manufacturer. However, if the internal resistance provides an inaccurate fit, equation 8.7 can be used. η is the battery efficiency at nominal current, which has been estimated to 99.5% by Tremblay et al. [100].
- The polarization constant K can be determined by equation 8.8. K depends on the curve fitting coefficients A and B, as well as V_{full} and V. Additionally the battery capacity Q and the nominal capacity Q_{nom} are taken into account.
- The battery constant voltage V_0 is determined based on the full voltage, the polarization constant K, internal resistance R and coefficient A. Note that i_{curve} is used, which is the specific current that is used to create the discharge curve by the manufacturer. Otherwise a mismatch will be made between the estimated parameters depicted in figure 8.2 and the battery constant voltage. Note that V_0 does not have to represent the exact nominal voltage of the battery.

8.3. Data extraction and parameter optimisation

8.3.1. Data extraction and preparation

The selected lithium-ion battery cell is the 200 Ah pouch cell from Kokam, provided by EST-Floattech. High capacity li-ion pouch cells are typically implemented in the maritime industry based on their relatively high energy density and specific energy. The cell specifications can be seen in table 7.2 and appendix A. The curves that describe the discharge behaviour of the battery can be seen in figure 8.3. The curves display the battery voltage related to the discharged capacity. In this figure a relative capacity of 0% means the SOC is equal to 100%. The specific curves are obtained at a temperature of 23°C. The battery capacity of 200 Ah has been determined at a discharge rate of 0.2C at 23°C. Note that the discharge curves at 0.2C and 0.3C can exceed 100% capacity. This means that at low discharge rates the battery capacity can be exceeded if discharging continues below the recommended lower voltage limit. A second observation that has to be made is that the discharge current is given in ”C”. This means that 0.5C = 100 A, 1.0C = 200 A, and 2.0C = 400 A. Figure 8.4 shows the charge curves based on a charge current of 0.3C, 0.5C and 1C. Note that the horizontal axis displays the time (minutes) instead of the relative capacity. A continuous charging voltage of 4.2V is applied in this figure. Figure 8.5 shows discharge curves based on a temperature range between -10°C and 55°C. The curves are obtained under a continuous current discharge of 0.5C. Similar to figure 8.3, the battery capacity can exceed 100%. Note that at temperatures of -10°C and 0°C the battery capacity is drastically reduced.

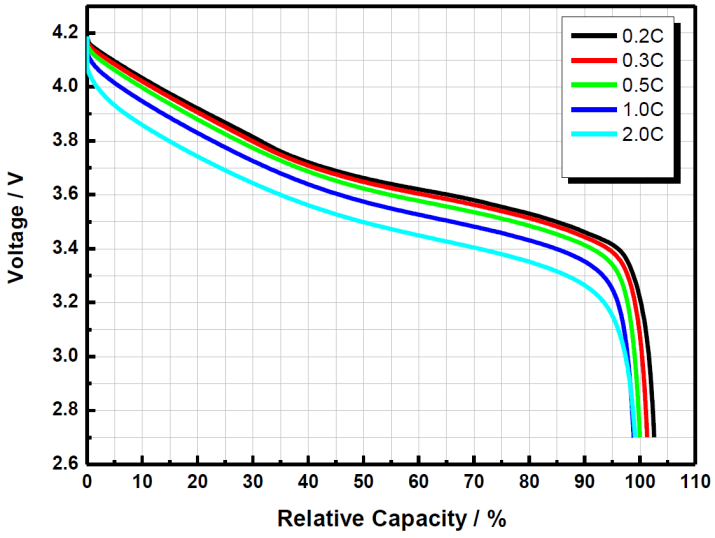

Figure 8.3: Kokam SLPB140460330 discharge curves at 23°C [31]

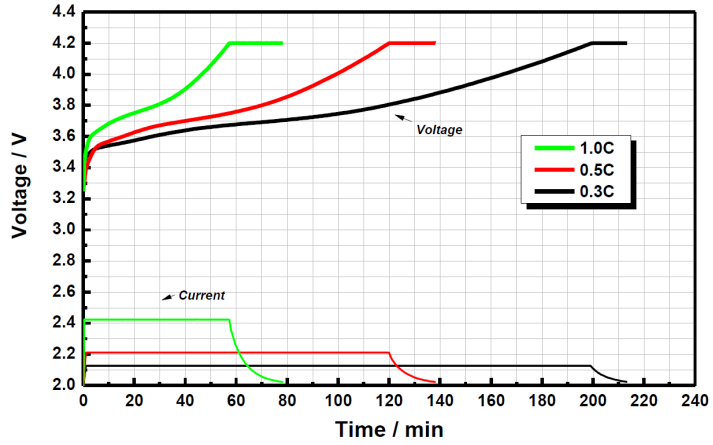

Figure 8.4: Kokam SLPB140460330 charge curves at 23°C [31]

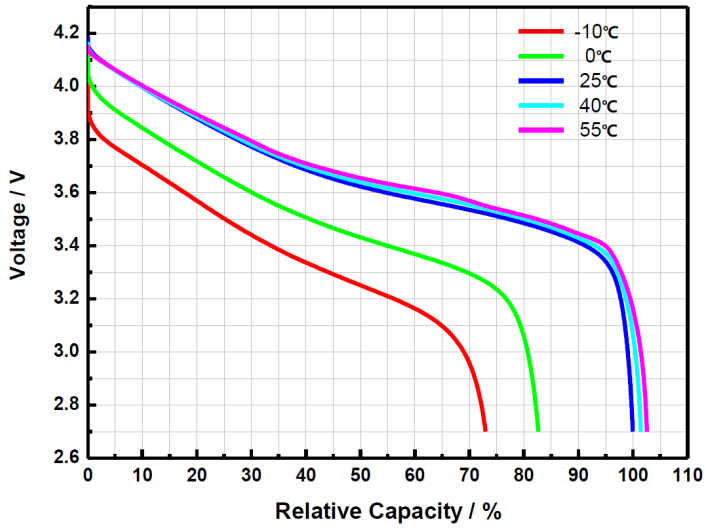

Figure 8.5: Kokam SLPB140460330 temperature curves at 0.5C [31]

8.3.2. Parameter optimisation

The initial parameters have been estimated by equations 8.5 to 8.9. The model output has been compared at 0.2C. However, the fit has a noticeable deviation throughout compared to figure 8.3. To fit the model better to the discharge curves, the initially calculated parameters will be optimised. First a sensitivity analysis is made to compare the effect individual parameter variations have on the model output. The parameters have been varied in a range between 20% and 180% related to the original values obtained by equations 8.5 to 8.9. The five parameter variations can be seen in appendix B. What can be concluded from this analysis is that parameter A strongly influences the exponential region. Parameter B influences both the exponential region as well as the gradient of the nominal zone. Parameter K influences the end of the nominal zone, and strongly describes the behaviour between 20% and 0% SOC. Parameters V_0 and R both have a similar influence on the voltage curve by adding or subtracting a constant value. Since parameter R is multiplied by the battery current, it is strongly influenced by the current. Therefore it is decided to omit parameter R for optimisation purposes. Parameters A, B, K and V_0 will be used to fit the model to discharge, charge and temperature-dependent curves.

The optimisation technique that is implemented is the Matlab function *fminsearch* [72]. This solver minimizes the error between the voltage obtained from the model and the voltage obtained from the data sheet through an objective function. The implemented objective function considers the least squares method, where the error is defined as the sum of the squared residuals. The residuals are the calculated voltages subtracted by the data voltages, as shown in equation 8.10:

$$L.SQ = \sum (V(n) - V_{data}(n))^2 \tag{8.10}$$

Besides optimising the model according to the least squares method, other indicators of accuracy have been implemented. The cumulative error has been calculated, defined as the sum of the residuals for each of the 250 data points. The cumulative error calculation can be seen in equation 8.11. A second measure of accuracy that has been used for analysis is the Mean Absolute Percentage Error (MAPE). This defines the average error relative to the calculated voltage percentage-wise. The MAPE is given by equation 8.12.

$$error = \sum (V(n) - V_{data}(n)) \tag{8.11}$$

$$MAPE = \frac{1}{n} \sum \left| \frac{V(n) - V_{data}(n)}{V(n)} \right| \cdot 100\% \tag{8.12}$$

8.4. Discharge model

The electrical model describes the voltage behaviour based on the state of charge of the battery cell. The voltage output of the electrical model is dependent on the state of charge, the current and the temperature. The goal is to simulate realistic behaviour of a lithium-ion battery cell. The behaviour has to be simulated as accurate as possible while preventing over-fitting which results in unrealistic behaviour outside the given data points.

8.4.1. Parameter configurations

The discharge model will be optimised according to three parameter configurations. The three configurations will be tested to see if they have a beneficial effect compared to the conventional method implemented in previously performed research.

Constant parameters

The initial parameter configuration optimizes the model according to the parameters A, B, K and V_0. The parameters will be optimised for all five discharge curves simultaneously. This means that the least squares error is the sum of all curves. This leads to four constant parameters that define the model. However, note that this parameter configuration can respond less accurately to nonlinear behaviour.

Cubic polynomial B

An alternative parameter configuration has been implemented based on an alternative composition of B. Parameters A, K and V_0 remain constant parameters. Based on research done by Verstraete et al. [107] parameter B has been replaced by a cubic polynomial dependent on the C-rate and four to be optimised coefficients. Higher order polynomials have been tested as well, without improved results. Therefore the polynomial described by Verstraete et al. [107] has been implemented. Parameter B has been selected instead of A, K or V_0, since parameter B has the largest influence on the discharge curve. The other parameters are less influential. Only parameter B is replaced by the cubic polynomial to prevent over-fitting of the model. The new formulation for parameter B is shown in equation 8.13. The parameter C is equal to the C-rate as formulated by equation 2.6 in chapter 2.

$$B = p_3 C^3 + p_2 C^2 + p_1 C + p_0 \tag{8.13}$$

Interpolated parameters

Another alternative parameter configuration remains at optimising parameters A, B, K and V_0 as described initially. However, the parameters are optimised for each discharge curve separately. This results in five data points for each parameter at discharge currents of 0.2C, 0.3C, 0.5C, 1.0C and 2.0C. Between these data points linear interpolation will be implemented. The result of this optimisation technique is that based on the discharge current, the parameters A, B, K and V_0 will be adjusted accordingly. Therefore these parameters are not fixed, but are determined based on linear interpolation.

8.4.2. Results & validation

Based on the three parameter configurations results have been obtained for the electrical model during discharge. The model is validated for the selected 200 Ah cell based on the discharge curves specified in figures 8.3, 8.4 and 8.5 as shown in appendix A. Note that if a different cell would be implemented, the optimisation process and validation process would have to be repeated. The results are given in table 8.1. The models are validated with an mean absolute percentage error below 0.4% for the given discharge curves. For each of the accuracy indicators, it can be seen that the interpolated parameter configuration performs best. Second best is the configuration implementing the cubic polynomial B. Finally the constant parameter configuration shows the lowest accuracy.

Although the interpolated configuration seems the best performing configuration, this is not the case. The configuration performs best at the dedicated discharge currents. However the various configurations have to be verified in terms of the voltage behaviour. The interpolated parameters prove to be irregular within the optimised range between 0.2C and 2.0C. This means the model can behave unpredictable outside the optimised discharge rates. Therefore the interpolated configuration will not be implemented. Similarly, the cubic polynomial B shows nonlinear and biased behaviour. The behaviour of the three configurations can be seen in appendix C in figures C.1, C.2 and C.3. Despite the slightly

lower accuracy for the constant parameter configuration, the behaviour is most generic. This is desired since the model should perform predictably within the entire operating range of a diesel-electric submarine. Therefore behaviour should be predictable outside the given data curves instead of a more accurate, but less predictable model.

To further analyse the accuracy of the parameter configurations, the Mean Absolute Percentage Error is calculated and plotted for the various discharge rates, as can be seen in table 8.2 and figure 8.6. The expected operating range for a diesel-electric submarine in terms of discharge rates can be estimated between at 1.0C and lower. A diesel-electric submarine has a large BESS capacity, meaning that in general lower currents are expected and a longer discharge duration of at least several hours [82] (A C-rate of 2.0 means the battery will be discharged in half an hour). It can be concluded that for low discharge rates between 0.2C and 1.0C, the constant parameter configuration and the interpolated parameter configuration have a similar accuracy around 0.3%. The model implementing polynomial B has a lower accuracy. The constant parameter configuration will be implemented in the electrical model based on the relatively higher accuracy between 0.2C and 1.0C and the more generic behaviour outside the given data points.

Table 8.1: Accuracy of three parameter configurations

Configuration	**L.SQ** [V^2]	**Error** [V]	**MAPE*** [%]
Constant parameters	0.950	16.7	0.394
Cubic polynomial B	0.715	16.3	0.378
Interpolated parameters	0.258	12.0	0.268

*Average of 5 curves

Table 8.2: Mean Absolute Percentage Error based on C-rate (discharge)

	MAPE [%]				
Configuration	**0.2C**	**0.3C**	**0.5C**	**1.0C**	**2.0C**
Constant parameters	0.255	0.168	0.285	0.308	0.954
Cubic polynomial B	0.232	0.188	0.400	0.416	0.652
Interpolated parameters	0.308	0.220	0.243	0.304	0.269

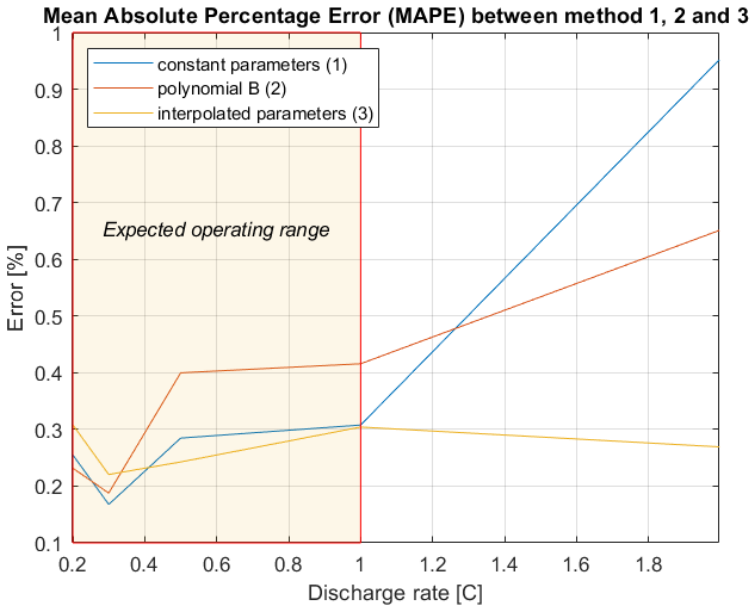

Figure 8.6: Mean Absolute Percentage Error for 3 parameter configurations based on C-rate

8.5. Charge model

Based on the curve fitting methodology applied in section 8.4, the model now describes the battery voltage based on a discharge current. However, the model needs to predict the battery voltage as well for a charging current, based on equation 8.4. The charge model will be based on three charge curves, as can be seen in figure 8.4. The charge curve is obtained by charging the battery with 4.2V and a continuous current of 0.3C, 0.5C and 1.0C. The same parameter configuration implementing constant parameters has been applied as described in section 8.4 to create consistency with respect to the discharge model. Parameters A, B, K and V_0 will be optimised based on the given charge curves. To omit ambiguity in parameter definition the charge model makes use of parameters A_c, B_c, K_c and V_{0c}. Since the charge curves are plotted on a graph with time (minutes) on the horizontal axis, a conversion has been made from time to the charged capacity [Ah] implementing equation 8.2.

The accuracy of the optimised charging model can be seen in table 8.3. The least squares error ranges around a value of 0.42V ^{2} on average, and the mean absolute percentage error ranges between 0.41% and 0.57%. This means that the charge model is validated for the selected lithium-ion cell with an average error below 0.6% for a charge current between 0.3C and 1.0C. The accuracy of the charging model is within the same order of magnitude as the accuracy of the discharge model. The behaviour of the charge model between 0C and 1.0C can be seen in figure C.4 in appendix C.

Table 8.3: Accuracy of charge model

Charge current	**L.SQ** [V^2]	**Error** [V]	**MAPE** [%]
0.3C	0.420	4.24	0.472
0.5C	0.404	3.58	0.411
1.0C	0.444	5.26	0.573

8.6. Temperature influence

Various models that simulate the electrical behaviour of a lithium-ion battery are usually dependent on the discharge current and the stage of charge of the battery. The temperature at which the cell operates is rarely modelled, meaning that very commonly the temperature has no influence on the charge and discharge characteristics. However, temperature effects that influence the voltage behaviour are present in lithium-ion batteries. Colder temperatures slow down the reaction rate within batteries, and can drastically reduce the ability to charge. The internal resistance usually increases at lower temperatures. Low temperatures can increase the viscosity of the electrolyte of lithium-ion batteries. This decreases the ionic conductivity and thus the reaction rate, as described in section 2.1.4. The temperature is therefore related to the battery voltage. Research has been done to implement temperature effects into the electrical model. Research done by Hemi et al. [42] implemented the modified Shepherd's model by Tremblay and Dessaint [99]. They optimised parameters A, B, K and V_0 based on several discharge curves at a temperature range. Based on these data points linear interpolation is used to relate the voltage to the operating temperature. Additionally polynomials are fitted on the parameter values. Another method is implemented by Wijewardana [112], who created temperature dependent coefficients which have been multiplied by parameters A, B, K and V_0. The new coefficients are third order polynomials fitted to temperature data similarly optimised as has been done by [42].

8.6.1. Parameter configurations

Based on the work of Hemi et al. [42] and Wijewardana [112], two parameter configurations have been defined to incorporate the temperature influence to the model. The original parameters defined in section 8.4 are kept, but additional temperature dependent coefficients have been added. The temperature-dependent model will be fitted to the data seen in figure 8.5. The initial temperature-dependent configuration can be seen in equation 8.14. The previously optimised parameters A, B, K and V_0 have been multiplied with X_A, X_B, X_K and X_{V0} respectively. Data above 55°C is not available. Therefore parameters will be kept constant from 55°C and higher. Based on the curves from figure 8.5, it can also be concluded that temperature effects on the cell voltage decrease at higher temperatures.

$$V = X_{V0} \cdot V_0 - X_K \cdot K\left(\frac{Q}{Q-it}\right)it - X_K \cdot K\left(\frac{Q}{Q-it}\right)i - R \cdot i + X_A \cdot Ae^{(-X_B \cdot B \cdot it)} \tag{8.14}$$

The second parameter configuration uses two parameters to fit the model to the temperature discharge data. A lower amount of parameters is chosen to prevent the model from over-fitting to a limited amount of data available. The goal is to try to capture the temperature behaviour with less parameters to better predict temperatures outside of the given discharge curves. Additionally, it is preferred to minimize the amount of parameters that have to be estimated when the model is applied to a different cell. The newly formulated temperature-dependent discharge model can be seen in equation 8.15. Only parameters X_K and X_A have been used. Parameter X_K has been selected since K has the largest influence on the voltage at a low SOC according to figure B.3 in appendix B. At low temperatures a significant reduction in battery capacity can be seen according to the discharge curves in figure 8.5. This can be realised by adjusting X_K. Either parameter X_A or X_B could have been selected to adjust the exponential zone at high SOCs. However, parameter X_A proved to be more effective by trial and error.

$$V = V_0 - X_K \cdot K\left(\frac{Q}{Q-it}\right)it - X_K \cdot K\left(\frac{Q}{Q-it}\right)i - R \cdot i + X_A \cdot Ae^{(-B \cdot it)} \tag{8.15}$$

8.6.2. Results & validation

Results have been obtained regarding the accuracy of the two selected parameter configurations. The temperature dependence of the electrical model is verified based on the research of Novák [81] and various temperatures curves of alternative lithium-ion cells based on their specification sheets. It can be concluded that for all analysed cells the voltage decreases with a decrease in temperature, as well as a decrease in voltage as the SOC decreases. The electrical model is validated for the selected 200 Ah cell based on the temperature curves in figure 8.5. The accuracy indicators for the total error based on 5 temperature-dependent discharge curves can be seen in table 8.4. Both configurations are validated between -10°C and 55°C with an average mean absolute percentage error below 0.7%. It can be concluded that for all 3 indicators, the 2 parameter model performs better. Secondly, an analysis has been performed on the MAPE based on each temperature separately. Those results are shown in table 8.5 and figure 8.7. Based on the two tables it can be concluded that the 4 parameter model performs better between 25°C and 55°C, although the error for both configurations is less than 0.6%. Temperatures between 20°C and 40°C are likely experienced in a BESS on board of a submarine. However, temperatures until freezing point could in theory be experienced in submarines, and temperatures below zero can be experienced in surface vessels. However, it is assumed that for this research battery temperatures will range between 20°C and 40°C, as indicated in figure 8.7. Finally an analysis has been made how both configurations perform outside the given temperatures. The behaviour of both models can be seen in figures C.5 and C.6 in appendix C. It can be seen that with the two parameter configuration good generic temperature behaviour can achieved. The 4 parameter configuration shows to be very inconsistent, and will therefore not be selected. This confirms the plausibility of over-fitting a model with too many parameters. Based on the results and the conclusions drawn, the 2 parameter temperature-dependent configuration will be implemented in the electrical model.

Table 8.4: Accuracy of 2 and 4 parameter configurations

Configuration	**L.SQ** [V^2]	**Error** [V]	**MAPE*** [%]
2 parameters	1.31	23.1	0.552
4 parameters	2.06	28.0	0.682

*Average of 5 curves

Table 8.5: Mean Absolute Percentage Error based on temperature

	MAPE [%]				
Configuration	**-10**°C	**0**°C	**25**°C	**40**°C	**55**°C
2 parameters	0.769	0.965	0.366	0.244	0.418
4 parameters	1.31	1.37	0.251	0.200	0.273

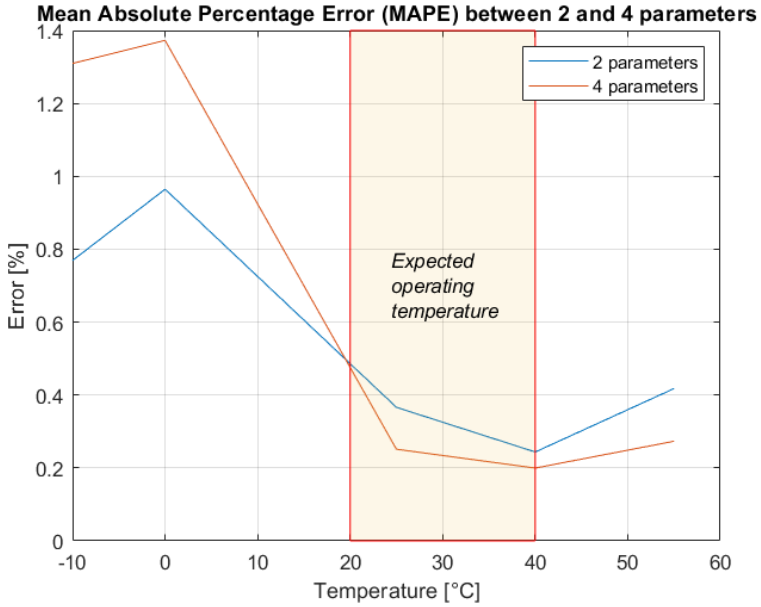

Figure 8.7: Mean Absolute Percentage Error for 2 and 4 parameters based on temperature

8.7. Conclusion

In this chapter the electrical behaviour of a lithium-ion battery cell has been modelled. The Shepherd's model has been implemented to simulate the voltage behaviour of a 200 Ah pouch cell from Kokam. The model has been optimised and validated based on the specification sheets of the cell. If a different cell would be implemented, the optimisation process and validation process would have to be repeated. Moreover, experimental data is desired as well for validation purposes. The battery voltage is a function of the discharge current, the SOC and the operating temperature. For the discharge model, constant parameters have been selected, having the result that consistent behaviour is realised and the chance of over-fitting is minimised. For the charge model, constant parameters have been optimised as well. The temperature-dependence has been modelled with 2 parameters. This shows more realistic behaviour compared to the four parameter model where over-fitting occurs. Therefore, realistic and consistent behaviour is favoured over the highest achievable accuracy. The selected modelling options for modelling the current and temperature dependence provide most realistic behaviour outside the given data points as shown in appendix C. Moreover, based on the fact that no specific battery is selected yet for the new submarines at a preliminary design stage, a high configurability is desired. A minimal configurational effort is desired when comparing different cells at this stage.

Various operational implications can be concluded for diesel-electric submarines based on the electrical model. The first implication is that a higher efficiency can be realised by lowering the discharge current. This results in a higher cell voltage as a consequence of minimal losses. This results in an increase in the submerged range. Secondly, discharge should be interrupted at a low SOC (dependent on the temperature) since the effective cell voltage decreases substantially. Finally, operation is not desired at temperatures below 20°C. Operation below this temperature drastically reduces the capacity and voltage, limiting the efficiency of the cell. As a consequence the submerged range is decreased.

9

Heat generation model - Cell

The process of charging and discharging a lithium-ion battery is not achieved at a 100% efficiency. Due to the change in entropy, the internal resistance, activation losses and concentration losses, heat is produced. The amount of heat produced is not constant and dependent on many factors, such as the battery chemistry, the operating temperature, the geometry and the charge or discharge rate, as described in chapter 5. The total generation of heat consists of two contributions, which are reversible heat and irreversible heat, as shown in equation 9.1. Based on these two contributions, the heat generation will be modelled as a function of the operating temperature, the SOC, the current, the cell voltage and battery specific factors such as the entropic coefficient. A schematic overview of the input and output of the heat generation model is given in figure 9.1.

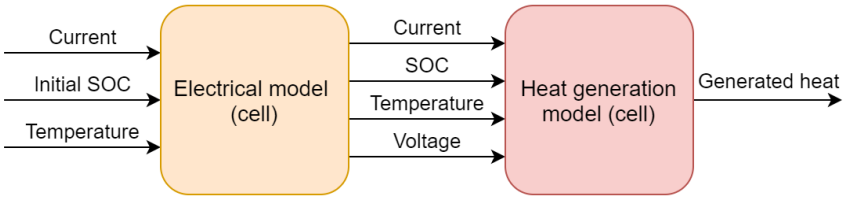

Figure 9.1: Schematic overview of the heat generation model - cell

$$\dot{Q}_{tot} = \dot{Q}_{rev} + \dot{Q}_{irr} \tag{9.1}$$

9.1. Reversible heat

The reversible heat consists of entropic heat. Entropic heat is related to the change in entropy of the battery cell. The entropy change occurs within the electrochemical reactions where lithium ions are intercalated and deintercalated in the electrodes of the cell. The entropy change can be both positive and negative based on the SOC and the chemistry of the battery. The contribution of entropic heat is particularly important at low C-rates, were irreversible losses have a much lower contribution. As explained in section 5.1.1, the entropic heat is given by equation 9.2, where I is the battery current (positive for discharge), T the battery temperature in Kelvin, and U_{OCV} the open circuit voltage.

$$\dot{Q}_{rev} = -I \cdot T \cdot \frac{\partial U_{OCV}}{\partial T} \tag{9.2}$$

The temperature derivative of the OCV, also named entropic coefficient, has to be determined experimentally. However, the determined values are chemistry and cell dependent. For that reason experimental data has to be obtained from a similar battery that matches the currently chosen cell as closely as possible. The SLPB140460330 pouch battery cell from Kokam has an NMC chemistry and a capacity of 200 Ah. Research on a very similar cell has been done by Abdul-Quadir et al. [1]. They

performed research on a Kokam SLPB100216216H cell, which is an NMC cell with a capacity of 40 Ah. Since this specific battery has the same manufacturer, the same chemistry and a similar pouch cell geometry, it is assumed that the temperature derivative of the OCV can be implemented for this research. Since entropy is an extensive quantity and is therefore proportional to the quantity of matter, scaling has a reduced impact [56]. Abdul-Quadir et al. [1] have measured the OCV for several different SOCs, where the temperature was raised while the SOC was kept constant. The entropic coefficient is given in table 9.1, where the values have been determined on an interval between 25°C and 30°C.

Table 9.1: Entropic coefficient based on the SOC between 25°C and 30°C [1]

SOC	**100**%	**80**%	**60**%	**40**%	**20**%	**0**%
dV/dT [mV/K]	-0.13	-0.03	0.06	0.02	-0.07	-0.44

Analysing the values of the entropic coefficient from table 9.1, it can be seen that the coefficient ranges between -0.44 and 0.06 mV/K. This shows that during discharge the entropic heat is exothermic for 100% and 80% SOC and 20% and 0%. For a SOC of 60% and 40%, the entropic heat is endothermic. Entropic coefficients for other lithium-ion chemistries vary significantly. Liu et al. [58] obtained an entropic coefficient between -0.3 to 0.1 mV/K for a 8 Ah prismatic LMO cell. Forgez et al. [35] obtained values between -0.31 and 0.13 mV/K for a cylindrical 26650 LFP cell, whereas Balasundaram et al. [5] obtained values between -0.28 and 0.23 mV/K for a cylindrical 18650 LFP cell. Nazari and Farhad [80] obtained values for LFP (-0.09 - 0.05 mV/K), LCO (-0.6 - -0.04 mV/K) and LMO (-0.25 - 0.23 mV/K). Lastly Lu et al. [62] investigated an NMC cell, obtaining an entropic coefficient between -0.06 and -0.12 mV/K. The entropic coefficient based on the SOC varies significantly between chemistries and researches, which concludes that only the order of magnitude is comparable. From the various researches and the data from table 9.1, it can be concluded that only the entropic coefficient at a SOC of 0% seems to be larger than other chemistries. According to Abdul-Quadir et al. [1], the high entropic coefficient can be caused by structural changes in the cathode side.

9.2. Irreversible heat

Irreversible heat is generated due to the difference between the open circuit voltage and the closed circuit voltage. The voltage difference is called the overpotential or polarization. As described in section 5.1.2, the total polarization consists of several sources, such as activation polarization, concentration polarization and Ohmic overpotential. The total polarization is defined by equation 9.3, and the heat generated due to the total polarization is given in equation 9.4, where η_{ohm} can be represented by $\eta_{ohm} = IR_{in}$, as described in 5.1.3.

$$\eta = U_{OCV} - V = \eta_{act} + \eta_{con} + \eta_{ohm} \tag{9.3}$$

$$\dot{Q}_{irr} = I \cdot \eta \tag{9.4}$$

Instead of calculating each polarization contribution separately, the total polarization is calculated. The battery voltage V is obtained through the electrical model described in chapter 8. Here the battery voltage is modelled based on the battery temperature, the charge or discharge current and the state of charge of the battery. The open circuit voltage has been obtained through data provided by EST-Floattech. The data has not been included due to confidentiality. By applying a pulse current to charge the battery, the OCV has been measured. After the current is interrupted, an immediate voltage drop occurs due to the absence of the Ohmic overpotential, commonly called the ”IR drop”. Afterwards the voltage will stabilize to the OCV value, where the cell potential is at chemical equilibrium. The OCV curves are obtained by measuring these OCV values at specific SOCs and temperatures. The OCV curves are linearly interpolated to predict the voltages at intermediate temperatures.

9.3. Results and verification

Based on the reversible heat and irreversible heat components, the total heat generation for the 200 Ah battery from Kokam has been modelled. Based on the entropic coefficients obtained through the research of Abdul-Quadir et al. [1] the entropic heat has been modelled. The irreversible heat has

been obtained through the overpotential between the OCV curves provided by EST-Floattech and the battery voltage from the electrical model described in chapter 8. The results have been verified based on experimental studies and modelling results found in literature. Note that in figures 9.3, 9.4, 10.17 and 9.6 the side planes are gray. This is to indicate that an SOC below 10% and above 90% are excluded from the operational range of the battery cell, as recommended by the manufacturer. This minimizes the risk of overcharge and overdischarge that potentially can cause a thermal runaway, as described in section 4.1. The limits are an initial indication and depend on the preferences of the engineer. For a diesel-electric submarine a higher minimum SOC of for instance 20% could be mandatory. Based on the operational profile, a specific remaining capacity is desired to account for evading a hostile area to search for a safe location to resurface or snort. By having a capacity reserve a situation can be avoided where no battery capacity is left while being submerged.

Reversible heat
An analysis has been made on the effect of the battery temperature and the C-rate on the reversible heat. Figure 9.3a shows the entropic heat for the SOC of the battery at a temperature range between 0°C and 60°C at 0.5C. It can be seen that initially the battery delivers heat at a rate of roughly 4 Watts. Around a SOC of 60% the battery absorbs heat at a rate near 2 W. At a SOC of 0% the reversible heat delivers between 12 W and 14 W of energy, accounted for by structural changes in the cathode. The temperature influence on the generated heat is minimal. However, it is assumed that the entropic coefficient itself remains constant for the various temperatures, due to the limited amount of suitable data found in literature. The order of magnitude of the reversible heat and the order of magnitude of the entropic coefficient is verified in literature, as described in section 9.1. Figure 9.3b shows the entropic heat at a temperature of 30°C for C-rates between 0.2C and 1.0C. As can be seen, the influence of the C-rate is more significant than the temperature. The relative difference in C-rate is much larger than the relative difference in absolute temperature. (0.2C to 1.0C is a 400% increase, while 273K (0°C) to 333K (60°C) is only a 22% increase). Equation 9.2 shows that the reversible heat is linearly related to the C-rate, which is noticeable in the figure.

Irreversible heat
The analysis of the irreversible heat has been made based on the same temperature interval and current interval as has been done with the reversible heat. Shown in figures 9.4a and 9.4b, the heat generation rate is plotted versus the state of charge of the battery. Analysing figure 9.4a, it can be seen that for lower temperatures more heat is generated. Especially at 0°C and 10°C the generated heat is substantially larger than at temperatures between 30°C and 60°C. The increase in heat generation at lower temperatures is verified by research from Esmaeili and Jannesari [30] and Liu et al. [58]. Moreover, as the SOC decreases, the heat generation rate increases. This is as expected since lithium ions are transferred from the anode to the cathode as the battery discharges. This changes the concentration gradients at the anode and the cathode, meaning that more energy is needed to transfer the ions from the anode to the cathode which results in more heat losses [1]. The increase in the heat generation rate can thus be related to the concentration polarization of the cell, which is verified by Esmaeili and Jannesari [30] and Ovejas and Cuadras [83]. At higher temperatures, temperature influences seem to decrease. The same effect can be seen from the temperature-dependent discharge curves in figure 8.5, where at higher temperatures no slight deviations in voltage can be seen. Importantly to note is that results between 10% and 0% SOC are unexpected and inconsistent with literature. Due to possible inaccuracies in the voltage modelling at low SOCs, unrealistic heat generation rates are realised. At higher temperatures the irreversible heat turns negative, which is impossible since irreversible heat is not endothermic. This is supported by the battery manufacturer advising to limit the voltage between 3.4 V and 4.1 V for a long life operating range (see appendix A).

Figure 9.4b shows the current dependence of the irreversible heat at 30°C. An exponential relationship can be seen in the irreversible heat generation, although not according to Ohm's law ($\dot{Q} = I^2 \cdot R$). This is accountable for by the activation polarization and concentration polarization. Between 10% and 0% SOC a slightly negative heat generation rate can be seen as in figure 9.4a. To validate the irreversible heat, a comparison has been made with the internal resistance given by confidential research performed by EST-Floattech. In their research, the total irreversible heat was assumed to be caused completely by the internal resistance. To compare the experimental resistance to the modelled resistance, the total overpotential has to be converted to a theoretical "total resistance". The total resistance

(R_{tot}) is calculated according equation 9.5, where the total overpotential is divided by the current. Figure 9.2 compares the given ranges by EST-Floattech (dashed lines) and the modelled values. At a temperature of 0°C, the total resistance (R_{tot}) is considerably higher than the internal resistance (R_{in}). At a temperature of 25°C, the total resistance lies within the margins between 100% and 40% SOC, and exceeds the margins at lower SOCs. At a temperature of 40°C, the total resistance is overestimated from an SOC of 85% and lower. Alternatively, Abdul-Quadir et al. [1] obtained a total resistance between 2.0 mΩ and 3.5 mΩ for a 40 Ah Kokam cell, indicating a higher total resistance.

$$R_{tot} = \frac{\eta}{I} \tag{9.5}$$

Total Heat

Figures 9.5a and 9.5b show the total heat generation based on a temperature range between 0°C and 60°C and 0.2C to 1.0C respectively. Compared to figures 9.3b and 9.4, it can be concluded that the total heat is mostly governed by the irreversible contribution. At a C-rate of 0.2C, the reversible heat is 23% of the total heat. At a rate of 1.0C, it decreased to 8.6% (at 30°C). This is in line with research done on a LFP cell by Balasundaram et al. [5] (33% at 1.0C and 11% at 5.0C, at 35°C). This confirms that the increase in irreversible heat is greater than the increase in reversible heat based on an increasing C-rate. These relationships are supported by equations 9.2 and 9.4. $\dot{Q}_{rev}$ increases linearly with an increase in C-rate, while $\dot{Q}_{irr}$ increases exponentially between I^1 and I^2. Although different in quantity, similar behaviour is seen with respect tot the total heat generation rate. The increase in heat as the SOC decreases is consistently confirmed by several researches [1] [83] [58] [115] [116].

Heat generation during charging

The heat generation rate has been determined based on a charging current as well. As described in section 8.5, the cell voltage has been modelled based on various charging rates. The charge model is however not temperature dependent, since no temperature-dependent charge data is available. Therefore it assumed that the heat generation profile will be the same at a temperature interval between 25°C and 55°C. Charging at lower temperatures is not advisable due to an increased internal resistance and increased viscosity of the electrolyte. Additionally, the temperature influence on the heat generation rate seems to decrease at 30°C and higher based on figures 8.5, 9.4a and 9.5a.

The reversible heat contribution is the same as for the discharge model, only opposite in sign according to equation 9.2. The irreversible heat generation rate and total heat generation rate are shown in figure 9.6a and 9.6b. The amount of heat that is generated during charging of the battery is lower than during discharging. The spike that can be seen at a SOC between 10% and 0% is likely caused by modelling inconsistencies, since an increase in charging resistance would usually be expected at high SOCs due to an increased resistance to reach a fully charged cell. The total overpotential during charging is converted to a theoretical total resistance to compare the heat generation rates to estimations from EST-Floattech. The result can be seen at a temperature of 25°C in figure 9.2. The heat generation rate seems to better fit between the ranges given by EST-Floattech. However, to properly validate the heat generation model, experimental data is needed.

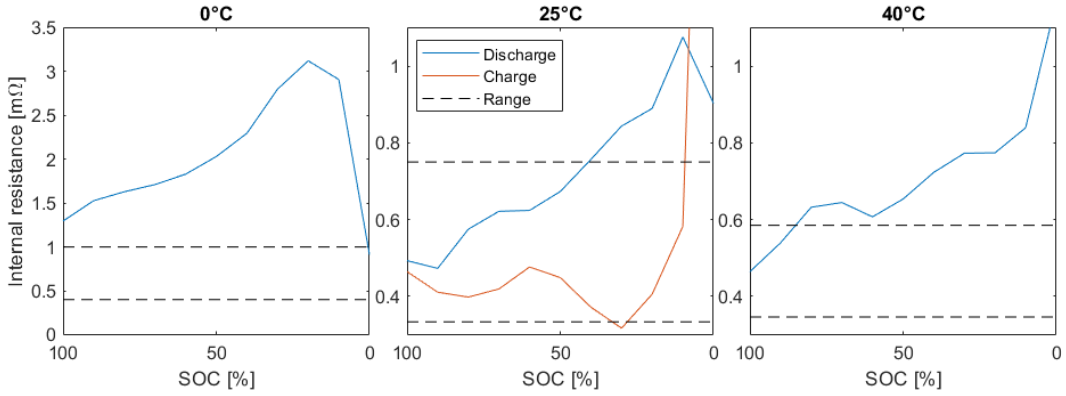

Figure 9.2: Comparison of total internal resistance (R_{tot}) for various temperatures (vertical axis at 0°C has larger range)

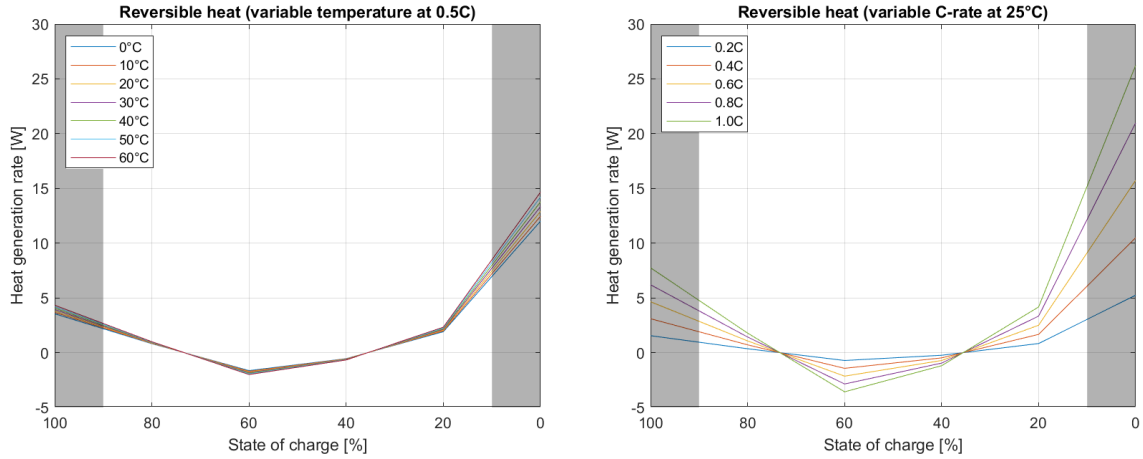

(a) Temperature dependence

(b) Current dependence

Figure 9.3: Reversible heat for various temperatures and C-rates

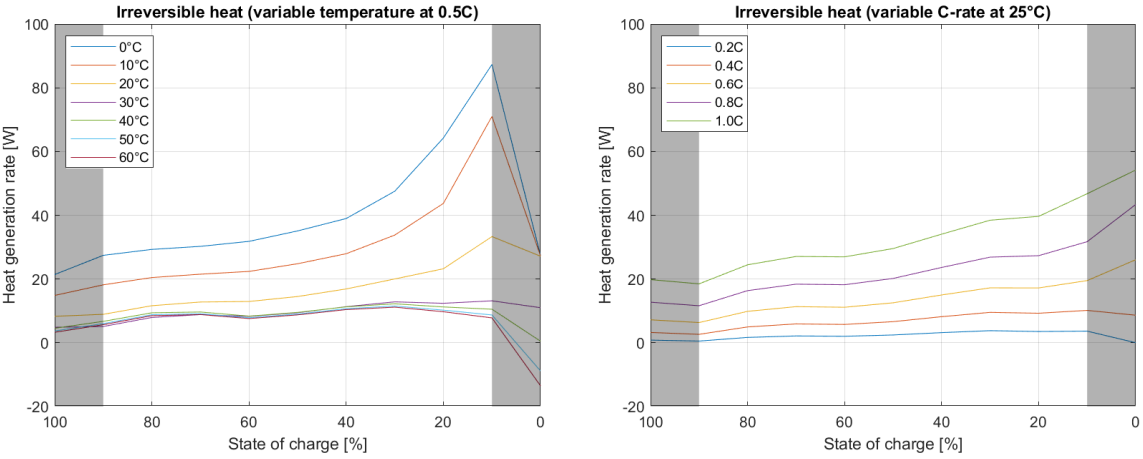

(a) Temperature dependence

(b) Current dependence

Figure 9.4: Irreversible heat for various temperatures and C-rates

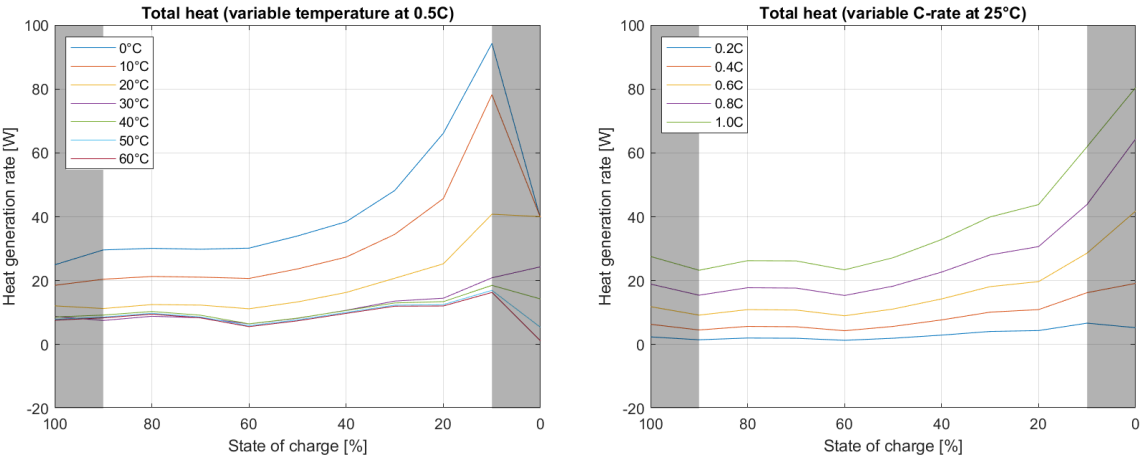

(a) Temperature dependence

(b) Current dependence

Figure 9.5: Total heat for various temperatures and C-rates

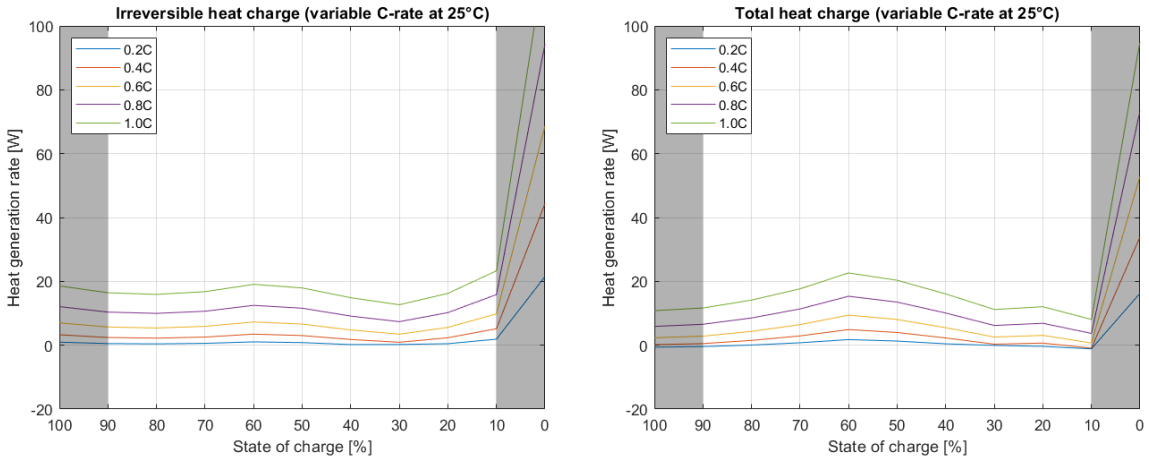

(a) Irreversible heat during charging

(b) Total heat during charging

Figure 9.6: Irreversible and total heat generation for charging at 25°C

9.4. Conclusion

The heat generation model incorporates the heat generation response of a 200 Ah lithium-ion battery cell. The model is based on reversible and irreversible heat. The contribution of reversible heat is based on the entropic coefficients obtained from research performed by Abdul-Quadir et al. [1]. The irreversible heat contribution is based on the overpotential between the open circuit voltage curves provided by EST-Floattech and the battery voltage obtained from the electrical model. The reversible heat and irreversible heat are both dependent on the charge and discharge current, the SOC of the cell and the temperature. The results have been verified based on experimental studies and modelling results found in literature. The total heat generation is mostly governed by the irreversible heat generation. The total heat generation increases with a decreasing temperature. Moreover, the total heat increases exponentially with an increase in the C-rate, although at a lower exponential factor than Ohm's law. The total heat generation rate increases with a decrease in the SOC.

Operational implications can be concluded based on the heat generation model. Discharging the cell below 20°C is not desired. Significantly more heat is generated at low temperatures, meaning that the efficiency decreases which consequently decreases the submerged range of the submarine. However, the increased heat generation rates can be utilised to increase the temperature of the cells, which means the heat generation rate will decrease as a consequence. The recommended operating temperature lies between 20°C and 30°C since high(er) temperatures reduce the battery lifetime [97]. It is recommended to maintain the state of charge between 10% and 90%. Exceeding the limits increases the risk of overcharge and overdischarge which can potentially cause a thermal runaway. Based on the operational profile of a diesel-electric submarine extra capacity up to 20% can be reserved to account for resurfacing or snorting. This depends on the user requirements.

10

Thermal model - Module

This chapter discusses the methodology of creating a thermal model of a lithium-ion battery module. The generated heat inside the battery module is modelled for each cell based on the heat generation model described in chapter 9. A schematic overview of the models is visualised in figure 10.1. First of all, the geometry of a typical module will be determined. Next, typical heat transfer rates are determined based on the module geometry. Heat transfer coefficients will be determined based on conduction, convection and radiation. Finally, the implementation is discussed based on a Lumped Thermal Capacity approach.

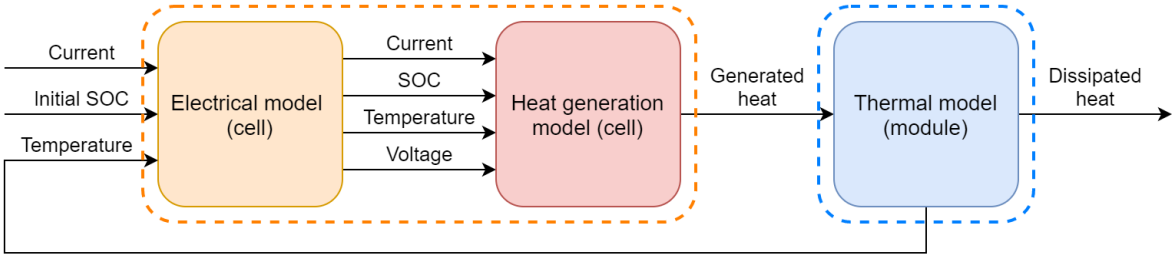

Figure 10.1: Schematic overview of the thermal model - module

10.1. Energy balance

The energy balance for each cell can be determined based on the first law of thermodynamics. The first law of thermodynamics states that the change in internal energy of a closed system is based on the added or subtracted heat and the delivered work, meaning that energy is conserved. The first law is shown in equation 10.1, where ΔU is the change in internal energy [J], Q is the added or subtracted heat [J] and W is the work done [J]. Under the assumption that all objects in the battery module are incompressible, there is no volume or pressure change. This means that the delivered work is equal to zero. This also means that the specific heats under constant pressure and constant volume are equal and constant [77]. Therefore the change in internal energy can be reformulated as shown in equation 10.2.

$$\Delta U = Q - W \tag{10.1}$$

$$\rho V c \frac{dT}{dt} = \dot{Q} + \dot{Q}_v \tag{10.2}$$

Where ρ is the density [kg/m^3], V the volume [m^3] and c the specific heat capacity of the object [J/(kg K)]. $\dot{Q}$ is the transferred heat [W] and $\dot{Q}_v$ is the generated heat [W]. This is a first order differential equation, where the change in internal energy is related to a change in temperature. The change in internal energy is dependent on the heat transfer in and out of the closed system and the generated heat.

10.2. Module geometry

A lithium-ion battery module consists of multiple cells within a module. The module geometry depends typically on the number of cells and the geometry of the cells. The implemented module geometry is inspired by the *Green Orca 1050* battery module from EST-Floattech [31]. EST-Floattech has implemented 200 Ah pouch cells in their modules. The cells are manufactured by Kokam and the cell dimensions can be seen in table 7.2 and appendix A. Note that the module described in this section is fictional and does not match the battery modules from EST-Floattech. The dimensions that are being described are therefore indications of a typical battery module based on large pouch cells.

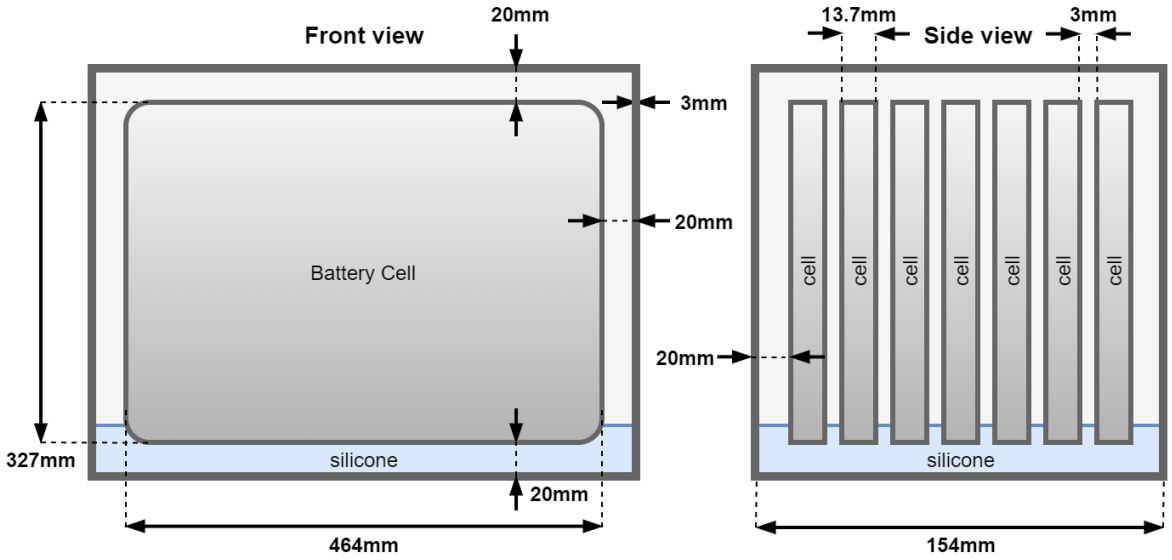

Figure 10.2: Implemented module geometry. For illustration purposes the module is not drawn to scale.

The battery module implemented in this research is shown in in figure 10.2. The battery module is assumed to be IP67 certified, meaning that the module is dust and waterproof. The cells have therefore no direct contact with the environment. The battery module consists of 7 lithium-ion cells. The cells are pouch cells with a height of 327 mm, a width of 464 mm and a thickness of 13.7 mm. The cells are modelled as cuboids, neglecting irregularities or excess material around the edges. The connecting tabs on the top side are neglected as well. The cells are aligned vertically, forming a row of cells. Between the cells a small spacing is realised, allowing room for the cells to expand during operation or in case of a failure mechanism. The air spacing between the cell is determined at 3 mm. The spacing between the cells and the module is determined at 2 cm at the top, bottom and sides. The surrounding spacing is usually needed to fixate the cells relative to each other and the casing. The bottom of the module is filled with a thermally conductive filler to dissipate the generated heat. The conductive material is usually an epoxy resin or a silicone based material. The properties of this material strongly depend on the manufacturer and desired properties. The thermally conductive material fixates the bottom of the cells to the casing and serves as a damper for any shocks and vibrations. The casing of the battery module is made of aluminium and has a thickness of 3 mm. aluminium is chosen as the casing material due to its high thermal conductivity, high strength and low weight compared to other materials. The module has an energy density of 209 Wh/kg and a specific energy of 135 Wh/kg.

The generated heat from the battery cells has to be dissipated to maintain the module at an acceptable temperature. Most heat is dissipated through the thermally conductive filler at the bottom of the module and the bottom module casing. The exterior side of the bottom casing is kept at a constant temperature by means of liquid cooling. Liquid cooling through the bottom casing is implemented. This method is initially chosen based on a relatively low complexity and potentially lower costs, as described in section 4.4.2. It will therefore be investigated if this configuration provides enough cooling capabilities. Alternatively cooling between the cells can be implemented, which increased the complexity of the module significantly. The front side and the back side of the battery module are in contact with

ambient air at a constant temperature. The left and right side of the module provide no heat exchange. Thermal resistant plates can be installed on either side to prevent a thermal runaway from propagating to adjacent modules. To idealize the thermal barrier, no heat transfer will be modelled between the left and right side. The top of the battery module has no heat exchange. Usually electrical hardware is mounted at the top side of a battery module, regulating the SOC of each cell and monitoring temperatures. The hardware is preferred to be thermally isolated from the module in case of a thermal runaway. Therefore no heat transfer will be modelled through the top side. Heat can only transfer out of the module by the front casing and the bottom casing.

10.2.1. Heat capacity

To investigate the thermal behaviour of the battery module, one needs to know the heat capacity to predict how quickly the module will heat up. The module is divided in several thermal objects as described in the previous section. A selection has to be made which thermal objects are significant to implement in the battery model. The heat capacity of each object can be calculated based on the initially chosen geometry and the thermal properties of the materials. The heat capacity of a thermal object can be calculated through equation 10.2. The heat capacity [J/K] is equal to the specific heat capacity [J/(kg K)] multiplied by the mass, leading to $C = \rho V c$. The density and thermal properties of materials used in the casing are given in table 10.1. Based on the material properties and the geometry described in section 10.2 and figure 10.2, the heat capacity can be calculated for each thermal object. The heat capacities are shown in table 10.2.

Table 10.1: Properties of selected materials at 300 K [77] [25] [4] [1]

Material	**Density** [kg/m^3]	**Specific heat capacity** [J/(kg K)]	**Thermal conductivity** [W/(m K)]
Air	1.177	1005	0.0267
aluminium	2790	883	168
Battery cell	2021	670	-
Silicone filler	3000	1100	1.5

Table 10.2: Heat capacities of thermal objects in the battery module

Thermal object	**Heat capacity** [J/K]
Air in module	22.94
Left/right casing	726.4
Bottom casing	997.5
Front casing	1367
Battery cell	2814
Filler	8908

The silicone filler selected for the thermal model is based on a thermally conductive gap filler by Electrolube [25]. The specified thermal conductivity from Electrolube is 3.0 W/(m K). however, the chosen conductivity is set at 1.5 since lower conductivities are also found at various manufacturers and different materials. A lower value means that the model will not be idealised, and offers more realistic results. The heat capacity is set at a value of 1100 J/(kg K), which is a typical value for silicone rubber [4].

The specific heat capacity of the lithium-ion battery cell is estimated at 670 J/(kg K) based on research performed by Abdul-Quadir et al. [1]. They determined the specific heat capacity of a 40 Ah lithium-ion pouch cell from Kokam. It is therefore assumed that the same chemistry and materials have been used, thus leading to the same specific heat capacity for the larger cell from Kokam. However, the specific heat capacity could potentially be higher. Doh et al. [22] analysed a 104 Ah NMC prismatic pouch cell having an average specific heat capacity of 1020 J/(kg K). The thermal conductivity of the battery cell is unknown. However, it is also unknown to what extend heat is generated at a specific internal location. Since the pouch is made of aluminium, it is assumed that the heat dissipates sufficiently to assume a uniform temperature distribution.

It can be concluded that the air has a relatively small heat capacity compared to the other objects. This means that the air has little influence on the thermal inertia of the model, meaning that hardly any thermal energy will be absorbed by the air surrounding the cells inside the module. The thermally conductive filler however has a high heat capacity of 4454 J/K. The filler has therefore a large influence on the thermal inertia of the module. The largest heat capacity is however realised by the 7 cells, having a combined heat capacity of 19698 J/K. Therefore the thermal inertia of the module will be governed by the battery cells. The heat capacity of the air in the module will be neglected, meaning that air will only serve as a medium for heat transfer.

10.3. Conduction

Heat conduction is the transfer of energy through direct contact. Conduction is most significant within solids, whereas liquids and gasses are less conductive. Conduction occurs through vibrating atoms and molecules interacting with neighbouring atoms and molecules [77]. Fourier's law of heat conduction states that the heat flux is proportional to the temperature gradient. The temperature varies therefore linearly through the thickness of the material. The degree of conduction is strongly dependent on the thermal conductivity k [W/(m K)] of the material and the thickness of the material L [m]. A higher thermal conductivity leads to a higher heat flux, whereas a thicker material leads to a lower heat flux, providing more resistance to the transfer of energy. The general formula for conduction is provided in equation 10.3 [77]:

$$\dot{Q}_{cond} = \frac{kA}{L}(T_1 - T_2) \tag{10.3}$$

$$h_{cond} = \frac{k}{L} \tag{10.4}$$

Where $\dot{Q}_{cond}$ is the heat flow by conduction [W], A is the conducting area [m^2], and T_1 and T_2 are the hot and cold surface temperatures [K]. Typically a conductive heat transfer coefficient can be determined indicated by equation 10.4, having the unit [W/(m^{2}K)]. Typical thermal conductivity values of the implemented materials in the battery module have been given in table 10.1. The heat transfer coefficients can be calculated for the thermally conductive filler with a thickness of 20 mm and the aluminium casing with a thickness of 3 mm, as can be seen in figure 10.2. For the filler: $h_{cond} = 1.5/0.02 = 75$ W/(m^{2}K). For the casing: $h_{cond} = 168/0.003 = 56$ kW/(m^{2}K). Both material provide therefore a high transfer of heat due to their high thermal conductivity.

10.4. Natural convection

Convection describes the heat transfer between a surface to a moving fluid. Convection can either be forced or natural. An example of forced convection is a liquid flowing through a pipe. Natural convection is driven by buoyancy forces due to the difference in density, such as air warming up and rising through a radiator. The flow for forced and natural convection can be both laminar and turbulent. The general formula for convective heat transfer is given by equation 10.5:

$$\dot{Q}_{conv} = \bar{h}_c A(T_s - T_e) \tag{10.5}$$

Where $\bar{h}_c$ is the average convective heat transfer coefficient [W/(m^{2}K)], A the area of the surface [m^2], and T_s and T_e the surface temperature and the fluid temperature respectively [K]. The heat transfer coefficient $\bar{h}_c$ is usually a function of the thermal conductivity k [W/(m K)], a characteristic length [m], and the average Nusselt number $\overline{Nu}$ [-], shown in equation 10.6. The Nusselt number may be viewed as a dimensionless heat transfer coefficient, indicating the ratio between convective and conductive heat transfer [77]. The Nusselt number has a lower limit of 1, indicating pure conduction.

$$\bar{h}_{conv} = \frac{k}{L}\overline{Nu} \tag{10.6}$$

10.4.1. Internal natural convection

Natural convection can either occur internally or externally. In the case of a lithium-ion battery module, layers of air exist between cells surfaces and between the cell and the casing. The heat transfer

through these air layers can be characterised by internal natural convection. Other examples of internal convection are for instance hollow walls or double-glazed windows. For convection to occur, an internal flow is needed. If the temperature difference is lower than the critical temperature, the fluid becomes unstable and starts flowing. This causes the transfer of heat to be caused by conduction only [77]. The criterion for instability and the onset of cellular convection is given by the Raleigh number according to equation 10.7. Since there is no characteristic velocity, the Reynolds number does not play a role. The Raleigh number is a function of the Grashof number and the Prandtl number.

$$Ra_L = Gr_L \cdot Pr = \frac{g\beta(T_H - T_C)L^3}{\nu^2} \cdot Pr = 1708 \tag{10.7}$$

where:

- T_h = temperature of the hot surface [K]
- T_c = temperature of the cold surface [K]
- g = gravitational acceleration [m/s^2]
- β = volumetric coefficient of expansion [1/K] (equal to $1/T_{avg}$ for an ideal gas)
- L = spacing between the two plates [m]
- ν = kinematic viscosity [m^2/s]
- Pr = Prandtl number [-]. For air equal to 0.69 between 150-600 K [77]

Note that T_h and T_c now represent the hot and cold temperatures of the two surfaces that contain the air instead of the average fluid temperature as was the case in equation 10.5. For a fluid contained between two parallel vertical plates at different temperatures, circulation will occur for any Raleigh number above 0. However, for $Ra_L < 10^3$, heat transfer is essentially by pure conduction. ElSherbiny et al. [28] have recommended correlations for the heat transfer across thin air layers between two vertical plates (equation 10.8).

$$\begin{aligned}
\overline{Nu}_L &= \max\{Nu_1, Nu_2, Nu_3\} \\
Nu_1 &= 0.0605 Ra_L^{1/3} \\
Nu_2 &= \left[1 + \left(\frac{0.104 Ra_L^{0.293}}{1 + (6310/Ra_L)^{1.36}}\right)^3\right]^{1/3} \\
Nu_3 &= 0.242\left(\frac{Ra_L}{H/L}\right)^{0.272}
\end{aligned} \tag{10.8}$$

Where H is the height of the air layer [m] and L the thickness of the air layer [m]. The correlations are valid for $10^3 < Ra_L < 10^7$ and for an aspect ratio of $H/L > 10$. For $Ra_L \leq 10^3, \overline{Nu}_L = 1$. In terms of the height of the currently selected battery cell, equation 10.8 holds for a maximum air layer of 3.27 cm. The convective heat transfer coefficient has been plotted in figure 10.3 between 1 mm and 3 cm. The implemented temperatures are $T_h = 40$°C and $T_c = 20$°C. What can be seen in figures 10.3a and 10.3b is that for a maximum air layer of 14.2 mm conduction predominates. Only after a thickness of 14.2 mm convection starts to influence the heat transfer coefficient, although minimal compared to the influence of conduction. The convective heat transfer coefficient from cell to cell is 8.8 W/(m^{2}K) at a distance of 3 mm and between cell to module 2 W/(m^{2}K) at a distance of 20 mm.

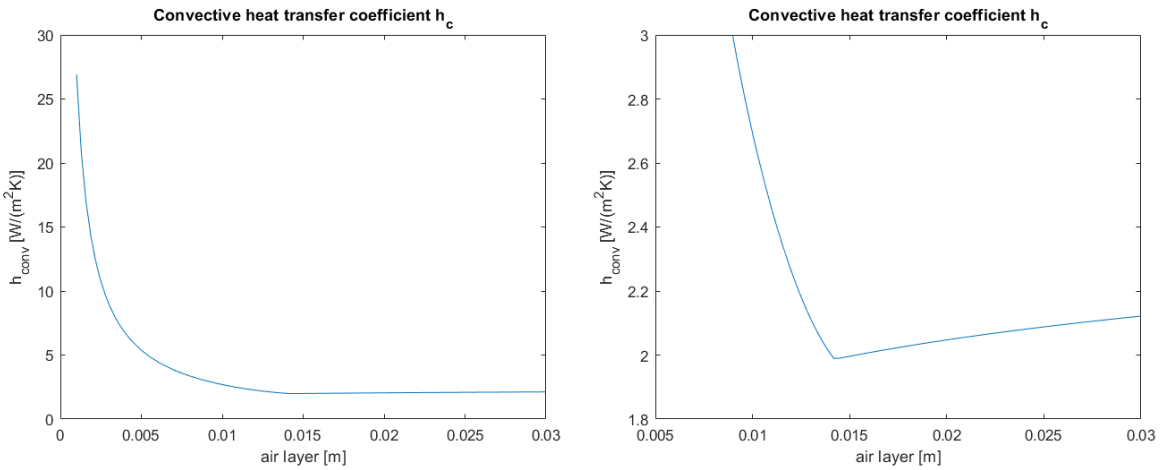

(a) h_c displayed between 0 and 3 cm

(b) h_c enlarged at critical point

Figure 10.3: Convective heat transfer coefficient for a thin air layer, typically cell-air-cell or cell-air-casing

10.4.2. External natural convection

External natural convection occurs at the surfaces of the battery module that are in contact with the ambient air. For the module described in section 10.2, the front casing will be subjected to external natural convection. The front of the casing is assumed as a vertical plate. The Raleigh number is used to calculate the critical value for which the transition occurs from a laminar flow to a turbulent flow. The critical value is $Ra_L = 10^9$ [77]. Based on equation 10.7, a maximum plate temperature $T_h = 60$°C and an ambient temperature $T_c = 20$°C, the maximum height can be calculated for which the flow remains laminar. Equation 10.7 is rewritten to equation 10.9, where the characteristic length is the height of the module:

$$H_{max} = \sqrt[3]{\frac{Ra_L \nu^2}{g\beta(T_h - T_c)Pr}} = 0.68\ m \tag{10.9}$$

It can be concluded that natural convection remains laminar since the module height is 0.373 m. The maximum temperature T_h for which natural convection remains laminar can be calculated using the same equation. The maximum temperature equals $T_h = 395$°C, which is far beyond the operating temperature range. Churchill and Chu [16] defined the Nusselt number for laminar natural convection on a vertical plate shown in equation 10.10, where Ψ is a function of the Prandtl number as shown in equation 10.11.

$$\overline{Nu}_L = 0.68 + 0.670(Ra_L \Psi)^{1/4} \tag{10.10}$$

$$\Psi = \left[1 + \left(\frac{0.492}{Pr}\right)^{9/16}\right]^{-16/9} \tag{10.11}$$

For analytical purposes, the convective heat transfer coefficient has been plotted in figure 10.4 for three specific cases of convection. Those cases are cell to cell convection (3 mm), cell to casing convection (2 cm) and casing to ambient convection. T_c is determined at 20°C, whereas the T_h is the variable surface temperature of the cell, cell and casing respectively. It can be concluded that the heat transfer coefficient between cell to cell is the highest, followed by the casing to ambient coefficient, and finally the cell to casing coefficient. Inside the module, the heat from the cells will be transferred via the cells to the front casing, where external natural convection occurs. This means that the heat flow is limited by the cell-casing convection. The heat transfer coefficient are however much lower compared to the conductive heat transfer coefficients stated in section 10.3 (filler: 75 W/(m^{2}K), casing: 56 kW/(m^{2}K)). This means that cooling through the front casing will be governed by the cell-casing convection, whereas the bottom casing cooling will be governed by the conductive heat transfer coefficient of the filler.

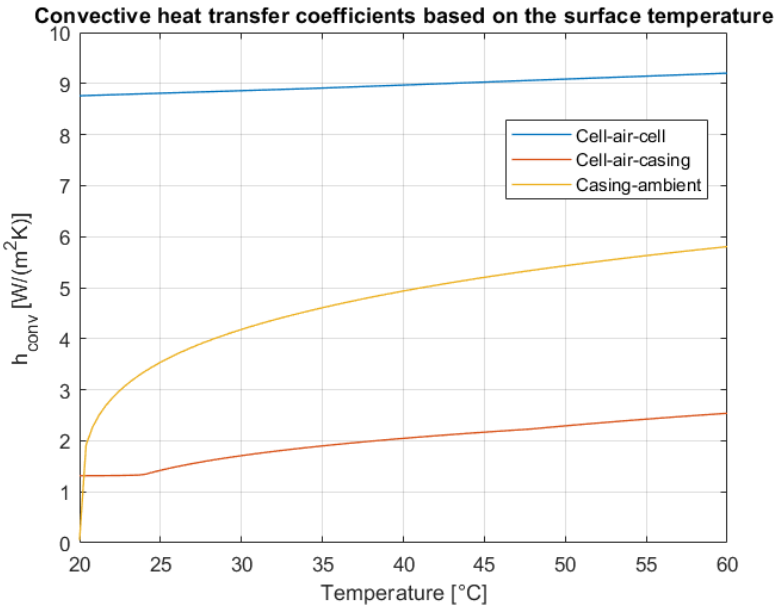

Figure 10.4: Heat transfer coefficients for cell-cell, cell-casing and casing-ambient convection

10.5. Radiation

Thermal radiation is a form of heat transfer based on electromagnetic radiation. Where conduction and convection require a medium for heat transfer to occur, radiation does not. Radiation can therefore occur in a vacuum. Every object with a temperature above absolute zero emits radiation [77]. Examples of radiation are for instance the heat experienced from a fire or sunlight reaching the earth and providing energy. Thermal radiation can both be absorbed and reflected. A black surface is defined as an object that emits and absorbs the maximum theoretical heat flux. Objects are commonly defined as gray objects, meaning that they emit and absorb a fraction of a theoretical black body. The fraction that is not absorbed is reflected. The fraction of the blackbody emissive power is called the emittance or emissivity (ϵ), which is a dimensionless number between 0 and 1 [77]. The emittance varies rather weakly with temperature, so it is convenient to assume the emittance as a constant value.

The radiative heat flux depends on the geometry of the two objects. Not all of the emitted radiation will be intercepted by the other object. A shape factor is therefore introduced (F_{12}), defining the fraction of radiation that is received by the other object. The total radiation heat transfer is therefore a function of the area of the emitting object, the shape factor between the two objects, the emittance of both objects and the temperatures of both objects. A general formula for thermal radiation is given by equation 10.12.

$$\dot{Q}_{rad} = A_1 \epsilon_1 F_{12} \sigma \left(T_1^4 - T_2^4\right) \tag{10.12}$$

Where:

- A_1 = radiating area of material 1 [m^2]
- ϵ_1 = emissivity of material 1 [-]
- F_{12} = shape factor between area 1 and area 2 [-]
- σ = Stefan-Boltzmann constant of $5.67 \cdot 10^{-8}$ [W/(m^{2}K^4)]
- T_1 = temperature of material 1 [K]
- T_2 = temperature of material 2 [K]

However, the general formula for thermal radiation defines the second object as a black body, absorbing all emitted radiation from the first object. If the second object is a gray surface, a fraction of the received radiation will be reflected back to object 1. Therefore a new formulation is needed where both emissivity factors are taken into account, as well as the areas of both surfaces and the shape factor.

Mills [77] has formulated this relationship according to the *Energy Balance Method*, based on the conservation of energy. The same result is obtained by implementing the electrical network analogy. The shape factor and both gray surfaces are represented by thermal resistances in series [77]. The new formulation for radiative heat transfer between two objects is given by equation 10.13. A radiative heat transfer coefficient is formulated according to equation 10.14.

$$\dot{Q}_{12} = \frac{1}{\frac{1-\epsilon_1}{\epsilon_1 A_1} + \frac{1}{A_1 F_{12}} + \frac{1-\epsilon_2}{\epsilon_2 A_2}} \cdot \sigma \left(T_1^4 - T_2^4\right) \tag{10.13}$$

$$h_{rad} = \frac{\dot{Q}_{12}}{A_1(T_1 - T_2)} = \frac{1}{\frac{1-\epsilon_1}{\epsilon_1 A_1} + \frac{1}{A_1 F_{12}} + \frac{1-\epsilon_2}{\epsilon_2 A_2}} \cdot \frac{\sigma \left(T_1^4 - T_2^4\right)}{A_1(T_1 - T_2)} \tag{10.14}$$

10.5.1. Shape factor

The shape factors have to be determined based on the module geometry described in section 10.2. The cells are represented by cuboids, from which each side is represented by a rectangle. The module casing can be represented by multiple rectangles as well. Therefore two shape factors have to be determined. The first shape factor concerns cell to cell radiation and the second shape factor concerns the cell to module radiation. It is thereby assumed that the cell always has a higher temperature than the casing. First the shape factor will be determined from cell to cell, where L is the spacing between the cells and W and H are the width and height of the cell. The formula for the shape factor of two opposite rectangles is given in equation 10.15 [77]. The shape factor has been plotted for a spacing between 0 and 10 cm based on the dimensions of the battery cell in figure 10.5.

$$F_{12} = \frac{1}{\pi x y}\left[\ln \frac{x_1^2 y_1^2}{x_1^2 + y_1^2 - 1} + 2x\left(y_1 \arctan \frac{x}{y_1} - \arctan x\right) + 2y\left(x_1 \arctan \frac{y}{x_1} - \arctan y\right)\right] \tag{10.15}$$

$$\text{with } x = \frac{W}{L},\ y = \frac{H}{L},\ x_1 = \sqrt{1 + x^2} \text{ and } y_1 = \sqrt{1 + y^2}$$

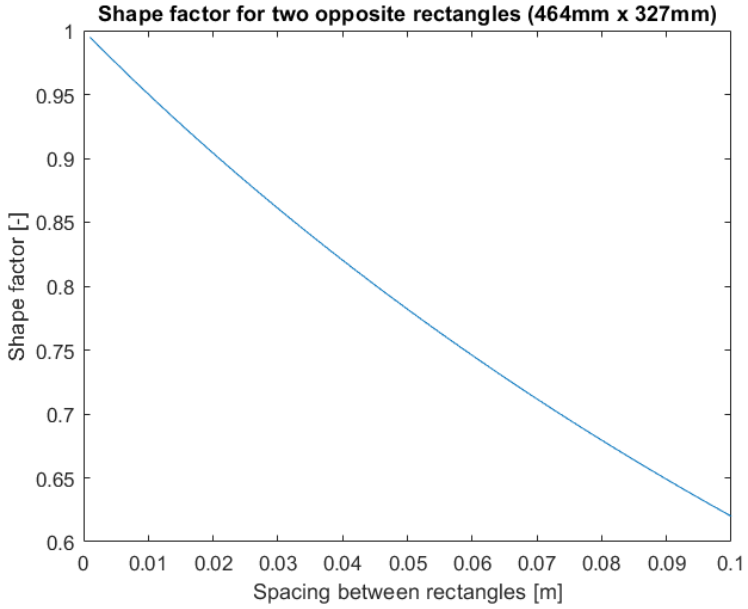

Figure 10.5: Shape factor for two opposite cells between 0 and 10 cm

Based on figure 10.5, it can be concluded that the shape factor decreases significantly with an increase in spacing. Note that the battery spacing in the module is only 3 mm. This results in a shape factor of 0.9846. A shape factor of 1 will be assumed for the radiation between the battery cells, meaning that the casing will not receive any radiation from the opposite facing cell sides. However, the small sides of the battery cell will radiate towards the module casing. Since the surface area of the module casing is larger than the area of the side of the cell, a shape factor of 1 is chosen. This means that all radiation from the sides of the cell is radiated onto the module casing. The radiative heat transfer is still dependent on the emissivity of the materials. The cell's pouch material and the casing material are assumed to be manufactured from ionised aluminium. For ionised aluminium, an emissivity of 0.8 has been selected [77]. Based on an emissivity of 0.8 and a shape factor of 1, the radiative heat transfer coefficient can be calculated with equation 10.13. The selected temperature of the hot surface varies between 20°C and 60°C and the cold surface is kept constant at 20°C. What can be concluded is that the heat transfer coefficient varies between a value of 3.8 and 4.66 W/(m^{2}K).

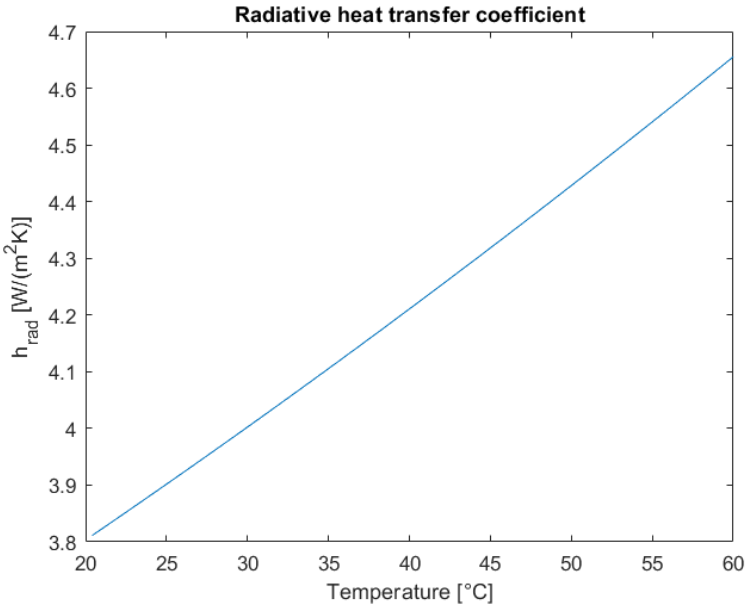

Figure 10.6: Radiative heat transfer coefficient between two aluminium surfaces implementing a shape factor of 1

10.5.2. Comparison of conduction, convection & radiation

The heat transfer coefficient shown in figure 10.6 is in the same range as the internal natural convective heat transfer coefficient described in section 10.4. This means that both radiation and convection are of equal importance in the thermal model. A comparison can be made in terms of conduction, convection and radiation based on the heat transfer coefficient. The heat transfer coefficient for the filler material is equal to 75 W/(m^{2}K), as explained in section 10.3. A comparison of the heat transfer coefficients for the three forms of heat transfer is depicted in figure 10.7. If all three forms of heat transfer would occur simultaneously, 89% can be attributed to conduction. 5% can be attributed to convection, and 6% to radiation. The contribution of conduction is close to nine times as much as convection and radiation combined. Conduction can thus be seen as the most significant form of heat transfer to dissipate the generated heat in the module. The implications on module design is to increase the contact area of the cells and the module to increase heat dissipation in terms of conduction.

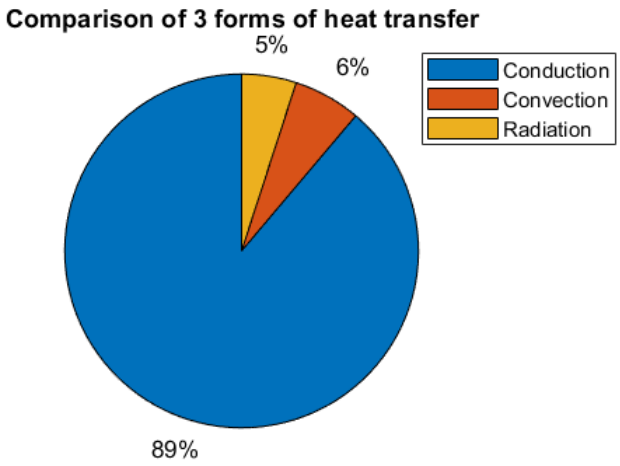

Figure 10.7: Comparison of the heat transfer coefficient of conduction, convection and radiation

10.6. Lumped Thermal Capacity Model

The thermal response of the battery module is modelled according to a Lumped Thermal Capacity approach. Each thermal object is assumed to have a uniform temperature distribution, meaning that there are no spatial temperature variations within the object. This assumption can be made if the internal resistance of the object is smaller than the external resistance across the boundary. This means that the internal heat conduction should be greater than the external forms of heat transfer to assume that the object has a uniform temperature. The assumption of negligible temperature gradients is based on the dimensionless Biot number. A Biot number smaller than 0.1 ensures that the core temperature differs no more than 5% from the surface temperature [77]. The Biot number is given by equation 10.16, where the internal resistance is divided by the external resistance. The internal resistance is given by conduction, while the external resistance is given by convection. When radiation is of significance, the sum of the convection and radiation heat transfer coefficients have to be taken into account.

$$Bi = \frac{Internal\,resistance}{External\,resistance} = \frac{L/(k \cdot A)}{1/(h_c \cdot A)} \tag{10.16}$$

Where L is typically the volume divided by the area where heat transfer occurs, but most often the thickness of the material: $L = V/A$. k is the thermal conductivity of the material and h_c the convective heat transfer coefficient. A is the area where heat transfer occurs.

10.6.1. Model implementation

Each thermal object can be seen as a node based on the lumped thermal capacity approach. Each node has a thermal mass, as well as a specific temperature. To determine the heat transfer between nodes subjected to multiple forms of heat transfer, the electrical resistance analogy can be implemented according to figure 10.8 and equation 10.17. Voltages represent temperatures, currents represent heat flows and electrical resistances represent thermal resistances [18]. The thermal resistance indicates at what rate heat can be transferred based on a temperature difference. Each heat transfer coefficient multiplied by its area can be viewed as a thermal resistance [K/W]. The resistances can be connected in series or parallel according to Kirchhoff's circuit laws [77]. The thermal resistances are formulated according to equation 10.18. The thermal resistances can be connected in series or in parallel according to equation 10.19 and equation 10.20. The total heat flow can then be calculated based on the total thermal resistance according to equation 10.17.

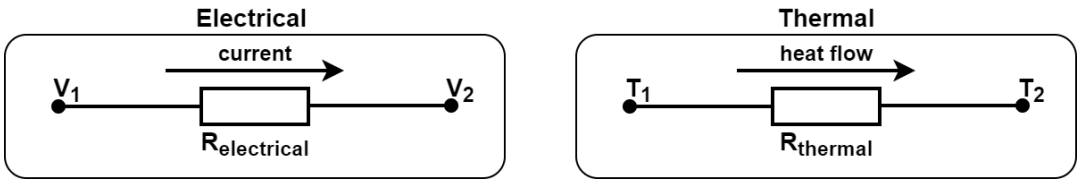

Figure 10.8: Electrical resistance analogy

$$I = \frac{U}{R} \quad \leftrightarrow \quad \dot{Q}_{tot} = \frac{\Delta T}{R_{tot}} \tag{10.17}$$

$$R_{cond} = \frac{L}{kA}, \quad R_{conv} = \frac{1}{h_{conv}A}, \quad R_{rad} = \frac{1}{h_{rad}A} \tag{10.18}$$

$$\text{Series} : R_{tot} = R_1 + R_2 + R_3 \tag{10.19}$$

$$\text{Parallel} : R_{tot} = \frac{1}{\frac{1}{R_1} + \frac{1}{R_2} + \frac{1}{R_3}} \tag{10.20}$$

The battery model is simulated implementing multiple nodes, where each node represents either a battery cell, one side of the casing or the thermally conductive filler. The model consists of 13 nodes. By implementing the electrical resistance analogy, a thermal network is created to calculate the heat flows and the temperatures within the battery module. For each cell, 6 heat flows are determined, as shown in figure 10.9. The cell generates its own heat. Additionally, the cell can receive heat from the adjacent cell to the right and transfer it to the cell on the left. The cell can also transfer heat to the left, right and bottom casing. As a result, the left, right and bottom casing can receive heat from the seven cells, whereas the front casing can only receive the heat from one cell directly.

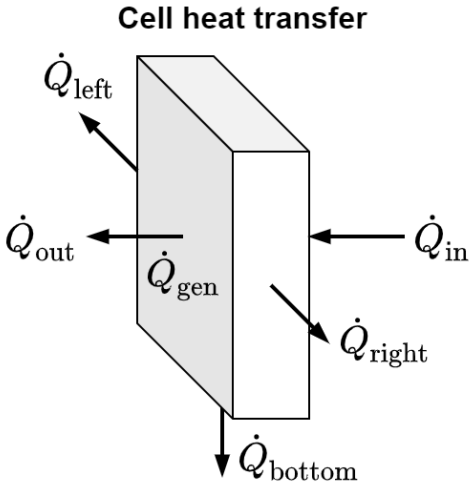

Figure 10.9: Modelled heat transfers for a battery cell

The implementation of the electrical analogy on a module level is visualised in figure 10.10. Only three cells are visualized in terms of simplicity, whereas the actual model consists of seven cells. Note that the figure is in 2D, while the actual model represents a module in 3D. It can be seen that each thermal object is represented by a node, meaning that each node has its own specific temperature. The left and right casing are represented by one node, while two nodes are modelled in reality. The network consists of parallel connections, as well as connections in series. The three forms of heat transfer are represented by thermal resistances as indicated in the legend. The ambient air temperature T_{amb} and the cooling water temperature T_{cool} serve as heat sinks in the model. A visualisation of the Simulink implementation can be visualised in appendix D.

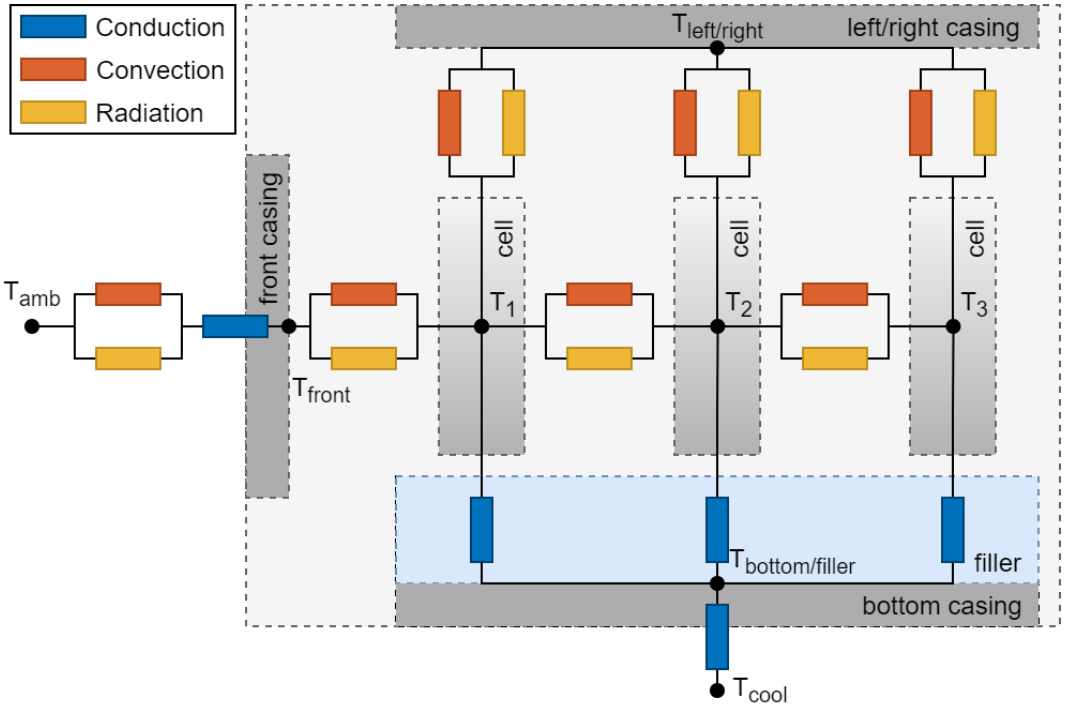

Figure 10.10: Electrical analogy of the battery module

10.6.2. Validity

The validity of the lumped thermal capacity approach has to be verified for each thermal object as described in section 10.2. The lumped thermal capacity approach is valid when the Biot number is smaller than 0.1. Instead of calculating the Biot number, the maximum allowable heat transfer coefficient can be calculated. This approach is chosen since heat transfer coefficients are not constant while discharging the battery module. Therefore it is chosen to analyze the maximum heat transfer coefficient to verify the lumped thermal capacity approach. Equation 10.16 has therefore been rewritten to equation 10.21.

$$h_{\max} = \frac{Bi \cdot k}{L} \tag{10.21}$$

Where $h_{\max}$ is the total maximum heat transfer coefficient of both radiation and convection. As explained in section 10.3, heat transfer is driven by a temperature difference. This means that for a thin plate, for example the module casing, there will always be a temperature gradient within the material for heat transfer to take place. This means that the temperature of the material in transverse direction is not uniform. The temperature distribution in longitudinal direction is most relevant to analyze. It is however assumed that in longitudinal direction the temperature is uniform as well for the casing. First of all, it was already assumed that the battery cell itself provides a uniform heat generation, as well as a uniform temperature distribution. Referring back to figure 10.2, it can be seen that the front casing, as well as the bottom casing, receive heat uniformly from the cells. Due to the relatively high thermal conductivity of the materials and the relatively small changes in temperature of the cells, it is assumed that the temperature can distribute itself uniformly within the bottom and front casing.

Based on equation 10.21, the maximum allowed heat transfer coefficient can be calculated for the casing. The maximum length in the module is the casing height. The maximum value of $h_{\max}$ is equal to 45.8 W/(m^{2}K). This is much larger than the sum of the maximum values of both convection and radiation for which the casing can receive heat, which is only $9 + 4.75 = 13.75$ W/(m^{2}K).

The conductive filler has however a much lower conductivity than the aluminium casing. For the filler, the maximum allowed $h_{\max}$ in transverse direction is 7.5 W/(m^{2}K). This seems more critical. However, heat will flow into the filler as well as out of the filler. This means that the temperature will rise minimally, meaning that the internal energy and temperature is close to a steady state. Therefore it is assumed that the filler has a conductivity high enough to reach a uniform temperature distribution in longitudinal direction.

10.7. Conclusion

This chapter describes the approach of formulating the thermal model of the battery module. The module geometry has been described based on an existing module from EST-Floattech. Liquid cooling through the bottom casing has been selected as a measure of cooling. Liquid cooling is effective in removing larger amounts of heat with relatively lower flow rates compared to air cooling. Liquid cooling on a module level has a lower complexity compared to liquid cooling between the cells, as described in section 4.4.2. To dissipate the generated heat, a silicone filler has been selected to provide heat dissipation through the bottom of the casing, as well as serving as a damper for any shocks. The relevant thermal objects have been determined based on their relative heat capacity. As a conclusion, the contribution of air has been neglected, only serving as a medium for heat transfer. Based on the determined geometry, heat transfer coefficients have been determined in terms of conduction, convection and radiation. On average, 89% can be attributed to conduction. 5% and 6% can be attributed to convection and radiation respectively. Conduction can thus be seen as the most significant form of heat transfer to dissipate the generated heat in the module.

An implications on module design is to increase the heat dissipation in the module by maximising the contact area of the cells. Convection and radiation therefore serve as a limiting factor in terms of heat transfer inside the battery module. The thermal properties of the filler material and the thickness of the filler have a large effect on the conductivity. The selected filler material has therefore a significant influence on the thermal behaviour of the module. To model the heat transfer of a lithium-ion battery module, a lumped thermal capacity approach has been implemented. The electrical analogy has been implemented in the thermal model to determine heat transfer rates simultaneously between cells within the module.

11

Results

This chapter provides the results for the simulated battery module described in chapter 10. The thermal behaviour of the battery module has been simulated for three operational profiles that can typically be experienced on a diesel-electric submarine. Results have been obtained for each scenario with and without cooling implemented. Next a geometry analysis has been performed to identify the effects of varying dimensions in the module. Finally an analysis has been made regarding the effects of a thermal runaway to the other cells in the module.

11.1. Operational profiles

The thermal behaviour of the lithium-ion battery module is simulated for three operational profiles. A typical mission profile for a diesel-electric submarine can consist of a submerged sprint, open transit, covert transit and covert surveillance. Open transit is not considered in the results, since the submarine can sail on the diesel generators and electric motor without the need of batteries. The actual charge or discharge rates and the duration are typically dependent on the submarine design. Therefore a typical range of charge and discharge currents is provided in the results that can be expected for a typical diesel-electric submarine. Two temperature limits are denoted in the following results. First of all a temperature limit of 30°C is indicated. A relatively longer life expectancy can be realised for a cell temperature between 20°C and 30°C [97]. A second temperature limit is indicated at 55°C. This is the cell's temperature limit stated by the manufacturer. Exceeding this limit significantly increases the risk of initiating the first phase of a thermal runaway, as described in chapter 4.

Submerged sprint

A submerged sprint means the submarine sails submerged at maximum speed. A submerged sprint can be initiated during an attack or when approaching convoys needs to be evaded. During a submerged sprint only a single discharge is available, since the submarine has to resurface or snort to recharge the battery system. The C-rate can be determined based on the power drawn by the main electric motor and the total battery capacity.

Covert transit

A covert transit typically occurs when a submarine travels to or from a desired location, having the consequence that the batteries are consecutively cycled. During transit, the submarine sails submerged at a constant speed and constant C-rate. Depending on operational circumstances, diesel-electric submarines typically charge the batteries at a lower sailing speed compared to the submerged speed to reduce the signature based on the wake of the masts during snorting. The purpose of this model is not to find the optimal indiscretion ratios, but to simulate the thermal limitations. Therefore the discharge rate is equal to the charge rate during a covert transit scenario.

Covert surveillance
Covert surveillance typically occurs at the operational area. The goal is to stay submerged as long as possible. This can be obtained by relatively low discharge rates. The batteries should be recharged as quickly as possible to reduce the time exposed at the surface. A ratio can be defined between the time at the surface (t_{snort}) and the submerged time (t_{sub}). This is called the Indiscretion Ratio (IR), defined according to equation 11.1 [13].

$$IR = \frac{t_{snort}}{t_{snort} + t_{sub}} \tag{11.1}$$

11.1.1. Submerged sprint

The thermal behaviour of the battery module has been simulated for a submerged sprint. A single discharge between 0.1C and 1.0C has been simulated, which are discharge rates that can be expected for a diesel-electric submarine. Figure 11.1 shows the cell temperatures for various discharge rates while no forced cooling is applied. The top half of the figure depicts the temperatures of the 7 battery cells. The lower half depicts the heat transfer rates through the bottom and front casing. The bottom casing (continuous line) does not function as a heat sink since no cooling is applied. Only the front casing (dashed line) transfers heat to the surroundings in this figure. The module is discharged from 90% to 10% SOC, which are the applied capacity limits of the module. Once a SOC of 10% is reached, the module will be switched off causing the abrupt temperature variation visible in the figure. From figure 11.1 it can be concluded that the temperature increases with an increase in C-rate. The same conclusion could be draw based on chapter 9. However, it is important to note that no equilibrium temperature is reached within a full discharge. Secondly, the maximum temperature at a discharge rate of 1.0C reaches up to 47.9°C. This is near the maximum discharge temperature of 55°C stated by Kokam, increasing the probability of initiating the first phase of a thermal runaway. At a discharge rate of 0.1C the maximum temperature is 30.3°C.

To lower the temperatures during a submerged sprint, forced cooling can be applied to the bottom casing. Figure 11.2 shows the cell temperatures with forced cooling implemented. The bottom plate is kept at a constant temperature of 15°C by implementing liquid cooling. Importantly to note is that the temperature at 0.1C and 0.2C stabilizes on average and is kept below 25°C. The maximum temperature that is reached is 44.5°C at 1.0C and 22.0°at 0.1C. This means that the temperature reduction of this forced cooling method is minimal for high discharge rates (3.4°C decrease) but more effective for low discharge rates (8.3°C decrease). It an also be concluded that the variation in temperature between the cells decreased with forced cooling. The heat transfer through the bottom casing varies between 20W and 100W. Higher cooling rates can be realised through the bottom casing compared to the front casing.

Mass flow cooling liquid
To ensure that the bottom casing is kept at a constant temperature of 15°C, liquid cooling is implemented to dissipate the heat. A mass flow and inlet temperature colder than the plate temperature are needed to dissipate the heat. Klein Woud and Stapersma [47] formulated equations to relate the mass flow of the coolant and the inlet temperature to the transferred heat. The formulations are based on the principle of heat exchangers, where the heat exchange of the cooler is taken into consideration. The formulation is shown in equation 11.2:

$$\dot{m} = \frac{\dot{Q}}{c_p(T_{out} - T_{in})} = \frac{100}{4200 \cdot (15 - 13)} = 0.012\ kg/s \tag{11.2}$$

Water is selected as a coolant, with a specific heat capacity of 4200 J/(kg K) [77]. Based on the upcoming results, average cooling rates of 100 W need to be dissipated. Assuming an inlet temperature of 13°C and an outlet temperature of 15°C, the average fluid temperature is equal to 14°C, below the bottom casing temperature of 15°. Assuming an efficient heat exchanger, a mass flow rate of 0.012 kg/s is needed. Additionally, the mass flow rate can be increased or the inlet temperature can be lowered to increase the heat dissipation. A mass flow rate of 0.012 kg/s is equal to 0.72 L/min. If the bottom casing is cooled via a single pipe of 1 cm diameter, the fluid flow speed is typically 1.5 m/s. However, typically multiple pipes can run through a cooling plate simultaneously. If for instance 3 separate circuits are implemented, the flow speed is 0.5 m/s per pipe. The flow speed and efficiency is strongly dependent on the cooler design.

The cooling rate is dependent on many variables, such as the heat capacity of the coolant, the inlet temperature, the cooler efficiency and the mass flow rate. The effects of the cooler design on the module temperature are excluded from the scope of this research. The thermal model of the battery module can serve as a tool or starting point to analyse the cooler design and effectiveness in future research.

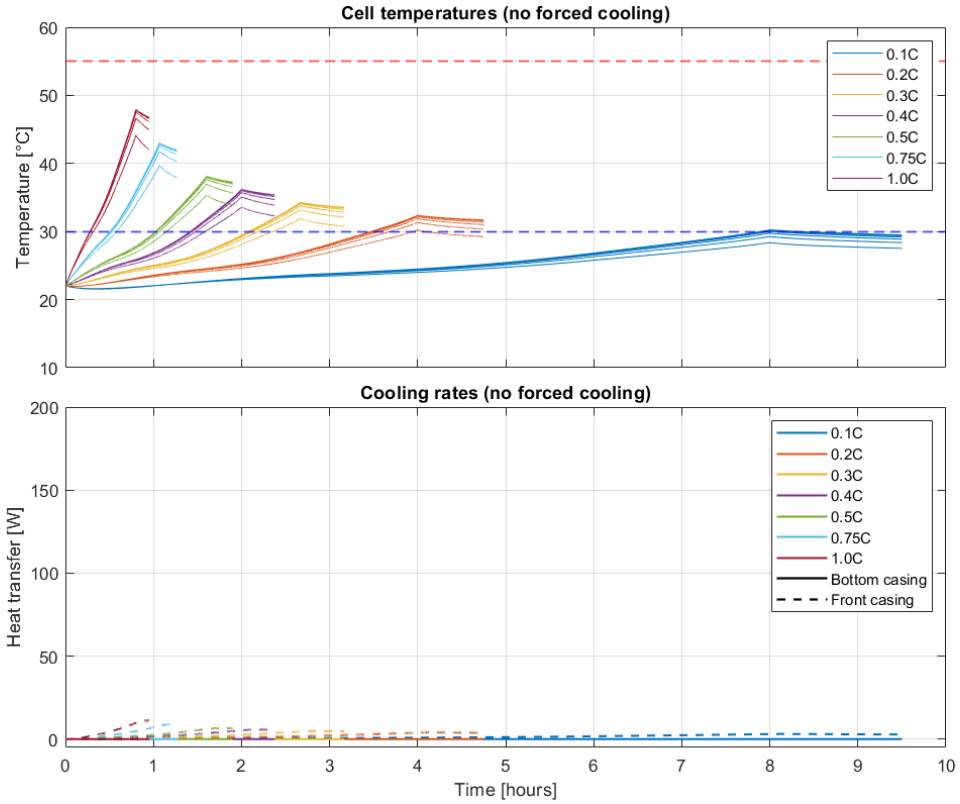

Figure 11.1: Submerged sprint: cell temperatures and cooling rates without forced cooling

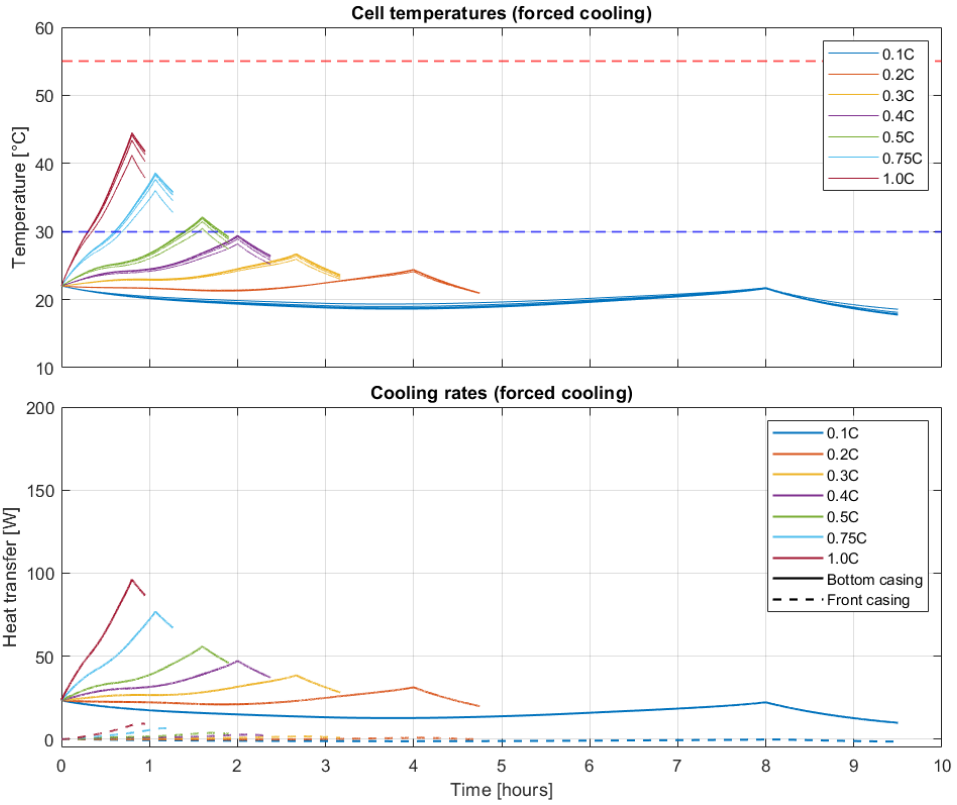

Figure 11.2: Submerged sprint: cell temperatures and cooling rates during various single discharges with forced cooling

11.1.2. Covert transit

A covert transit is simulated in the from of three consecutive cycles, which is assumed as a typical operation on a diesel-electric submarine. The three cycles are based on an equal charge and discharge currents ranging between 0.1C and 1.0C. Figure 11.3 shows the thermal behaviour of the module without forced cooling implemented. For C-rates above 0.3C, critical temperatures are reached causing failure of the cells. The temperature variation between cells increases as the C-rate increases. Only for a C-rate of 0.1C the cell temperatures are maintained at a maximum temperature of 35.8°C. C-rates are desirably limited to 0.1C without cooling to ensure safe operating temperatures. Temperatures are however exceeded for a longer life expectancy.

Figure 11.4 shows the thermal behaviour of a covert transit when cooling is enabled. It can be seen that temperatures are relatively stable for C-rates up to 0.5C. Since less heat is developed during the charging of the battery, more heat can be dissipated than is generated, having the consequence that the temperatures of the cells reach an equilibrium. For C-rates of 0.75C and 1.0C, cooling is still insufficient for consecutive cycles, where the temperature increases significantly with each cycle. At 1.0C, the maximum operating temperature of 55°C is exceeded. Temperatures reach up to 61.9°C, increasing the chance of a thermal runaway and causing permanent damage to the cells. It can therefore be concluded from the results that a typical module could be employed up to C-rates of 0.5C during a covert transit for at least three cycles. Maximum cooling rates that can achieved with the current module geometry reach up to 150 W.

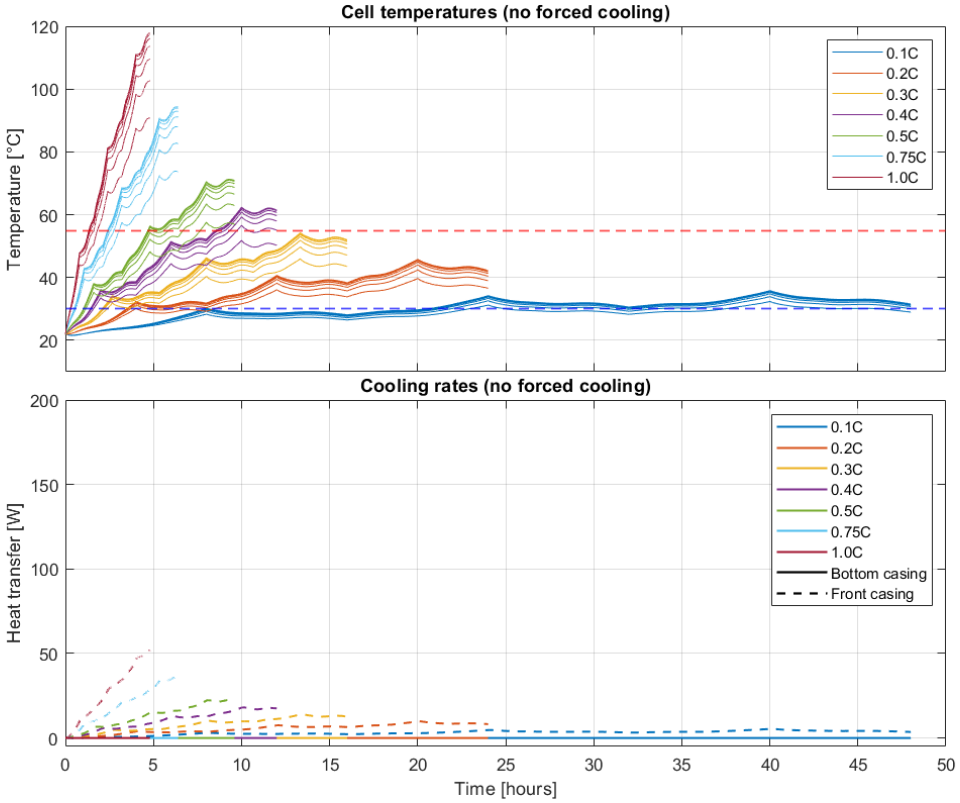

Figure 11.3: Covert transit: cell temperatures and cooling rates without forced cooling

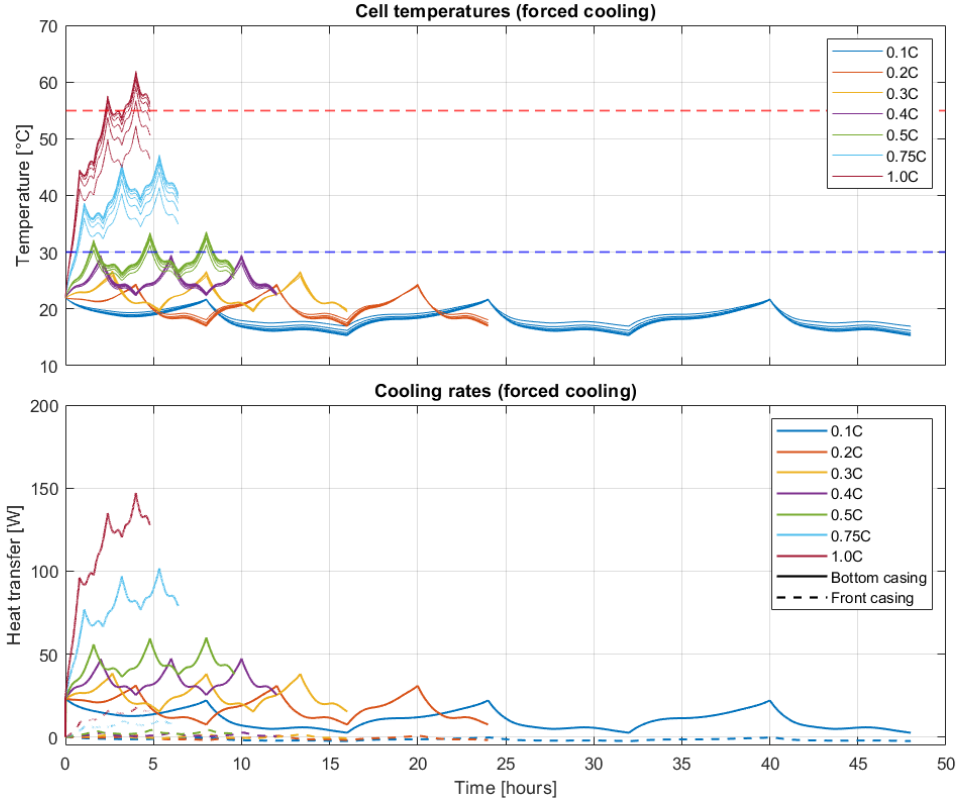

Figure 11.4: Covert transit: cell temperatures and cooling rates with forced cooling

11.1.3. Covert surveillance

A covert surveillance operation is simulated in the form of three consecutive cycles. A high indiscretion ratio is desired. As a consequence high charge currents and low discharge currents are desired. Therefore four simulations have been performed where the charge and discharge currents have been varied. The charge current is either 0.5C or 1.0C, while the discharge current is either 0.1C or 0.2C. The C-rates and indiscretion ratios can be seen in table 11.1. The indiscretion ratio varies between 9% and 29%, which are typical IR rates for diesel-electric submarines. To verify, the IR can typically range from 7% to 10% on patrol and 20% to 30% during transit [96]. Figure 11.5 shows the cells temperatures without forced cooling initiated. ”C” and ”D” mean charge and discharge respectively in the legend. It can be seen that for each scenario the 30°C boundary is crossed. However, only for a discharge rate of 0.1C and a charge rate of 0.5C the cells remain below the critical limit of 55°C. Moreover, significant temperature variations between the cells in the module are visible, potentially causing performance and lifetime variations.

Table 11.1: Modelled covert surveillance scenarios

#	**Discharge rate** [C]	**Charge rate** [C]	t_{sub} [h]	t_{snort} [h]	**IR**
1	0.1	0.5	8	1.6	0.17
2	0.2	0.5	4	1.6	0.29
3	0.1	1	8	0.8	0.09
4	0.2	1	4	0.8	0.17

Figure 11.6 shows the cell temperatures during a covert surveillance operation with cooling initiated. Important to note is that forced cooling is able to limit the temperature below the 30°C limit. Only during charging at 1.0C the temperature limit is exceeded for a minimal time. Based on the modelling results it can be concluded that for a typical covert surveillance operation cooling is needed if cell temperatures are desired below 30°C. Typical cooling rates vary between 30 W and 60 W.

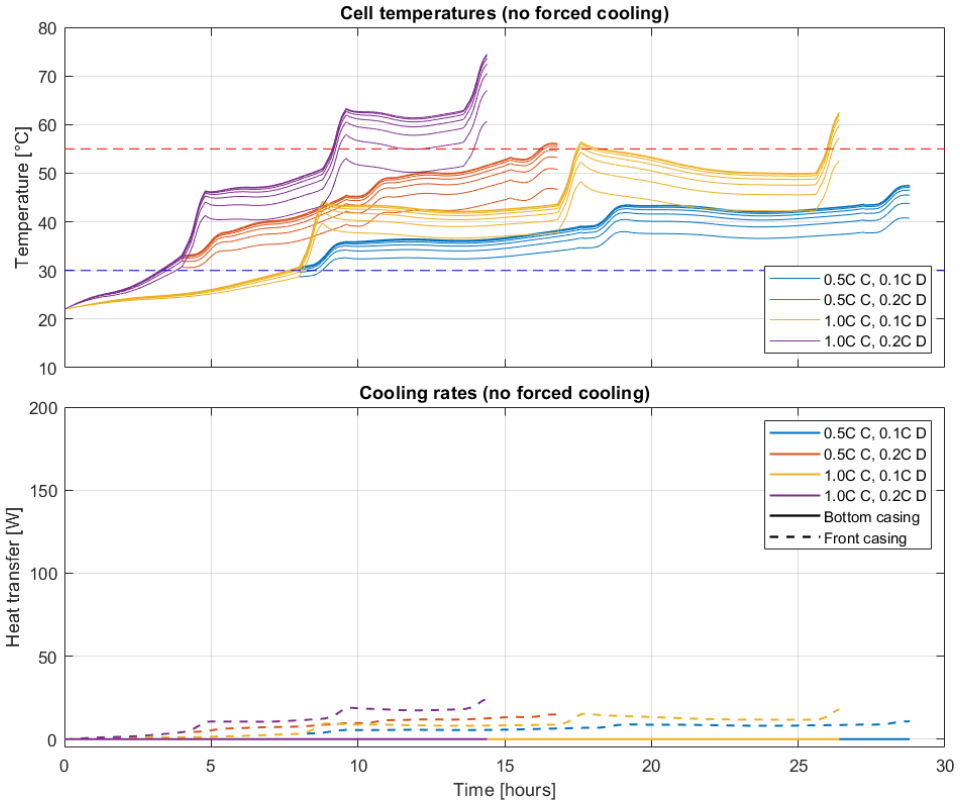

Figure 11.5: Covert surveillance: cell temperatures and cooling rates without forced cooling

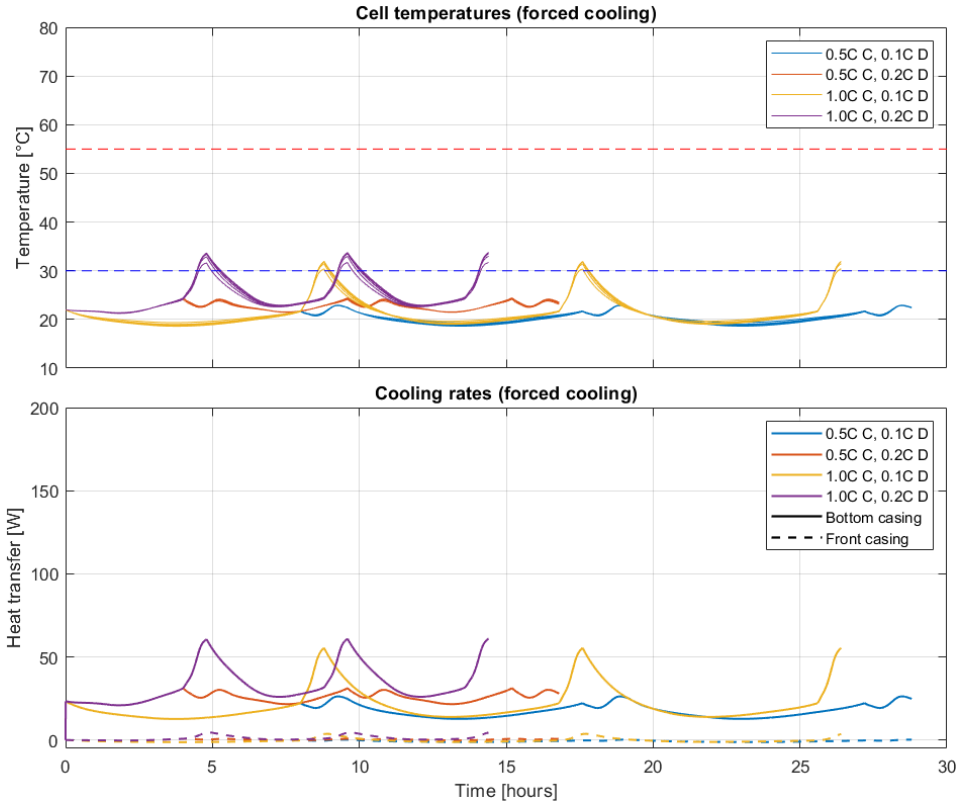

Figure 11.6: Covert surveillance: cell temperatures and cooling rates with forced cooling

11.2. Geometry optimisation

For analytic simplicity, the heat generation rate has been assumed at a constant value of 10 W for all cells. This reduces the fluctuations in temperature and heat transfer rates and ensures that the only influences in the results are caused by the changes in the geometry. Figure 11.7a shows the maximum cell temperatures for a variable cell to cell spacing. The spacing is varied between 20% and 180% of its initial value of 3 mm. What can be concluded is that the temperature variations between the cells increase as the spacing between the cells increases. Therefore it is desired to maintain this spacing as small as possible. However, a minimum spacing is needed between the cells in case of expansion of the cells.

Figure 11.7b shows the maximum cell temperatures for a variable cell to casing spacing. Most importantly is to conclude that the overall temperature decreases slightly for a minimal spacing. The temperature variations between the cells increase as well. The cell adjacent to the casing ensures more cooling from the front casing since higher heat transfer rates can be obtained due to a smaller air spacing.

The strongest influence on the maximum cell temperatures is realised by the filler thickness and the filler conductivity, as can be seen in figures 11.8a and 11.8b. A small filler thickness below 1 cm ensures a higher heat transfer so all generated heat can be dissipated almost instantly. The thickness is however limited by any excess material around the cell's edges, as well as a minimum thickness of the filler material to ensure as a shock absorber. The thermal conductivity is desired as high as possible to ensure a higher heat flow. The thickness of the module casing has no influence on the cell temperatures due to the high thermal conductivity of aluminium. Moreover, a minimal thickness is needed to provide robustness for the pouch cells. As described in section 3.2, pouch cells need an additional casing to satisfy a required level of robustness since their individual robustness is low.

The original module has an energy density of 209 Wh/kg and a specific energy of 135 Wh/kg. This is in the same range as the existing modules described in section 7.2 and table 7.1. Based on the

optimised geometry where the cell to cell spacing is minimised to 1 mm and the filler thickness to 1 cm, the energy density an specific energy have increased. The results are shown in table 11.2. The energy density has mainly increased due to the minimised cell spacing and filler thickness, resulting in an improvement of 12.9%. Based on the minimised filler thickness, the total filler weight has decreased, as well as the specific energy. This resulted in an improvement of 6.7%. Moreover, it can be concluded that by decreasing the volume and mass of the module, the thermal efficiency has increased. Based on the large amount of cells present on a diesel-electric submarine, a volumetric improvement of 6.7% per module can result in a significant amount of extra space for an entire battery system. Since the cell temperature remains relatively constant after the fourth cell in a row, a larger battery module can be developed resulting in a higher energy density and specific energy as well. Note that the described module does not include appendages such as a battery management system. Based on the auxiliary systems the energy density and specific energy can decrease.

Table 11.2: Optimised module in terms of energy density and specific energy

	Original	**Optimised**	**Improvement**
Specific energy [Wh/kg]	135	144	6.7%
Energy density [Wh/L]	209	236	12.9%

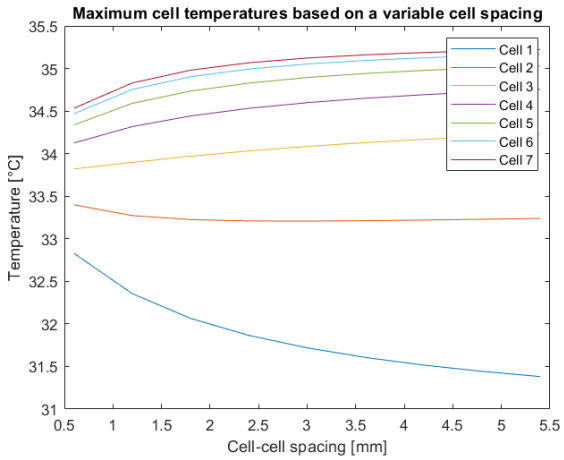

(a) Varying cell-cell spacing between 20% and 180%

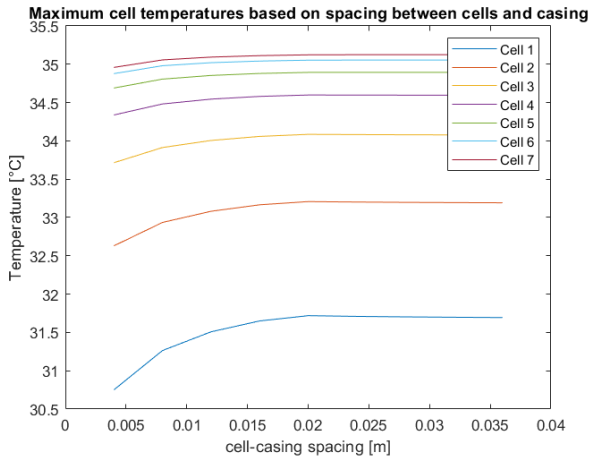

(b) Varying cell-casing spacing between 20% and 180%

Figure 11.7: Maximum cell temperatures based on the cell-cell spacing and the cell-casing spacing

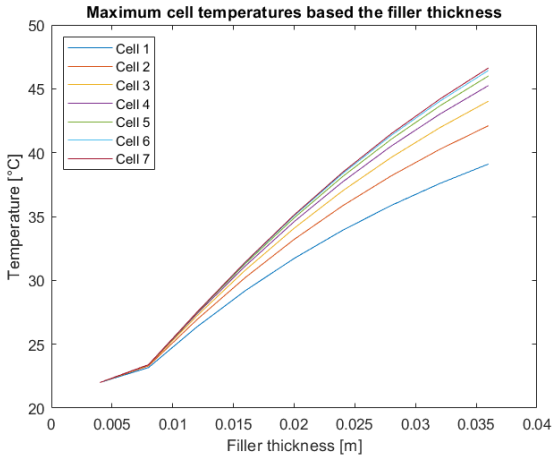

(a) Varying filler thickness between 20% and 180%

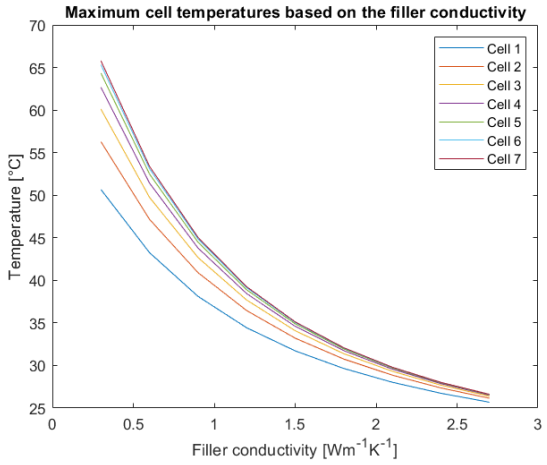

(b) Varying filler conductivity between 20% and 180%

Figure 11.8: Maximum cell temperatures based on the filler thickness and the filler conductivity

11.2.1. Results based on optimised geometry

Based on the previous section, optimised parameters regarding the module geometry have been obtained. The spacing between the cells is minimised to 1 mm to minimize the temperature difference between the cells and lower the maximum temperatures in the module. The spacing between the cells and the module is kept at 2 cm to provide enough space for the cells to expand, since the temperature reduction is minimal based on a varying cell-module spacing. The filler thickness is minimised as much as possible. Taking into account the space needed for excess material of the cells, the minimal thickness is set at 1 cm. Additionally the conductivity could be increased, but this is dependent on the manufacturer. Therefore the conductivity remains unchanged. Similarly, the cooling liquid temperature could be lowered. However, this is seen as an external factor and will not be taken into consideration.

Figure 11.9 shows the thermal behaviour of the optimised module based on a submerged sprint. The peak temperature during a 1.0C discharge has decreased from 44.5°C to 39.0°C. Up to a C-rate of 0.5C cell temperatures remain below 30°C. As a consequence, the cooling rates have increased up to 150 W. Figure 11.10 shows the thermal behaviour for a covert transit. Based on the data it can be concluded that for C-rates up to 0.5C temperatures remain below 30°C. At a C-rate of 1.0C temperatures reach a maximum of 43.8°C. This is a significant improvement where temperatures remain within the operating range of 55°C. Moreover, temperature variations between cells have decreased significantly, minimising discrepancies in performance such as cycle life. Based on the results it can be concluded that the optimised module could be employed for C-rates up to 0.5C without temperatures exceeding 30°C. Alternatively, C-rates up to 1.0C can be realised if higher operating temperatures are accepted. Cooling rates reach up to 185 W based on the optimised geometry. Finally figure 11.11 shows the temperatures of the optimised module during a covert surveillance. It can be noted that temperatures do not exceed the 30°C boundary, and overall temperatures are slightly decreased. The improvements in temperature reduction are smaller compared to the covert transit profile. Cooling rates have increased up to peak values of 90 W.

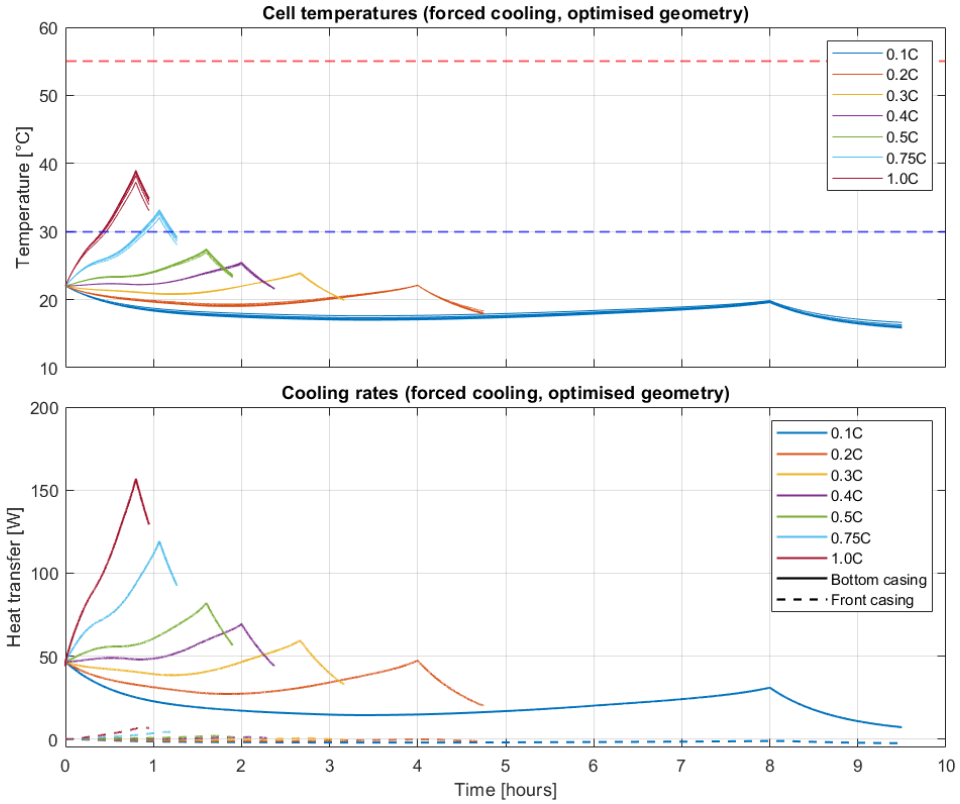

Figure 11.9: Optimised geometry, submerged sprint: cell temperatures and cooling rates with forced cooling

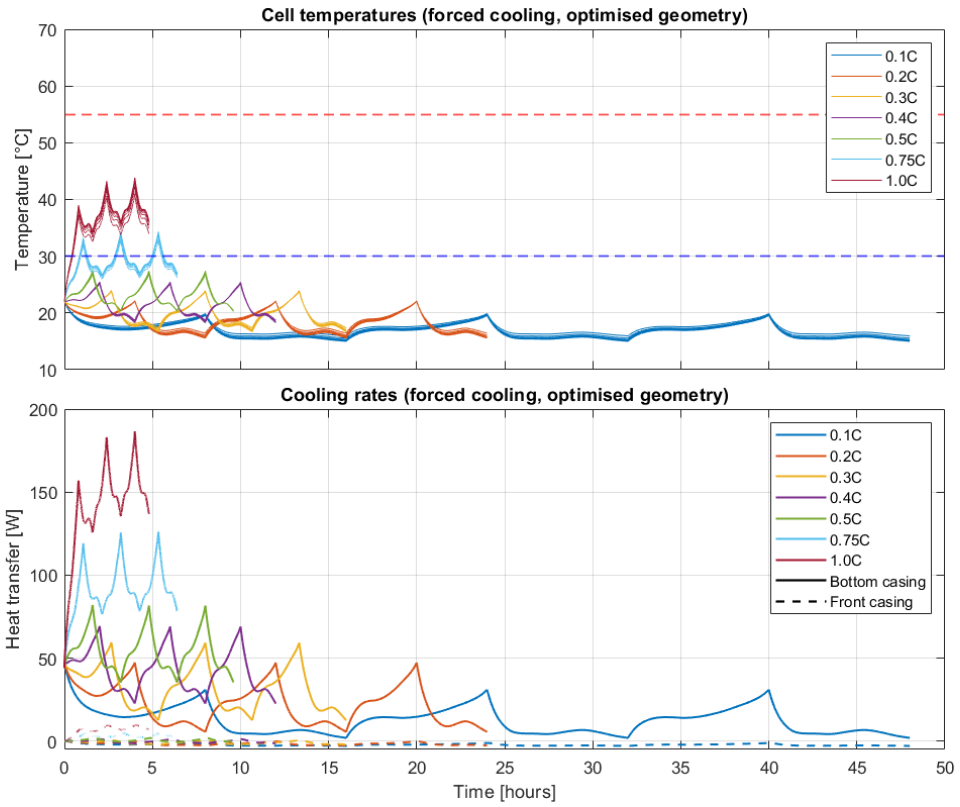

Figure 11.10: Optimised geometry, covert transit: cell temperatures and cooling rates with forced cooling

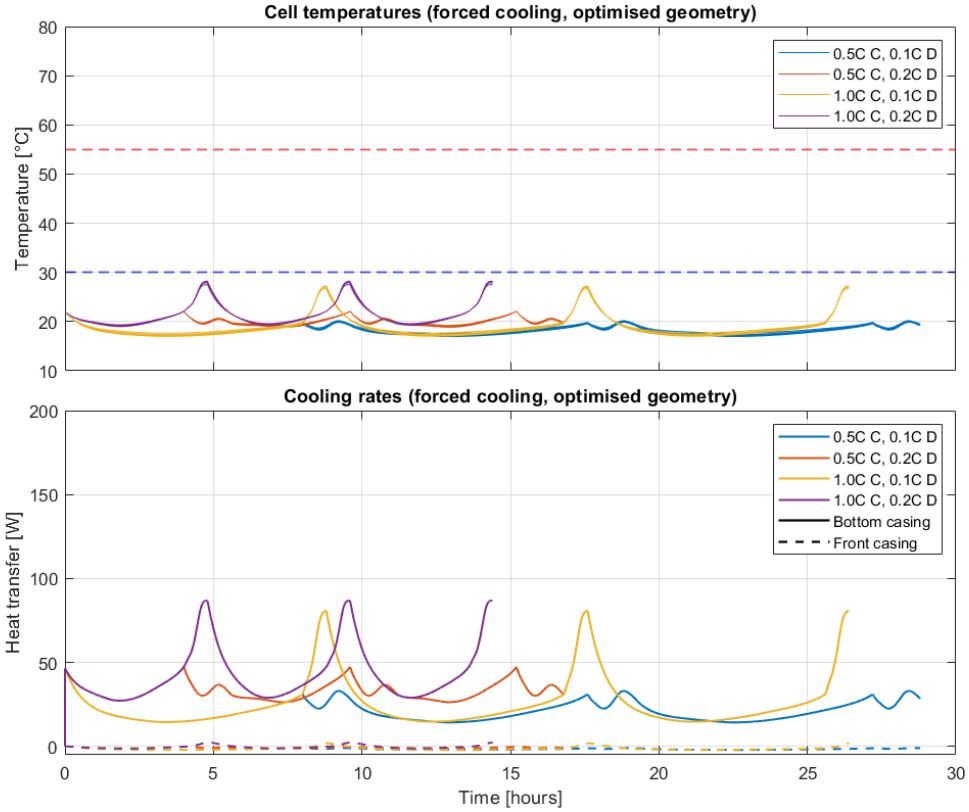

Figure 11.11: Optimised geometry, covert surveillance: cell temperatures and cooling rates with forced cooling

11.3. Overview results operational profiles

An overview of the obtained results is shown in figure 11.12. The figure shows the maximum cell temperatures that have been reached during each operational profile. During a submerged sprint, C-rates up to 1.0C can be sustained without cooling. The critical temperature limit at 55°C is not reached. If cooling is initiated, C-rates up to 0.4C (regular module) and 0.5C (optimised module) can be realised without exceeding the 30°C limit desired for a longer lifetime. For a covert transit scenario cooling is essential above C-rates of 0.3C. Otherwise the critical temperature limit is exceeded which results in an increased chance of a thermal runaway. With cooling initiated, C-rates up to 0.75C and 1.0C can be sustained for the regular module and optimised module respectively. Below the limit of 30°C only 0.4C and 0.5C can be sustained, similar to the submerged sprint. Finally the maximum temperatures during covert surveillance are depicted. Note that the horizontal axis correspond to the four different scenarios instead of a constant C-rate. It can be concluded that cooling is necessary for three of the four surveillance scenario's. Moreover, the optimised geometry has the implication that temperatures for each scenario are kept below 30°C.

It can be concluded that the effects of cooling are minimal for a submerged sprint. For covert transit and covert surveillance, cooling is of significance. Consecutive cycles are significantly limited in terms of C-rate. Therefore it is concluded that for the operational profile either low charge and discharge rates have to be accepted, or cooling has to be implemented to fulfill higher C-rate requirements.

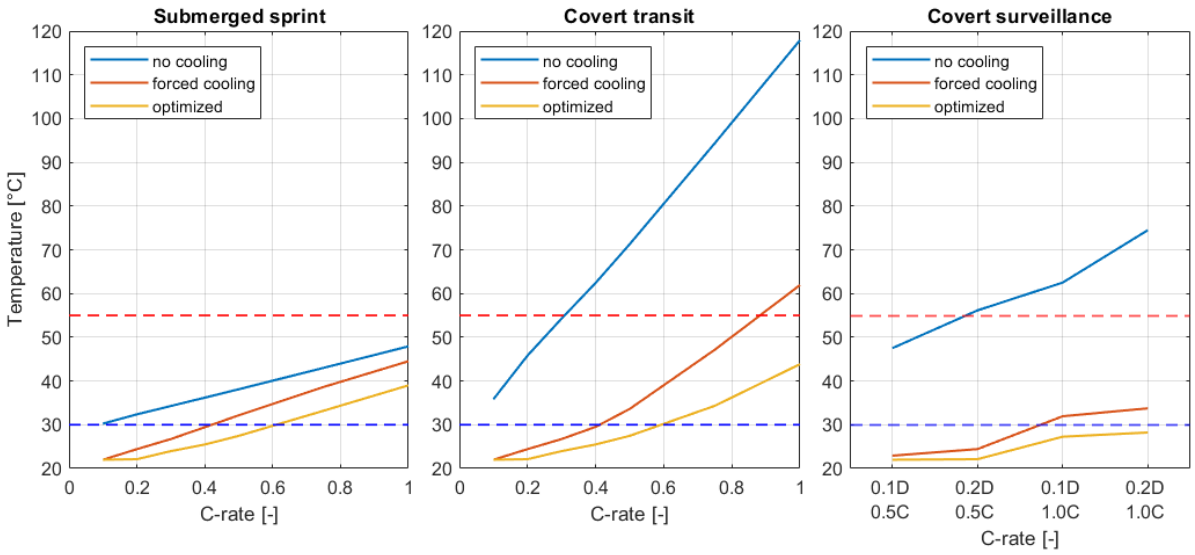

Figure 11.12: Comparison of maximum temperatures of the three operational profiles

11.4. Thermal runaway

As described in section 4.2, a thermal runaway event consists of four stages. First of all, the SEI layer decomposes (1). Next, the anode reacts with the electrolyte (2). This is followed by the separator melting (3). Finally the cathode reacts with the electrolyte (4). The thermal runaway is usually characterised by the fourth stage, where a large amount of heat is released. This can occur at a temperature of roughly 180°C. The event of the battery cell heating up to this point is usually caused by one of the failure mechanisms as described in section 4.1. The various failure modes that can initiate a thermal runaway will not be modelled. The thermal runaway profile will focus on the maximum temperature that is reached, the time it takes to reach that temperature and the heat that is generated during the event.

11.4.1. Thermal runaway profile

The thermal runaway profile has been based on several experimental researches. The mentioned researches all implement an NMC cell, which is the same chemistry as the battery cell from Kokam implemented in the model. Lithium-ion battery cells are commonly overheated to initiate a thermal runaway. Liao et al. [55] analysed multiple cylindrical cells of 2.4Ah. They concluded that the maximum temperature during a thermal runaway decreases with a decrease in the SOC of the cell, since the internal energy decreases. Liu et al. [60] have analysed a prismatic 38 Ah NMC cell at a SOC of 100%. They concluded that within 40 seconds, a maximum surface temperature of 577°C is reached (starting at roughly 80°C). Feng et al. [34] concluded that a 25 Ah prismatic cell reached a peak temperature of 751°C. DNV GL [20] overheated a 63 Ah NMC pouch cell. At 100% SOC, the onset temperature was approximated at 173°C and the maximum temperature was determined at 475°C. The time it took to reach its peak temperature was roughly 60 seconds. Besides overheating, they overcharged the cell, where a maximum temperature during the thermal runaway event was determined at 602°C. Table 11.3 shows an overview of several thermal runaway experiments performed on NMC cells.

Table 11.3: Maximum thermal runaway temperatures for various NMC cells

Research	**Capacity** [Ah]	**Cell design**	**Thermal runaway T_{max}** [°C]
DNV GL [20]	63	pouch	475
DNV GL [20]	63	pouch	602
Liu et al. [60]	38	prismatic	577
Feng et al. [34]	25	prismatic	751
Liao et al. [55]	2.4	cylindrical (18650)	883
Golubkov et al. [38]	1.5	cylindrical (18650)	678

From table 11.3, a trend can be seen that the maximum temperature during a thermal runaway decreases with an increase in capacity. Based on these results, a thermal runaway profile will be constructed for the 200 Ah NMC pouch cell implemented in the model. A thermal runaway will be simulated for a cell with a SOC of 100%. Based on table 11.3 and section 4.2, a thermal runaway onset temperature of 180°C is selected. The time that is needed to reach that temperature is estimated at roughly 1000 seconds based on research performed by DNV GL [20]. The duration of the thermal runaway is estimated at 50 seconds. To calculate the energy that is needed to reach those temperatures, equation 10.2 is implemented. For the cell to reach a temperature of 180°C from 22°C, 445 kJ of energy is needed, as can be seen in equation 11.3. This is equal to a heat generation rate of 445 W for 1000 seconds. However, to accelerate the process and module cooling happens at the same time, a heat generation rate of 1000 W will be assumed. For the thermal runaway event itself, 1041 kJ of heat is needed, according to equation 11.4. This equals a heat generation rate of 20.8 kW for 50 seconds. To verify if these amounts of energy can be delivered, the electrical energy of the cell will be calculated in equation 11.5. The internal electrical energy is almost twice the theoretical energy that is delivered during a thermal runaway according to these calculations, meaning that the simulated event is plausible.

$$Q = m \cdot c \cdot (T_2 - T_1) = 4.2 \cdot 670 \cdot (180 - 22) = 445kJ \tag{11.3}$$

$$Q = m \cdot c \cdot (T_2 - T_1) = 4.2 \cdot 670 \cdot (550 - 180) = 1041kJ \tag{11.4}$$

$$E_{electrical} = V_{nom} \cdot Q = 3.7V \cdot 200Ah = 3.7 \cdot 200 \cdot 3600 = 2664kJ \tag{11.5}$$

11.4.2. Thermal runaway results

Figure 11.13 shows the cell temperatures as cell 4 initiates a thermal runaway. The lower half of the figure shows the cooling rates of the bottom casing an the front casing. Cell 4 depicts a typical thermal runaway profile, where a peak temperature of 550°C is reached. What can be seen is that the adjacent cells, cell 3 and 5, reach a temperature above 180°C. Likely, they will initiate the final phase of a thermal runaway as well, causing a cascading effect. An important factor in is the reaction time before the next cell initiates a thermal runaway. 214 seconds after cell 4 reached 180°C and initiated the final phase of

the thermal runaway, cells 3 and 5 reach a temperature of 180°C. This provides a reaction time of less than 214 seconds to cool down the battery module to prevent a cascading effect. Cooling through the bottom casing proves to be insufficient to prevent thermal runaway propagation. Therefore alternative cooling configurations, for instance liquid cooling between cells, could provide enough heat dissipation. Alternatively, as described in chapter 4.4 and figure 4.1, suppression methods such as water mist or foam could be injected.

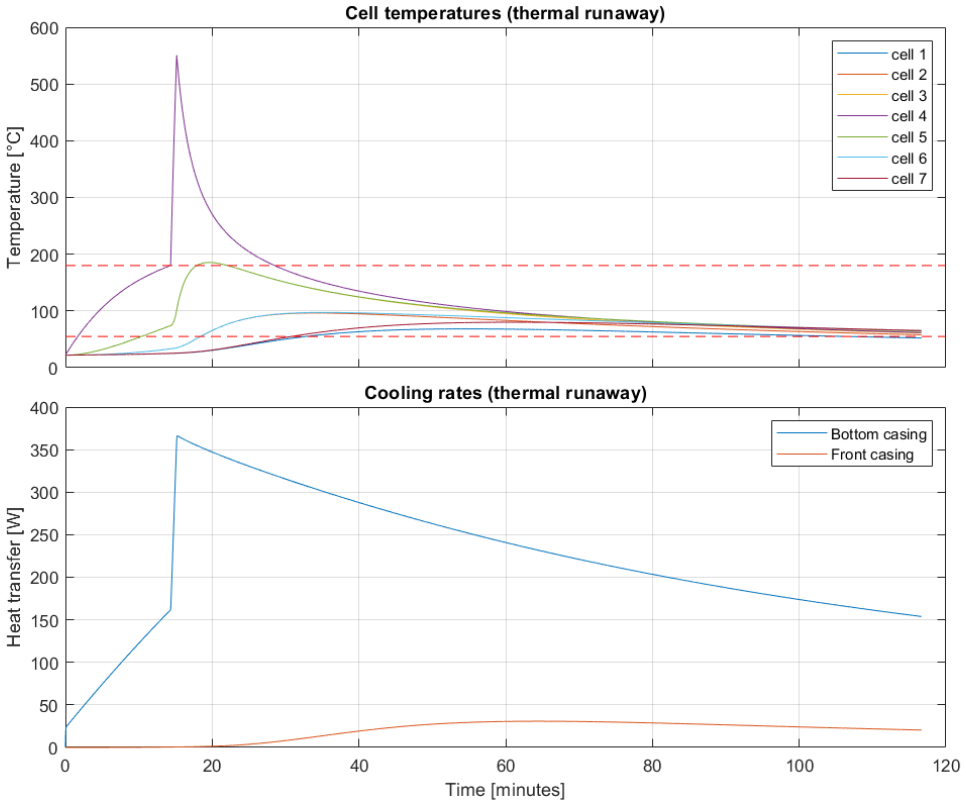

Figure 11.13: Simulation of a thermal runaway in a battery module

11.5. Conclusion

In this chapter, the thermal behaviour of a lithium-ion battery module has been analysed. The cell temperatures and cooling rates have been obtained for three operational profiles. Specifically a submerged sprint, covert transit and covert surveillance have been analysed based on typical C-rate expectations. The operational profiles are simulated with and without cooling through the bottom casing in the form of forced liquid cooling. Natural cooling takes place through the front casing in the form of convection and radiation. The cooling rate is dependent on many variables, such as the heat capacity of the coolant, the inlet temperature, the cooler efficiency and the mass flow rate. The developed thermal model can serve as a tool or starting point to analyse cooler design and the effectiveness in future research.

To improve heat dissipation rates from the cells to the surroundings, the module geometry has been optimised. The most significant reduction in maximum temperature is obtained by minimising the cell to cell spacing and minimising the thickness of the thermal conductive filler. The cell to cell spacing and filler thickness have been minimised from 3 mm to 1 mm and from 2 cm to 1 cm respectively. As a result, the energy density and specific energy have increased by 12.9% and 6.7% respectively. The simulation results for the operational profiles have been summarised in figure 11.12. The conclusions are given below:

- During a submerged sprint, C-rates up to 1.0C can be sustained without cooling. The critical temperature limit at 55°C is not reached, although temperatures can reach up to 47.9°C. If cooling is initiated, C-rates up to 0.4C (regular module) and 0.5C (optimised module) can be realised without exceeding the 30°C limit desired for a longer lifetime.
- For a covert transit scenario cooling is essential above C-rates of 0.3C. Otherwise the critical temperature limit is exceeded which results in an increased chance of a thermal runaway. With cooling initiated, C-rates up to 0.75C and 1.0C can be sustained for the regular module and optimised module respectively. Below the limit of 30°C only 0.4C and 0.5C can be sustained with forced cooling, similar to a submerged sprint scenario.
- In terms of covert surveillance, it can be concluded that cooling is necessary for three of the four scenario's. Only at a 0.1C discharge rate and a 0.5C charge rate, cell temperatures remain below 55°C without cooling implemented. With forced cooling, all typical covert surveillance scenario's can be fulfilled. Moreover, the optimised geometry has the implication that temperatures for each scenario are kept below 30°C. Typically, temperatures are raised during charging, after which sufficient time is realised to dissipate the generated heat.

It can be concluded that the effects of cooling are minimal for a submerged sprint. For covert transit and covert surveillance, cooling is of significance. Consecutive cycles are significantly limited in terms of C-rate. Therefore it is concluded that for the operational profile either low charge and discharge rates have to be accepted, or cooling has to be implemented to fulfill higher C-rate requirements. Typical cooling rates are quantified between 60 W and 185 W. Moreover, it can be concluded that by decreasing the volume and mass of the module, the thermal efficiency has increased. Based on the large amount of cells present on a diesel-electric submarine, a volumetric improvement of 6.7% per module can result in a significant amount of extra space for a battery system on board of a submarine. Since the cell temperatures remain relatively constant after the fourth cell in a row, a larger battery module consisting of more cells can be developed, resulting in a higher energy density and specific energy.

Finally, a thermal runaway has been simulated in the battery module. From the results it can be concluded that forced cooling through the bottom casing is insufficient to prevent a cascading effect to adjacent cells. The adjacent cells reach a temperature above 180°C within 214 seconds, significantly increasing the chances of a thermal runaway on module level. Moreover, this indicates that the reaction time for propagating measures is minimal on board of a submarine. Alternatively cooling between the cells or suppression methods such as water mist or foam could be employed in the case of a thermal runaway.

12

Conclusion & recommendations

12.1. Conclusion

In part II of the thesis, the methodology and results have been discussed of the thermal model of a lithium-ion battery module. To support preliminary submarine design, thermal behaviour has been analysed based on the generated heat during charge and discharge cycles based on various C-rates. The first model that has been created describes the electric behaviour of a lithium-ion battery cell. The second model determines the generated heat based on the electrical model and cell specific properties. The third model implements a lithium-ion battery module, where heat is generated by multiple cells and heat transfer rates with the environment are modelled. An overview of the created models is given in figure 12.1 reproduced from figure 7.1. The objective of the follow-up research has been discussed in the second part of the thesis (1). Based on the conclusions drawn, answers have been formulated for the main research question of the thesis (2).

Develop a thermal model of a lithium-ion battery module to support preliminary submarine design. *(1)*

What are the implications on preliminary submarine system design based on the thermal behaviour of lithium-ion batteries and how can the thermal behaviour and design implications be quantified? *(2)*

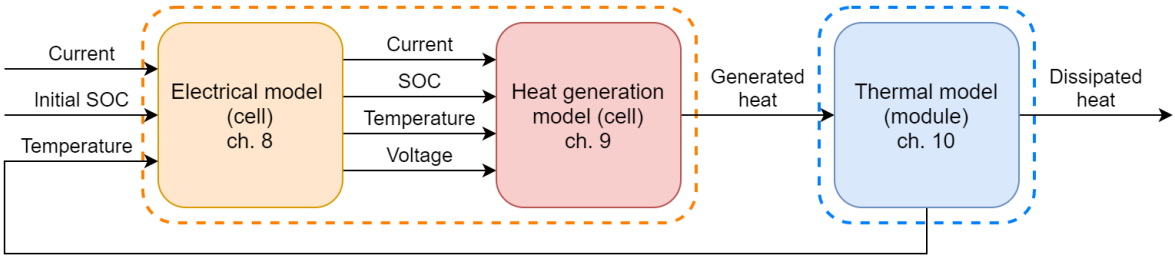

Figure 12.1: Schematic overview of the thermal model of a lithium-ion battery module (reproduced from figure 7.1)

In chapter 8 the electrical behaviour of a lithium-ion battery cell has been modelled. The Shepherd's model has been implemented to simulate the voltage of a 200 Ah pouch cell that is typically implemented in marine applications. The implication of implementing pouch cells is that an additional casing is required to provide the desired level of robustness. The cell voltage has been modelled based on the state of charge, the charge or discharge current and the influence on the operating temperature. The electrical model has been validated based on measurements provided in appendix A. The first implication based on the electrical model is that a higher efficiency can be realised by lowering the discharge current. Secondly, discharge should be interrupted at a low SOC based on a low voltage output, resulting in a lower power output. The third implication is that operation is not desired below

20°C which causes a great reduction in cell capacity and voltage. This decreases the submerged range of a diesel-electric submarine.

Chapter 9 described the methodology to model the heat generation rate based on reversible and irreversible heat generation. The reversible heat has been based on the entropic coefficients determined for a 40Ah pouch cell by Kokam. The irreversible heat is based on the overpotential between the OCV curves from EST-Floattech and the battery voltage obtained from the electrical model. The total heat generation is mostly governed by the irreversible heat generation. The total heat generation increases with a decrease in temperature. Moreover, the total heat increases exponentially with an increased C-rate. High C-rates can imply that more sophisticated cooling systems are required based on increased sprint speeds and covert transit speeds. The operational implication concluded from the heat generation model is that discharging below 20°C is not desired since the efficiency drops due to increased losses in the form of heat. The recommended operating temperature is estimated between 20°C and 30°C since high(er) temperatures reduce the battery lifetime.

Chapter 10 described the approach of formulating the thermal model of the battery module. The module geometry has been determined based on an existing module from EST-Floattech. Based on the geometry, heat transfer coefficients have been determined in terms of conduction, convection and radiation. It can be concluded that conduction is most significant in the transfer of heat, whereas convection and radiation are of equal importance. In terms of the heat transfer coefficient, 89% can be contributed to conduction, and 5% and 6% to convection and radiation respectively. A lumped thermal capacity approach has been implemented using the electrical analogy to create a thermal network. Liquid cooling through the bottom casing has been selected since this has a higher cooling capacity and lower system volume compared to air cooling. Alternatively liquid cooling between the cells could be selected, although this increases the system complexity. Therefore, module cooling through the bottom casing has been selected as an initial choice.

The thermal behaviour of the previously described lithium-ion battery module has been discussed in chapter 11. The cell temperatures and cooling rates have been obtained for three operational profiles. Specifically a submerged sprint, covert transit and covert surveillance have been analysed based on typical C-rate expectations.

- During a submerged sprint, C-rates up to 1.0C can be sustained without cooling. The critical temperature limit at 55°C is not reached, although temperatures can reach up to 47.9°C. If cooling is initiated, C-rates up to 0.4C (regular module) and 0.5C (optimised module) can be realised without exceeding the 30°C limit desired for a longer lifetime.

- For a covert transit scenario cooling is essential above C-rates of 0.3C. Otherwise the critical temperature limit is exceeded which results in an increased chance of a thermal runaway. With cooling initiated, C-rates up to 0.75C and 1.0C can be sustained for the regular module and optimised module respectively. Below the limit of 30°C only 0.4C and 0.5C can be sustained with forced cooling, similar to a submerged sprint scenario.

- In terms of covert surveillance, it can be concluded that cooling is necessary for three of the four scenario's. Only at a 0.1C discharge rate and a 0.5C charge rate, cell temperatures remain below 55°C without cooling implemented. With forced cooling, all typical covert surveillance scenario's can be fulfilled. Moreover, the optimised geometry has the implication that temperatures for each scenario are kept below 30°C. Typically, temperatures are raised during charging, after which sufficient time is realised to dissipate the generated heat.

- Module geometry optimisation provides a reduction in temperature for each operational profile, as well as a reduction in volume and weight. The energy density and specific energy have increased by 12.9% and 6.7% respectively based on a reduction in cell-cell spacing and filler thickness. A temperature reduction up to 30% can be realised based on the optimised geometry, while reducing the mass and volume of the module. Based on the large amount of cells present on a diesel-electric submarine, a volumetric improvement of 6.7% per module can result in a significant amount of extra space for a battery system on board of a submarine.

- In the case of a thermal runaway in one of the cells, it can be concluded that forced cooling through the bottom casing is insufficient to prevent a cascading effect to adjacent cells. The adjacent cells reach a temperature above 180°C within 214 seconds, indicating a minimal reaction time for propagation preventive measures. Alternative methods such as cooling between the cells or suppression methods such as water mist or foam have to be analysed to prevent a thermal runaway on a module level.

- The effects of cooling are most significant for covert transit and covert surveillance compared to a submerged sprint scenario. Therefore it is concluded that for the operational profile either low charge and discharge rates have to be accepted, or cooling has to be implemented to fulfill higher C-rate requirements. Typical cooling rates are quantified between 60 W and 185 W. Since the cell temperature remains relatively constant after the fourth cell in a row, meaning that modules are typically not limited by the number of cells. A battery module consisting of more than the modelled seven cells can result in a higher energy density and specific energy.

- The largest improvement in thermal management can be realised by choosing the right thermal conductive filler and minimising the filler thickness. This is however strongly dependent on the thermal properties of the material. Moreover, the cooling capacity has a large influence on the cell temperatures. The developed model can serve as a tool to analyse the cooler design in future research.

12.2. Recommendations

Several recommendations can be made to improve the discussed thermal model of the battery module. Suggestions for further research are proposed based on the findings of the literature review and the follow-up research.

- Based on the literature review, the conclusion was drawn that a comparative analysis between different chemistries based on their thermal behaviour was absent. To partially fill this gap, behaviour from other cells designs and chemistries could be modelled on a cell level. Additionally, the behaviour on a cell level could be implemented on a module level. This could provide a comparison between modules regarding other alternative cells available. To improve the electrical and heat generation models on cell level, physical modelling could be implemented to increase the model accuracy. A basis for this could be electrochemical modelling.

- To improve the accuracy and validity of the thermal behaviour of the cells implemented in this research, experimental validation of the model is desired. Thermal measurements of the selected cell is absent, which is desirable for validation. As described, the methodology of the model has been verified based on previous research. Moreover, it would be desired to obtain thermal measurements of a representative model to be able to validate the model.

- Cooling has been modelled through the bottom casing as an initial cooling method. A recommendation for further research is to analyze alternative cooling methods. For instance cooling between cells or cooling on multiple sides could be incorporated. Moreover, a combination between air cooling and liquid cooling could be proposed. Additionally, the design and dimensioning of a cooling system could be suggested for further research. This could focus on extracting the total heat from a BESS from the cooling liquid with the use of heat exchangers and alternative methods. The dimensioning of the cooling system has a large influence on the submarine design. Especially the heat exchangers, which are typically in contact with the seawater and have to withstand high pressure requirements.

- In terms of a thermal runaway, only cooling during regular operation has been implemented as a preventive measure. For future research an analysis on the effectiveness of other thermal runaway prevention measures is desired. An analysis of the various methods stated in section 4.4 could be a starting point for this. Additionally, the effects of propagation prevention measures can be analysed. The current thermal model can function as a starting point. However, the proposed methods of cooling as explained in the previous recommendation, can be analysed as well in terms of the cooling capabilities during a thermal runaway.

- Another recommendation is to incorporate a gas generation model. The buildup of toxic and flammable gasses is especially important for a submarine, since getting rid of those gasses is difficult when submerged. Additional research towards the risks of accumulated gasses during a thermal runaway could provide a starting point for the gas generation model. Additionally, methods to prevent propagation of the gasses and gas extraction methods can be developed.
- The final recommendation is to perform further research on the influence of the module geometry. As described in the conclusion, the geometry has a strong correlation with the maximum cell temperatures. Moreover, the energy density and specific energy have increased. In further research even more efficient geometries might be found, resulting in a more efficient cooler design while limiting the size and weight of the module.

Bibliography

[1] Yasir Abdul-Quadir, Tomi Laurila, Juha Karppinen, Kirsi Jalkanen, Kai Vuorilehto, Lasse Skogström, and Mervi Paulasto-Kröckel. Heat generation in high power prismatic li-ion battery cell with limnnicoo2 cathode material. *International Journal of Energy Research*, 38(11): 1424–1437, 2014. ISSN 1099114X. doi: 10.1002/er.3156.

[2] S. Al Hallaj, H. Maleki, J. S. Hong, and J. R. Selman. Thermal modeling and design considerations of lithium-ion batteries. *Journal of Power Sources*, 83(1-2):1–8, 1999. ISSN 03787753. doi: 10.1016/S0378-7753(99)00178-0.

[3] Parisa Amiribavandpour, Weixiang Shen, Daobin Mu, and Ajay Kapoor. An improved theoretical electrochemical-thermal modelling of lithium-ion battery packs in electric vehicles. *Journal of Power Sources*, 284:328–338, 2015. ISSN 03787753. doi: 10.1016/j.jpowsour.2015.03.022. URL http://dx.doi.org/10.1016/j.jpowsour.2015.03.022.

[4] Azom. Silicone rubber, December 2020. URL https://www.azom.com/properties.aspx?ArticleID=920.

[5] Manikandan Balasundaram, Vishwanathan Ramar, Christopher Yap, Li Lu, Andrew A.O. Tay, and Balaya Palani. Heat loss distribution: Impedance and thermal loss analyses in lifepo4/graphite 18650 electrochemical cell. *Journal of Power Sources*, 328:413–421, october 2016. ISSN 03787753. doi: 10.1016/j.jpowsour.2016.08.045.

[6] EAS Batteries. Marine, January 2021. URL https://eas-batteries.com/markets/marine.

[7] Morris Beck. Battery energy storage systems market 2019: Global industry analysis, type, applications, players, size, share, growth, trends and forecast to 2024, May 2020. URL https://themarketresearchnews.wordpress.com/2019/04/15/battery-energy-storage-systems-market-2019-global-industry-analysis-/type-applications-players-size-share-growth-trends-and-forecast-/to-2024/.

[8] Dawn Bernardi, Ellen Pawlikowski, and John Newman. A general energy balance for battery systems. *J. Electrochem. Soc.*, 132:1(April), 1984. doi: 10.1149/1.2113792.

[9] K Brandt. Historical development of secondary lithium batteries. *Solid State Ionics*, 1994.

[10] Polina Brodsky. Real-time modeling of battery pack temperature for thermal limit prevention in electric race vehicles. pages 1–53, 2016.

[11] Isidor Buchmann. *Batteries in a Portable World*. Cadex Electronics Inc, 2011.

[12] Isidor Buchmann. When was the battery invented?, May 2020. URL http://www.arrl.org/when-was-the-battery-invented#:~:text=%201859%2C%20French%20physician,and%20cadmium%20for%20the%20negative.

[13] R. Burcher and L. J. Rydill. *Concepts in Submarine Design*. Cambridge University Press, 1994. ISBN 9780521559263.

[14] S. C. Chen, C. C. Wan, and Y. Y. Wang. Thermal analysis of lithium-ion batteries. *Journal of Power Sources*, 140(1):111–124, 2005. ISSN 03787753. doi: 10.1016/j.jpowsour.2004.05.064.

[15] Ashok Vijh Christian Julien, Alain Mauger. *Lithium Batteries, Science and Technology*. Springer International Publishing, 2016. ISBN 978-3-319-19107-2.

[16] Stuart W. Churchill and Humbert H.S. Chu. Correlating equations for laminar and turbulent free convection from a vertical plate. *International Journal of Heat and Mass Transfer*, 18(11):1323–1329, 1975. ISSN 00179310. doi: 10.1016/0017-9310(75)90243-4.

[17] Green Car Congress. Design of the daimler s400 mild hybrid system, May 2020. URL https://www.greencarcongress.com/2009/06/s400-20090611.html.

[18] Nicolas Damay, Christophe Forgez, Marie Pierre Bichat, and Guy Friedrich. Thermal modeling of large prismatic lifepo4/graphite battery. coupled thermal and heat generation models for characterization and simulation. 283:37–45, 2015. ISSN 03787753. doi: 10.1016/j.jpowsour.2015.02.091. URL http://dx.doi.org/10.1016/j.jpowsour.2015.02.091.

[19] DNV GL. Li-ion battery safety wiki 2: Li-ion battery rooms. 2019.

[20] DNV GL. Technical reference for li-ion battery explosion risk and fire suppression. 2019.

[21] DNV GL. Preventing thermal runaway propagation in li-ion batteries. 2020.

[22] Chil Hoon Doh, Yoon Cheol Ha, and Seung wook Eom. Entropy measurement of a large format lithium ion battery and its application to calculate heat generation. *Electrochimica Acta*, 309:382–391, 2019. ISSN 00134686. doi: 10.1016/j.electacta.2019.04.026. URL https://doi.org/10.1016/j.electacta.2019.04.026.

[23] Ze'ev Drori. We have begun regular production of the tesla roadster, May 2020. URL https://www.tesla.com/nl_NL/blog/we-have-begun-regular-production-tesla-roadster?redirect=no.

[24] James Edmondson. Immersion of electric vehicle batteries: The best way to keep cool?, May 2020. URL https://www.idtechex.com/en/research-article/immersion-of-electric-vehicle-batteries-the-best-way-to-keep-cool/20169.

[25] Electrolube. Gf300 gap filler, December 2020. URL https://res.cloudinary.com/electrolube/images/v1603184573/GF300_wa75g6_2224505bfc/GF300_wa75g6_2224505bfc.pdf.

[26] Electropaedia. Battery comparison chart, June 2020. URL https://www.mpoweruk.com/specifications/comparisons.pdf.

[27] Electropaedia. High temperature batteries, June 2020. URL https://www.mpoweruk.com/high_temp.htm.

[28] S. M. ElSherbiny, G. D. Raithby, and K. G.T. Hollands. Heat transfer by natural convection across vertical and inclined air layers. *American Society of Mechanical Engineers (Paper)*, 104, 1980. ISSN 04021215.

[29] Xalt Energy. Xmp 111e, January 2021. URL https://www.xaltenergy.com/portfolio/xmp-111e/.

[30] Javad Esmaeili and Hamid Jannesari. Developing heat source term including heat generation at rest condition for lithium-ion battery pack by up scaling information from cell scale. *Energy Conversion and Management*, 139:194–205, 2017. ISSN 01968904. doi: 10.1016/j.enconman.2017.02.052.

[31] EST-Floattech. Our modules, December 2020. URL https://www.est-floattech.com/est-technology/our-modules/.

[32] EST-Floattech. Clean, compact, safe & reliable energy, September 2020. URL https://www.est-floattech.com/.

[33] X. Feng, H. B. Gooi, and S. X. Chen. An improved lithium-ion battery model with temperature prediction considering entropy. *IEEE PES Innovative Smart Grid Technologies Conference Europe*, (December), 2012. doi: 10.1109/ISGTEurope.2012.6465668.

[34] Xuning Feng, Xiangming He, Minggao Ouyang, Languang Lu, Peng Wu, Christian Kulp, and Stefan Prasser. Thermal runaway propagation model for designing a safer battery pack with 25ah $lini_xco_ymn_zo_2$ large format lithium ion battery. *Applied Energy*, 154:74–91, 2015. ISSN 03062619. doi: 10.1016/j.apenergy.2015.04.118. URL http://dx.doi.org/10.1016/j.apenergy.2015.04.118.

[35] Christophe Forgez, Dinh Vinh Do, Guy Friedrich, Mathieu Morcrette, and Charles Delacourt. Thermal modeling of a cylindrical LiFePO4/graphite lithium-ion battery. *Journal of Power Sources*, 195(9):2961–2968, 2010. ISSN 03787753. doi: 10.1016/j.jpowsour.2009.10.105.

[36] Lijun Gao, Shengyi Liu, and Roger A. Dougal. Dynamic lithium-ion battery model for system simulation. *IEEE Transactions on Components and Packaging Technologies*, 25(3):495–505, 2002. ISSN 15213331. doi: 10.1109/TCAPT.2002.803653.

[37] Florian Geifes, Christoph Bolsinger, Paul Mielcarek, and Kai Peter Birke. Determination of the entropic heat coefficient in a simple electro-thermal lithium-ion cell model with pulse relaxation measurements and least squares algorithm. *Journal of Power Sources*, 419(March):148–154, 2019. ISSN 03787753. doi: 10.1016/j.jpowsour.2019.02.072. URL https://doi.org/10.1016/j.jpowsour.2019.02.072.

[38] Andrey W. Golubkov, David Fuchs, Julian Wagner, Helmar Wiltsche, Christoph Stangl, Gisela Fauler, Gernot Voitic, Alexander Thaler, and Viktor Hacker. Thermal-runaway experiments on consumer li-ion batteries with metal-oxide and olivin-type cathodes. *RSC Advances*, 4(7):3633–3642, 2014. ISSN 20462069. doi: 10.1039/c3ra45748f.

[39] Rui Guo, Languang Lu, Minggao Ouyang, and Xuning Feng. Mechanism of the entire overdischarge process and overdischarge-induced internal short circuit in lithium-ion batteries. *Scientific Reports*, 6(July):1–9, 2016. ISSN 20452322. doi: 10.1038/srep30248.

[40] Taeyoung Han, Bahram Khalighi, Erik C. Yen, and Shailendra Kaushik. Li-ion battery pack thermal management: Liquid versus air cooling. *Journal of Thermal Science and Engineering Applications*, 11(2), 2019. ISSN 19485093. doi: 10.1115/1.4041595.

[41] Ali Hanif. A suitable battery technology for pv-battery integrated module. 2018.

[42] Hanane Hemi, Nacer K. M'Sirdi, and Aziz Naamane. A new proposed shepherd model of a li-ion open circuit battery based on data fitting. *12th International Conference on Integrated Modeling and Analysis in Applied Control and Automation, IMAACA 2019*, pages 83–92, 2019.

[43] Joey Hoogendoorn. Fuel cell and battery hybrid system optimization: Towards increased range and endurance. 2018. URL https://repository.tudelft.nl/islandora/object/uuid:6e274095-9920-4d20-9e11-d5b76363e709.

[44] Ala Al Haj Hussein and Issa Batarseh. An overview of generic battery models. *IEEE Power and Energy Society General Meeting*, (August), 2011. ISSN 19449925. doi: 10.1109/PES.2011.6039674.

[45] N. Imanishi and O. Yamamoto. Perspectives and challenges of rechargeable lithium–air batteries. *Materials Today Advances*, 4:100031, 2019. ISSN 25900498. doi: 10.1016/j.mtadv.2019.100031. URL https://doi.org/10.1016/j.mtadv.2019.100031.

[46] Indiamart. Papal lithium ion cell, 3.7v, May 2020. URL https://www.indiamart.com/proddetail/lithium-ion-cell-18920788848.html.

[47] H. Klein Woud and D. Stapersma. *Design of Auxiliary Systems, Shafting and Flexible Mounting*. Delft University of Technology, 2016.

[48] Kokam. Kokam li-ion cell, December 2020. URL https://kokam.com/cell.

[49] Kokam. Marine battery module, January 2021. URL https://kokam.com/module-marine.

[50] Lingxi Kong, Chuan Li, Jiuchun Jiang, and Michael G. Pecht. Li-ion battery fire hazards and safety strategies. *Energies*, 11(9):1–11, 2018. ISSN 19961073. doi: 10.3390/en11092191.

[51] Akos Kriston, Andreas Pfrang, Harry Döring, Benjamin Fritsch, Vanesa Ruiz, Ibtissam Adanouj, Theodora Kosmidou, Jürgen Ungeheuer, and Lois Boon-Brett. External short circuit performance of graphite-lini1/3co1/3mn1/3o2 and graphite-lini0.8co0.15al0.05o2 cells at different external resistances. *Journal of Power Sources*, 361:170–181, 2017. ISSN 03787753. doi: 10.1016/j.jpowsour.2017.06.056.

[52] Xin Lai, Yuejiu Zheng, Long Zhou, and Wenkai Gao. Electrical behavior of overdischarge-induced internal short circuit in lithium-ion cells. *Electrochimica Acta*, 278:245–254, 2018. ISSN 00134686. doi: 10.1016/j.electacta.2018.05.048. URL https://doi.org/10.1016/j.electacta.2018.05.048.

[53] D. Larcher and J. M. Tarascon. Towards greener and more sustainable batteries for electrical energy storage. *Nature Chemistry*, 7(1):19–29, 2015. ISSN 17554349. doi: 10.1038/nchem.2085.

[54] Fredrik Larsson, Petra Andersson, Per Blomqvist, and Bengt Erik Mellander. Toxic fluoride gas emissions from lithium-ion battery fires. *Scientific Reports*, 7(1):1–13, 2017. ISSN 20452322. doi: 10.1038/s41598-017-09784-z. URL http://dx.doi.org/10.1038/s41598-017-09784-z.

[55] Zhenghai Liao, Shen Zhang, Kang Li, Mingyue Zhao, Zongjia Qiu, Dong Han, Guoqiang Zhang, and Thomas G. Habetler. Hazard analysis of thermally abused lithium-ion batteries at different state of charges. *Journal of Energy Storage*, 27(November 2019):101065, 2020. ISSN 2352152X. doi: 10.1016/j.est.2019.101065. URL https://doi.org/10.1016/j.est.2019.101065.

[56] Chemistry Libretexts. Entropy changes in reversible processes, October 2020. URL https://chem.libretexts.org/Bookshelves/General_Chemistry/Map%3A_Principles_of_Modern_Chemistry_(Oxtoby_et_al.)/UNIT_4%3A_EQUILIBRIUM_IN_CHEMICAL_REACTIONS/13%3A_Spontaneous_Processes_and_Thermodynamic_Equilibrium/13.4%3A_Entropy_Changes_in_Reversible_Processes.

[57] Xinfan Lin, Hector E. Perez, Shankar Mohan, Jason B. Siegel, Anna G. Stefanopoulou, Yi Ding, and Matthew P. Castanier. A lumped-parameter electro-thermal model for cylindrical batteries. *Journal of Power Sources*, 257:12–20, 2014. ISSN 03787753. doi: 10.1016/j.jpowsour.2014.01.097. URL http://dx.doi.org/10.1016/j.jpowsour.2014.01.097.

[58] Guangming Liu, Minggao Ouyang, Languang Lu, Jianqiu Li, and Xuebing Han. Analysis of the heat generation of lithium-ion battery during charging and discharging considering different influencing factors. *Journal of Thermal Analysis and Calorimetry*, 116(2):1001–1010, 2014. ISSN 13886150. doi: 10.1007/s10973-013-3599-9.

[59] Kai Liu, Yayuan Liu, Dingchang Lin, Allen Pei, and Yi Cui. Materials for lithium-ion battery safety. *Science Advances*, 4(6), 2018. ISSN 23752548. doi: 10.1126/sciadv.aas9820.

[60] Yujun Liu, Qiangling Duan, Jiajia Xu, Huang Li, Jinhua Sun, and Qingsong Wang. Experimental study on a novel safety strategy of lithium-ion battery integrating fire suppression and rapid cooling. *Journal of Energy Storage*, 28(July 2019):101185, 2020. ISSN 2352152X. doi: 10.1016/j.est.2019.101185. URL https://doi.org/10.1016/j.est.2019.101185.

[61] Melanie J. Loveridge, Guillaume Remy, Nadia Kourra, Ronny Genieser, Anup Barai, Mike J. Lain, Yue Guo, Mark Amor-Segan, Mark A. Williams, Tazdin Amietszajew, Mark Ellis, Rohit Bhagat, and David Greenwood. Looking deeper into the galaxy (note 7). *Batteries*, 4(1), 2018. ISSN 23130105. doi: 10.3390/batteries4010003.

[62] W. Lu, I. Belharouak, D. Vissers, and K. Amine. In situ thermal study of $li_{1+x}[ni_{1/3}co_{1/3}mn_{1/3}]_{1-x}o_2$ using isothermal micro-clorimetric techniques. *Journal of The Electrochemical Society*, 153(11): A2147, 2006. ISSN 00134651. doi: 10.1149/1.2349287.

[63] Christopher Lyness, Meike Fleischhammer, Michael Abert, Brian Barnett, Christopher H. McCoy, David Ofer, Suresh Sriramulu, Martin Gilljam, Helge Weydahl, Sissel Forseth, Preben J.S. Vie, and Torleif Lian. *Lithium-secondary cell: Sources of risks and their effects*. 2018. ISBN 9780444637772. doi: 10.1016/B978-0-444-63777-2.00007-4.

[64] Shuai Ma, Modi Jiang, Peng Tao, Chengyi Song, Jianbo Wu, and Jun Wang. Temperature effect and thermal impact in lithium-ion batteries: a review. 28(October):653–666, 2018. doi: 10.1016/j.pnsc.2018.11.002.

[65] Seyed Saeed Madani, Erik Schaltz, and Søren Knudsen Kær. An electrical equivalent circuit model of a lithium titanate oxide battery. *Batteries*, 5(1), 2019. ISSN 23130105. doi: 10.3390/batteries5010031.

[66] Hossein Maleki and Jason N. Howard. Internal short circuit in li-ion cells. *Journal of Power Sources*, 191(2):568–574, 2009. ISSN 03787753. doi: 10.1016/j.jpowsour.2009.02.070.

[67] T. Maloney. Lithium battery thermal runaway vent gas analysis. page 35, 2016.

[68] Binbin Mao, Haodong Chen, Zhixian Cui, Tangqin Wu, and Qingsong Wang. Failure mechanism of the lithium ion battery during nail penetration. *International Journal of Heat and Mass Transfer*, 122:1103–1115, 2018. ISSN 00179310. doi: 10.1016/j.ijheatmasstransfer.2018.02.036. URL https://doi.org/10.1016/j.ijheatmasstransfer.2018.02.036.

[69] James Marcicki, Marcello Canova, A. Terrence Conlisk, and Giorgio Rizzoni. Design and parametrization analysis of a reduced-order electrochemical model of graphite/lifepo4 cells for soc/soh estimation. *Journal of Power Sources*, 237:310–324, 2013. ISSN 03787753. doi: 10.1016/j.jpowsour.2012.12.120.

[70] Koninklijke Marine. Zr.ms. walrus, March 2021. URL https://www.defensie.nl/organisatie/marine/eenheden/schepen/zr-ms-walrus.

[71] Koninklijke Marine. Onderzeeboten, March 2021. URL https://www.defensie.nl/organisatie/marine/materieel/schepen/onderzeeboten.

[72] Mathworks. Fminsearch, July 2020. URL https://www.mathworks.com/help/matlab/ref/fminsearch.html.

[73] Mathworks. Battery, generic battery model, July 2020. URL https://www.mathworks.com/help/physmod/sps/powersys/ref/battery.html.

[74] Johnson Matthey. Our guide to batteries. 2017.

[75] Celina Mikolajczak, Pe Michael Kahn, Kevin White, and Richard Thomas Long. *Lithium-Ion Batteries Hazard and Use Assessment Final Report*. 2011. ISBN 9781461434856.

[76] Peter Miller. Automotive lithium-ion batteries. *Johnson Matthey Technology Review*, 59:4–13, 2015.

[77] A.F. Mills. *Basic Heat and Mass Transfer*. Pearson Education Limited, 2nd edition, 2014. ISBN 9781292042480.

[78] XING Mobility. Immersion cooling: The safest battery technology on the market?, May 2020. URL https://www.xingmobility.com/news/immersion-cooling-the-safest-battery-technology-on-the-market.

[79] Seung Taek Myung, Yashiro Hitoshi, and Yang Kook Sun. Electrochemical behavior and passivation of current collectors in lithium-ion batteries. *Journal of Materials Chemistry*, 21(27):9891–9911, 2011. ISSN 09599428. doi: 10.1039/c0jm04353b.

[80] Ashkan Nazari and Siamak Farhad. Heat generation in lithium-ion batteries with different nominal capacities and chemistries. *Applied Thermal Engineering*, 125:1501–1517, 2017. ISSN 13594311. doi: 10.1016/j.applthermaleng.2017.07.126. URL http://dx.doi.org/10.1016/j.applthermaleng.2017.07.126.

[81] David Novák. Design of a li-ion battery pack emulator. 2015.

[82] Defensie Materieel Organisatie. Confidential information.

[83] V. J. Ovejas and A. Cuadras. State of charge dependency of the overvoltage generated in commercial li-ion cells. *Journal of Power Sources*, 418(July 2018):176–185, 2019. ISSN 03787753. doi: 10.1016/j.jpowsour.2019.02.046. URL https://doi.org/10.1016/j.jpowsour.2019.02.046.

[84] Panasonic. Panasonic develops high energy lithium-ion battery module with high reliability, May 2020. URL https://phys.org/news/2009-10-panasonic-high-energy-lithium-ion-battery.html.

[85] Jung-Ki Park. Principles and applications of lithium secondary batteries, April 2020. URL https://wiley-vch.e-bookshelf.de/products/reading-epub/product-id/644991/title/Principles.

[86] Qnovo. 82. the cost components of a lithium ion battery, May 2020. URL https://batteryuniversity.com/index.php/learn/article/bu_1006_cost_of_mobile_power.

[87] Ravishankar Rao, Sarma Vrudhula, and Daler N. Rakhmatov. Battery modeling for energy-aware system design. *Electrochemical Society Interface*, 14(4):39–42, 2005. ISSN 10648208. doi: 10.1002/9781118970553.ch12.

[88] L. H. Saw, Y. Ye, and A. A.O. Tay. Electro-thermal analysis and integration issues of lithium ion battery for electric vehicles. *Applied Energy*, 131:97–107, 2014. ISSN 03062619. doi: 10.1016/j.apenergy.2014.06.016.

[89] Samsung SDI. Ess batteries by samsung sdi, January 2021. URL https://www.samsungsdi.com/upload/ess_brochure/201902_Samsung%20SDI%20ESS_EN.pdf.

[90] C. M. Shepherd. Design of primary and secondary cells. *Journal of The Electrochemical Society*, 112(7):657, 1965. ISSN 00134651. doi: 10.1149/1.2423659.

[91] Leclanché Energy Storage Solutions. Modules, January 2021. URL https://www.leclanche.com/our-technologies/modules/.

[92] Chunwen Sun, Jin Liu, Yudong Gong, David P. Wilkinson, and Jiujun Zhang. Recent advances in all-solid-state rechargeable lithium batteries. *Nano Energy*, 33(January):363–386, 2017. ISSN 22112855. doi: 10.1016/j.nanoen.2017.01.028.

[93] Peiyi Sun, Roeland Bisschop, Huichang Niu, and Xinyan Huang. *A Review of Battery Fires in Electric Vehicles*. Number January. 2020. ISBN 1069401900. doi: 10.1007/s10694-019-00944-3.

[94] Sunlight. Training course system description, theory & fundamentals, 2012.

[95] Delta Energy Systems. Delta energy systems es30: energy storage system with 78 kilowatt hours capacity, May 2020. URL https://www.pveurope.eu/Products/Storage/Batteries/Delta-Energy-Systems-ES30-energy-storage-system-with-78-kilowatt-/hours-capacity.

[96] Naval Technology. Ssk scorpene-class attack submarine, france, March 2021. URL https://www.naval-technology.com/projects/scorpene-class/#:~:text=The%20ratio%20between%20this%20time,30%25%20in%20transit%20at%208k.

[97] S. ten Cate Hoedemaker. Battery aging in full electric ships, 2017.

[98] Karen E. Thomas and John Newman. Heats of mixing and of entropy in porous insertion electrodes. *Journal of Power Sources*, 119-121:844–849, 2003. ISSN 03787753. doi: 10.1016/S0378-7753(03)00283-0.

[99] Olivier Tremblay and Louis A. Dessaint. Experimental validation of a battery dynamic model for ev applications. *24th International Battery, Hybrid and Fuel Cell Electric Vehicle Symposium and Exhibition 2009, EVS 24*, 2:930–939, 2009.

[100] Olivier Tremblay, Louis A. Dessaint, and Abdel Illah Dekkiche. A generic battery model for the dynamic simulation of hybrid electric vehicles. *VPPC 2007 - Proceedings of the 2007 IEEE Vehicle Power and Propulsion Conference*, (V):284–289, 2007. doi: 10.1109/VPPC.2007.4544139.

[101] Fritz Ullmann. *Encyclopedia of industrial chemistry, fifth edition*. Weinheim, 1985.

[102] Battery University. Bu-203: Nickel-based batteries, April 2020. URL https://batteryuniversity.com/learn/article/nickel_based_batteries.

[103] Battery University. Bu-1006: Cost of mobile and renewable power, May 2020. URL https://batteryuniversity.com/index.php/learn/article/bu_1006_cost_of_mobile_power.

[104] Battery University. Bu-502: Discharging at high and low temperatures, May 2020. URL https://batteryuniversity.com/learn/article/discharging_at_high_and_low_temperatures.

[105] J.J.A. van der Burgt. Li-ion safety wiki 1: safety aspects of li-ion chemistries. 2019.

[106] Petr Vanýsek. Electrochemical series. 2010.

[107] Dries Verstraete, Andrew Gong, Dylan D.C. Lu, and Jennifer L. Palmer. Experimental investigation of the role of the battery in the aerostack hybrid, fuel-cell-based propulsion system for small unmanned aircraft systems. *International Journal of Hydrogen Energy*, 40(3): 1598–1606, 2015. ISSN 03603199. doi: 10.1016/j.ijhydene.2014.11.043. URL http://dx.doi.org/10.1016/j.ijhydene.2014.11.043.

[108] Aiping Wang, Sanket Kadam, Hong Li, Siqi Shi, and Yue Qi. Review on modeling of the anode solid electrolyte interphase (sei) for lithium-ion batteries. *npj Computational Materials*, 4(1), 2018. ISSN 20573960. doi: 10.1038/s41524-018-0064-0. URL http://dx.doi.org/10.1038/s41524-018-0064-0.

[109] Qingsong Wang, Jinhua Sun, Xiaolin Yao, and Chunhua Chen. Thermal stability of lipf6/ec + dec electrolyte with charged electrodes for lithium ion batteries. *Thermochimica Acta*, 437(1-2): 12–16, 2005. ISSN 00406031. doi: 10.1016/j.tca.2005.06.010.

[110] Qingsong Wang, Binbin Mao, Stanislav I. Stoliarov, and Jinhua Sun. A review of lithium ion battery failure mechanisms and fire prevention strategies. *Progress in Energy and Combustion Science*, 73:95–131, 2019. ISSN 03601285. doi: 10.1016/j.pecs.2019.03.002. URL https://doi.org/10.1016/j.pecs.2019.03.002.

[111] John T. Warner. *Lithium-ion battery operation*. 2019. ISBN 9780128147788. doi: 10.1016/b978-0-12-814778-8.00003-x.

[112] S. M. Wijewardana. New dynamic battery model for hybrid vehicles and dynamic model analysis using simulink. *Engineer: Journal of the Institution of Engineers, Sri Lanka*, 47(4):53, 2014. ISSN 1800-1122. doi: 10.4038/engineer.v47i4.6883.

[113] Martyn Williams. Sony explains battery problems, May 2020. URL https://www.pcworld.com/article/127637/article.html.

[114] Spring wise. A dutch company has developed all-electric, fully autonomous cargo barges, May 2020. URL https://www.springwise.com/worlds-first-electric-autonomous-ships/.

[115] Meng Xiao and Song Yul Choe. Theoretical and experimental analysis of heat generations of a pouch type limn2o4/carbon high power li-polymer battery. *Journal of Power Sources*, 241:46–55, 2013. ISSN 03787753. doi: 10.1016/j.jpowsour.2013.04.062. URL http://dx.doi.org/10.1016/j.jpowsour.2013.04.062.

[116] Bo Yan, Cheolwoong Lim, Leilei Yin, and Likun Zhu. Simulation of heat generation in a reconstructed licoo2 cathode during galvanostatic discharge. *Electrochimica Acta*, 100:171–179, 2013. ISSN 00134686. doi: 10.1016/j.electacta.2013.03.132. URL http://dx.doi.org/10.1016/j.electacta.2013.03.132.

[117] Jiana Ye, Haodong Chen, Qingsong Wang, Peifeng Huang, Jinhua Sun, and Siuming Lo. Thermal behavior and failure mechanism of lithium ion cells during overcharge under adiabatic conditions. *Applied Energy*, 182:464–474, 2016. ISSN 03062619. doi: 10.1016/j.apenergy.2016.08.124.

[118] Kisoo Yoo and Jonghoon Kim. Thermal behavior of full-scale battery pack based on comprehensive heat-generation model. *Journal of Power Sources*, 433(June):226715, 2019. ISSN 03787753. doi: 10.1016/j.jpowsour.2019.226715. URL https://doi.org/10.1016/j.jpowsour.2019.226715.

[119] Rui Zhao, Junjie Gu, and Jie Liu. An investigation on the significance of reversible heat to the thermal behavior of lithium ion battery through simulations. *Journal of Power Sources*, 266:422–432, 2014. ISSN 03787753. doi: 10.1016/j.jpowsour.2014.05.034. URL http://dx.doi.org/10.1016/j.jpowsour.2014.05.034.

[120] Rui Zhao, Jie Liu, and Junjie Gu. The effects of electrode thickness on the electrochemical and thermal characteristics of lithium ion battery. *Applied Energy*, 139:220–229, 2015. ISSN 03062619. doi: 10.1016/j.apenergy.2014.11.051. URL http://dx.doi.org/10.1016/j.apenergy.2014.11.051.

[121] Rui Zhao, Jie Liu, and Junjie Gu. Simulation and experimental study on lithium ion battery short circuit. *Applied Energy*, 173:29–39, 2016. ISSN 03062619. doi: 10.1016/j.apenergy.2016.04.016. URL http://dx.doi.org/10.1016/j.apenergy.2016.04.016.

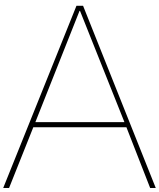

Kokam SLPB140460330

SLPB140460330

Kokam
Great Power for Everyone

SUPERIOR LITHIUM POLYMER BATTERY TECHNICAL SPECIFICATION

• Model # : SLPB140460330 • Issued date: Oct. 01, 2012

SLPB 200Ah HIGH ENERGY
SUPERIOR LITHIUM POLYMER CELL

Kokam's patented manufacturing process produces battery cells for applications that require:

- Excellent energy density(140 – 200 Wh/kg)
- Excellent power-to-energy balance
- High cycle life
- Longer battery life
- Low impedance and heat generation provide improved safety
- Light weight

Advantages of SLPB

Lower Cost/Consistent Quality/Greater Reliability

Innovative SLPB manufacturing technology: Simple and fast manufacturing process with Z-Folding technology

Applications

- Transportation
  - Fully electric vehicles
  - Plug-in electric vehicles
- Military
- Aviation
- UPS(uninterrupted power supply)
- Industrial Machinery
- Marine
- Grid Storage
- Telecom

1.1 Typical Properties

Items	Unit	Specification			Remarks
Rated Capacity	Ah	**200.0**			*Charge@0.2C, 23℃* *Discharge@0.2C, 23℃*
Energy Density	Wh/kg	**176**			
Energy Density[(1)]	Wh/L	**356**			
AC Impedance	mΩ	**Max. 0.45**			*@ 1kHz, AC*
Weight	kg	**4.2 ±0.1**			
Cell Dimension [Maximum]	㎜	**Thickness[(C)]**		**13.7**	*0.5kgf/㎠, 3.7 ±0.1V*
	㎜	**Width[(A)]**		**464**	*Unfolded*
	㎜	**Length[(B)]**		**327**	*Except for tab length*
Voltage	V	**Average**		**3.7**	
	V	**Lower limited**		**3.0**	
	V	**Upper Limited**		**4.2**	
Current [Maximum]	A	**Charge**	**Cont.**	**200 (1C)**	*@ 23 ±3℃*
	A	**Discharge**	**Cont.**	**400 (2C)**	*@ 23 ±3℃*
	A		**Peak**	**600 (3C)**	*<10sec , > SOC 50%*
Available Operating Temperature	℃	Charge		**0 ~ 10℃**	*<0.3C*
				10 ~ 35℃	*≤ 2C*
				35 ~ 45℃	*< 1C*
	℃	Discharge		**-10 ~ 55℃**	
Available Storage Condition	-	-20 ~ 25℃		**1 year**	*@60±25% R.H.* *SOC 50 ±5%*
	-	25 ~ 40 ℃		**3 months**	
	-	40 ~ 60 ℃		**1 week**	
Cycle Life	Times	23±3℃		**> 4,000**	*Cycles @1C/1C to 80% of Capacity* *80% DOD or 3.4~4.1V*
Self Discharge	%	23±3℃ / Year		**< 2%**	*50% SOC*
Certification	**UL1642**				

[(1)]Volume calculated using core cell demensions, excluding tabs and seals

SUPERIOR LITHIUM POLYMER CELL

2. Technical Information

2.1 Charge Characteristics

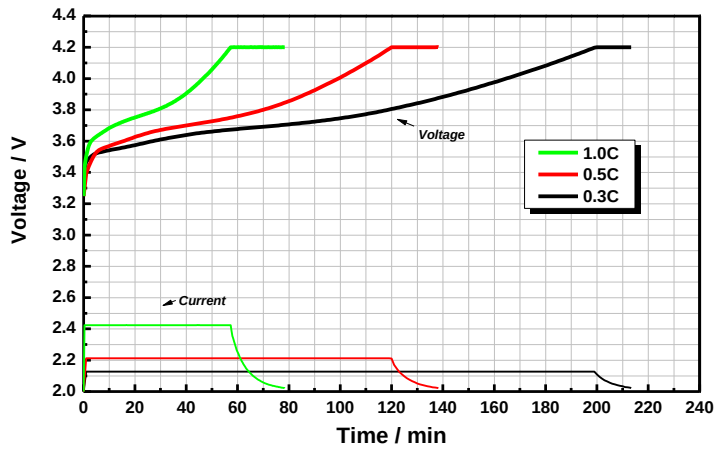

Charge	0.3C	< 250 min	CC-CV, 0.5C ~ 3.0C, 4.2V, 0.05C cut off @23℃±2℃
	0.5C	< 150 min	
	1.0C	< 100 min	

2.2 Discharge Characteristics

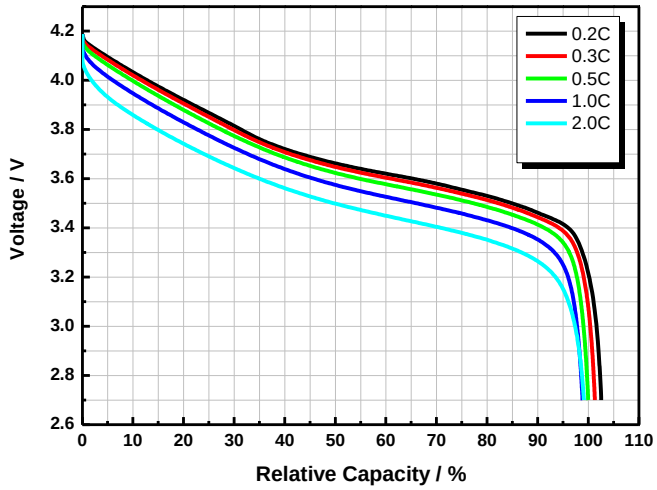

Discharge	0.2C	< 100 %	Charge : CC-CV, 1.0C, 4.2V, 0.05C cut off @23℃±2℃ Discharge : CC, 0.5~8.0C, 3.0V cut-off @23℃±2℃
	0.5C	< 100 %	
	1.0C	< 95 %	
	2.0C	< 93%	

2.3 Temperature Characteristics

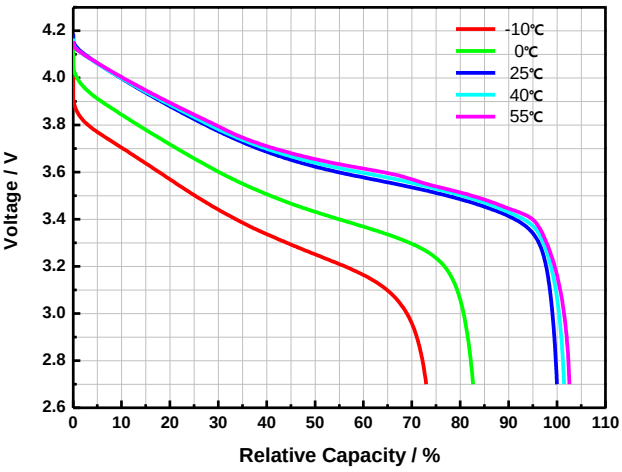

Discharge	-10℃	< 60 %	Charge : CC-CV, 1.0C, 4.2V, 0.05C cut off @23℃±2℃ Discharge : CC, 0.5C, 3.0V cut-off @Each temp.
	0℃	< 80 %	
	25℃	100 %	
	55℃	> 100%	

2.4 Mechanical Characteristics

Note: dimensions shown in mm

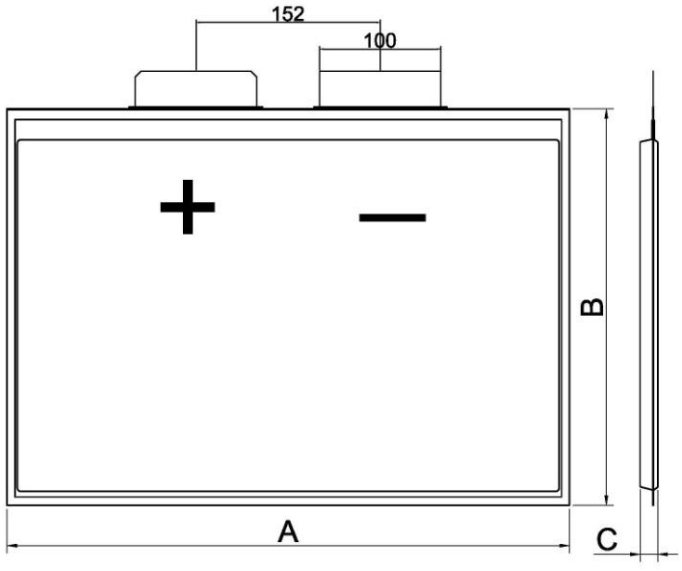

3. Operating Manual

3.1 Operating Voltage Range

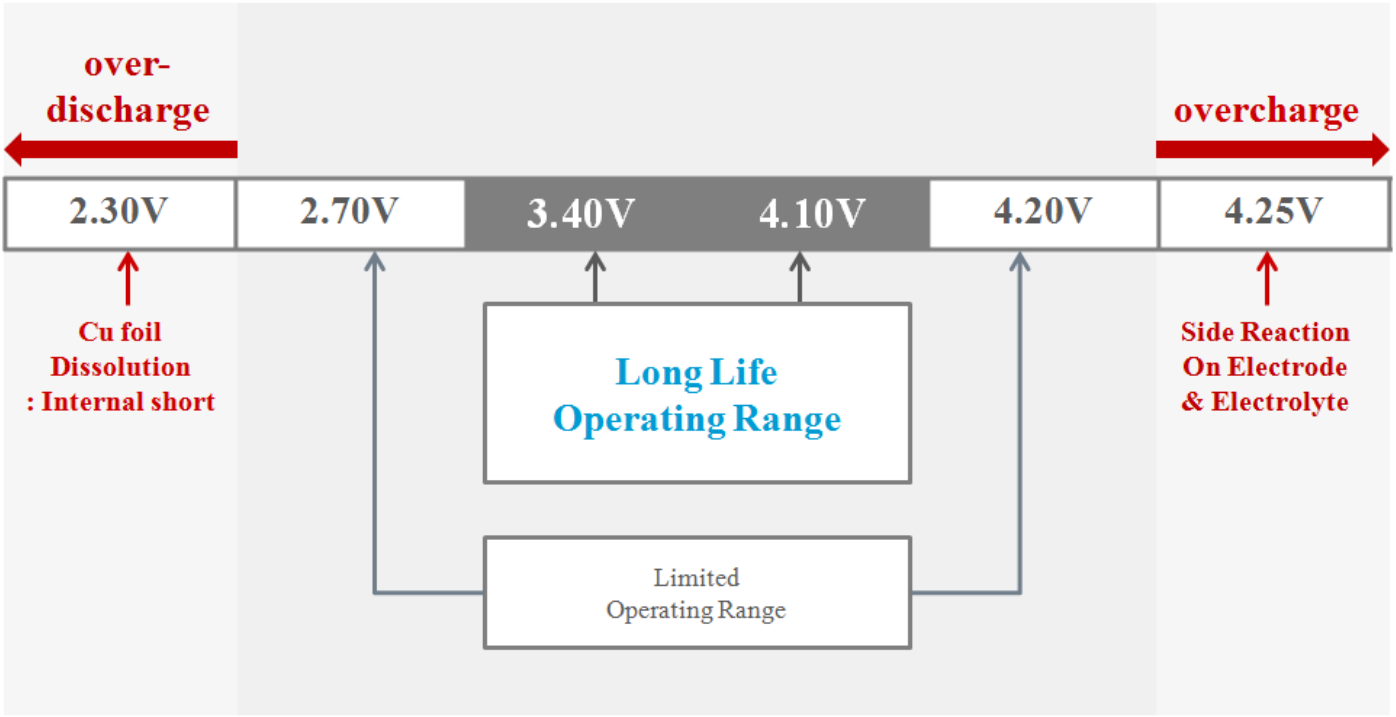

3.2 Operating Temperature Range

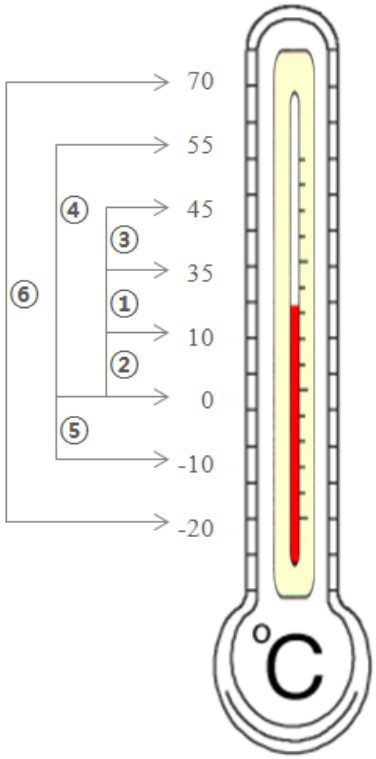

① 10~35°C: Fast charging Range

② 0~10°C: Pre-charging Range(<0.3C)

③ 35~45°C: Charging Range(<1.0C)

④ 0~55°C: Charge Protection Temp.(Shut down)

⑤ -10~55°C: Discharge Operating Range

⑥ -20~70°C: Discharge Protection Temp.(Shut down)

4. Handling Precautions & Prohibitions

Danger

1. Do not disassemble or alter the battery. The battery contains a safety mechanism and a protecting device in order to avoid any danger. If these are damaged, heat generation, smoke emission or ignition may be caused.
2. Do not let the battery terminals (+ and -) contact a wire or any metal (like a metal necklace or a hair pin) with which it carried or stored together. In such a case, the battery is shorted and causes an excessive current, which may result in heat generation, smoke emission or ignition.
3. Do not put the battery into a fire or heat it. In such a case, the insulator in the battery may be damaged, all of which may cause heat generation, smoke emission or ignition.
4. Do not use or leave the battery near a heat source such as a fire or heater (80℃ or higher). Such a high temperature may cause damage of the protecting device in the battery, which may result in heat generation, smoke emission or ignition.
5. Do not dip or wet the battery in water, seawater, or other liquid. If the protecting device assembled in the battery is damaged, the battery may be charged with an abnormal current and voltage, which may result in the cause of heat generation, smoke emission or ignition of the battery.
6. Do not apply heavy impact to the battery, or throw or drop it. Strong impact may damage the protecting device, which may result in heat generation, smoke emission or ignition of the battery.
7. Do not drive a nail in, hit with a hammer, or stamp on the battery. In such a case, the battery may be deformed and shorted, and the protecting device may be damaged, which may cause heat generation, smoke emission or ignition of the battery.
8. The battery has a predetermined polarity. If the battery will not connect well to the charger or equipment, do not try to connect the battery forcefully. Check the polarity first. In the case the battery is connected in reverse, it is charged reversely and may cause leakage, heat generation, smoke emission or ignition due to an abnormal chemical reaction.
9. Do not connect the battery reversed in positive (+) and negative (-) terminals in the charger or equipment. In the case the battery is connected in reverse, it is charged reversely during charge, and causes an excessive current during discharge, and may cause heat generation, smoke emission or ignition due to an abnormal chemical reaction.
10. The battery to be charged must be placed on a non-flammable, heat resistant and non-conductive surface. Keep inflammable and volatile materials well away from the charging area. Batteries must not be left on charge unsupervised.
11. Do not charge battery without proved safety circuit. If unexpected errors occur in charger, it might cause overcharging and it could be resulted in safety accident. Safety Guard made by Kokam or better quality circuit must be used for charging.
12. Do not use any unqualified charger or not specified by Kokam, also, follow the charge conditions specified by Kokam. If the battery is charged under other conditions (a high temperature, a high voltage / current, or an altered charger) not specified by Kokam, the battery may cause heat generation, smoke emission or ignition with abnormal chemical reactions.
13. Do not connect the battery directly to an electric outlet or cigarette heater socket in a car. Applying a high voltage may generate an excessive current, and get an electric shock. Possibly leading to leak electrolyte, heat generation, smoke emission or ignition.
14. Do not use the battery for a purpose other than those specified. Otherwise, its guaranteed performance will be lost and/or its service life will be shortened. Depending on the equipment in which the battery is used, excessively high current can flow through battery, possibly damaging it and leading to leakage, heat generation smoke emission or ignition.
15. If the battery leaks, and the electrolyte gets into the eyes, do not rub them. Instead, rinse the eyes with clean running water and immediately seek medical attention. Otherwise, eye injury may result.
16. Be careful that conductivity material should not touch on the surface of battery.

Warning

1. Do not use the battery together with a dry battery or other primary battery or other battery of a different capacity, types and / or brand. In such a case, over-discharge during use, or over-charge during charge may occur and abnormal chemical reactions may cause heat generation, smoke emission or ignition of the battery.
2. Discontinue charging after specified charging time even if the charge is not complete. Otherwise, the battery might cause heat generation, smoke emission or ignition.
3. Do not put the battery in a microwave oven or a pressure cooker. Sudden heat may damage the seal of the battery and may cause heat generation, smoke emission or ignition of the battery.
4. If you notice any malodor, heating, discoloration, deformation, or any other change from what you are used to while using, charging, storing the battery, take it out of equipment or charger, and avoid using it. Using it in such state may result in heat generation, smoke emission or ignition.
5. If the battery leaks or emits a malodor, take it away from any fire immediately. The electrolyte may catch fire, which may cause heat generation, smoke emission or ignition.
6. Do not use the battery in the place where the static electricity (more than the limit of the manufacturer's guarantee) occur.
7. Do not use the battery in other than the following conditions
   Discharge: -10 deg. C — + 55 deg. C
   Store: -20 deg. C — + 25eg. C (on the charge of 50 %)

Caution

1. Do not use or leave the battery in a place exposed to strong direct sunlight, or in a car under the blazing sun, or high temperature sources. Such a high temperature may cause performance will be lost and/or its service life will be shortened.
2. If you find the battery rusty, malodor, heating, or any other defective before using the battery for the first time after purchase, do not use it. Take it back to the dealer instead.
3. Store the battery in a location where children cannot reach it. Also, make sure that a child does not take out the battery from the battery charger or equipment.
4. If the battery leaks and its electrolyte contact with skin or clothes, wash it well with tap water or other clean water right away. Otherwise, skin inflammation can occur.
5. Read the instructions of your equipment regarding the battery installation and removal from the equipment so as not to mishandle and waste the battery.
6. The battery was charged a little before shipment for temporary use by an end user. In case your equipment does not operate with the battery or in the case of a long use, charge the battery with a specified charger once
7. In the case the battery terminals are dirty, clean the terminals with a dry cloth before use, otherwise, the contact with equipment might cause insufficiency, and power failure or charge failure
8. Carefully read the instructions for the specified charger to learn how to charge the battery.
9. Do not charge the battery over the specified time described in the instruction

Kokam
Great Power for Everyone

1261-3 Jeongwang-dong, Siheung-City, Gyeonggi-Do, South Korea • +82 31 3620 100
483-42 Yachon-ri, Gayagok-Myun, Nonsan-Si, Chungnam • +82 41 740 3800

Email: battery@kokam.com
Web: www.kokam.com

B

Sensitivity analysis

Appendix B shows the battery voltage while varying the parameters A, B, K, V_0 and R. The parameters have been varied in a range between 20% and 180% related to the original values. The original values have been calculated with the use of equations 8.5 to 8.9. From figures B.1 to B.5, it can be seen that parameter A strongly influences the exponential region. Parameter B influences the exponential region as well as the slope of the nominal zone. Parameter K influences the end of the nominal zone, determining how gradually the voltage starts to decrease. Parameter V_0 and R both influence the entire curve by adding or subtracting a constant voltage.

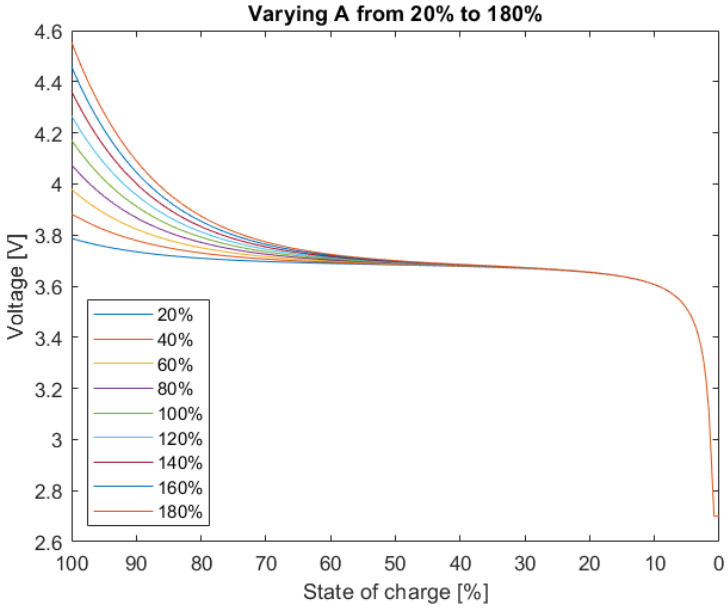

Figure B.1: The effect of varying parameter A

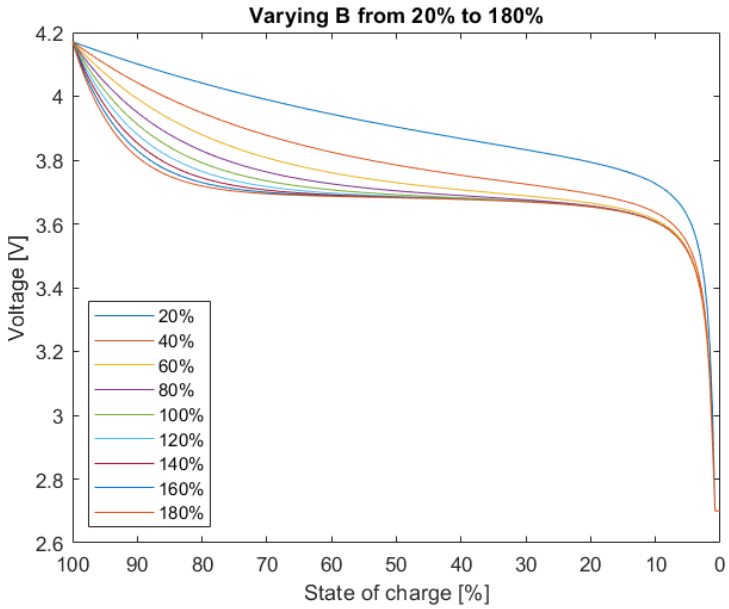

Figure B.2: The effect of varying parameter B

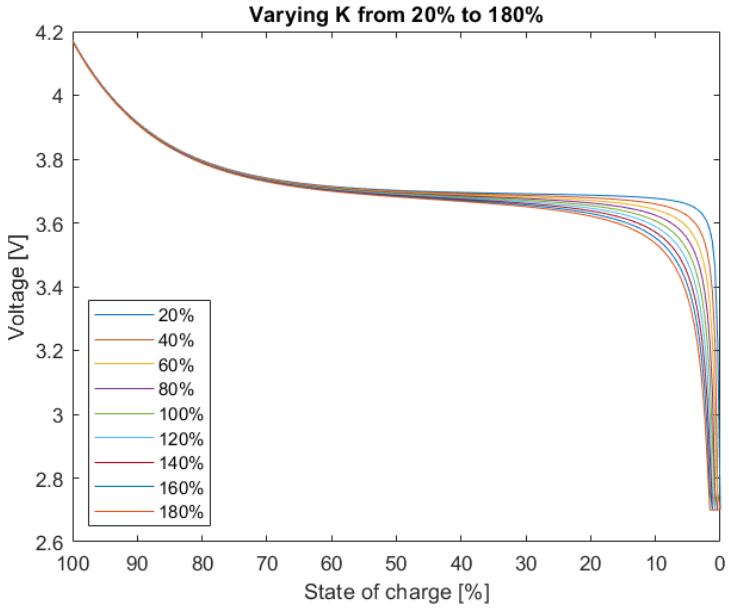

Figure B.3: The effect of varying parameter K

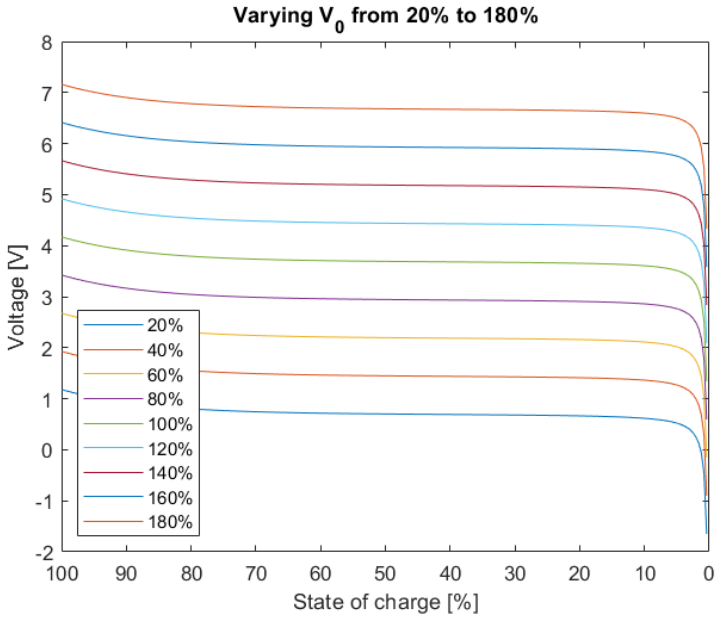

Figure B.4: The effect of varying parameter V_0

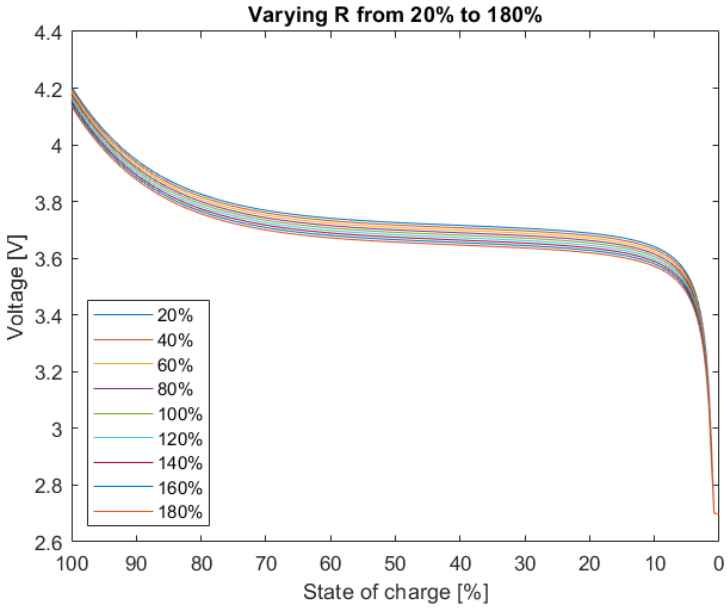

Figure B.5: The effect of varying parameter R

C

Model behaviour

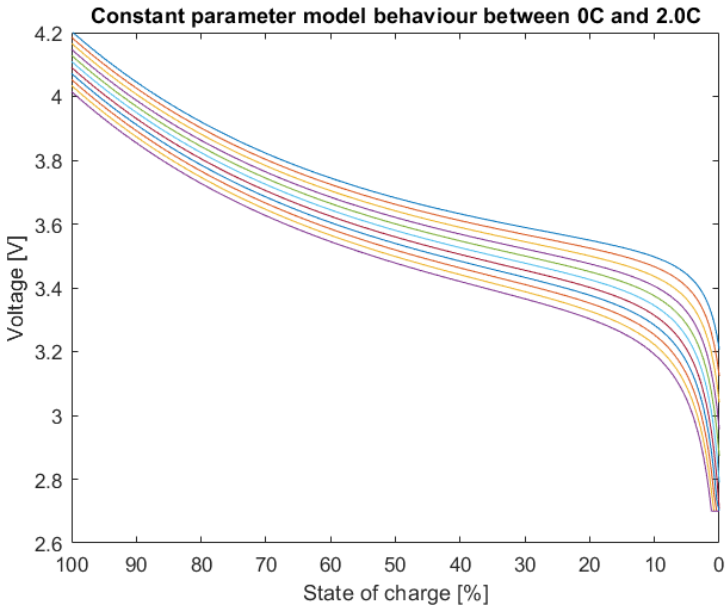

Figure C.1: Constant parameter model behaviour between 0C and 2.0C

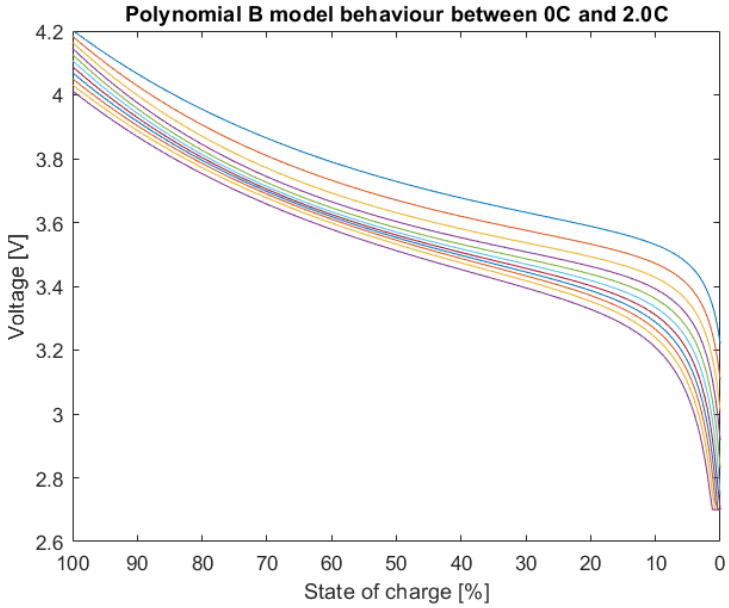

Figure C.2: Polynomial B model behaviour between 0C and 2.0C

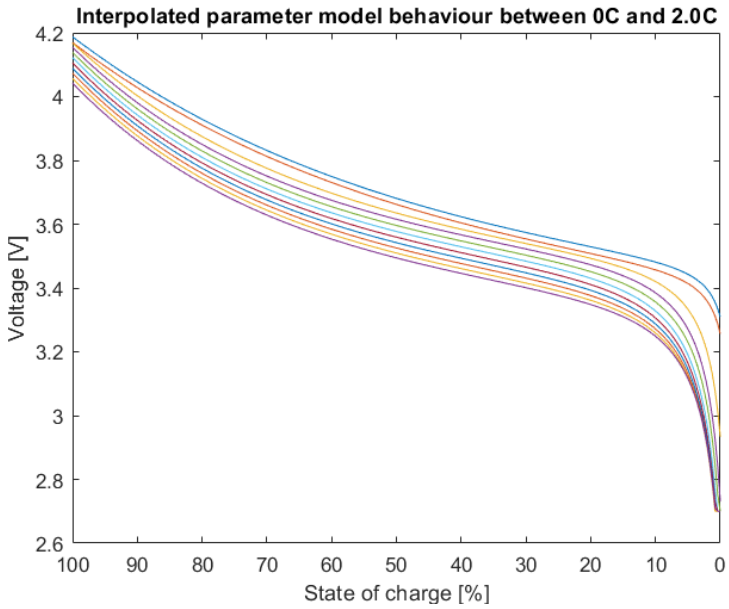

Figure C.3: Interpolated parameter model behaviour between 0C and 2.0C

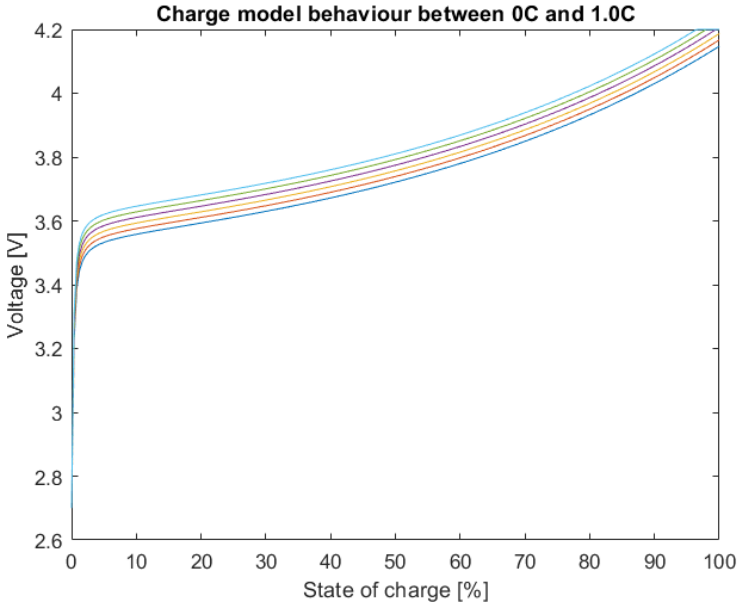

Figure C.4: Constant parameter charge model between 0C and 1.0C

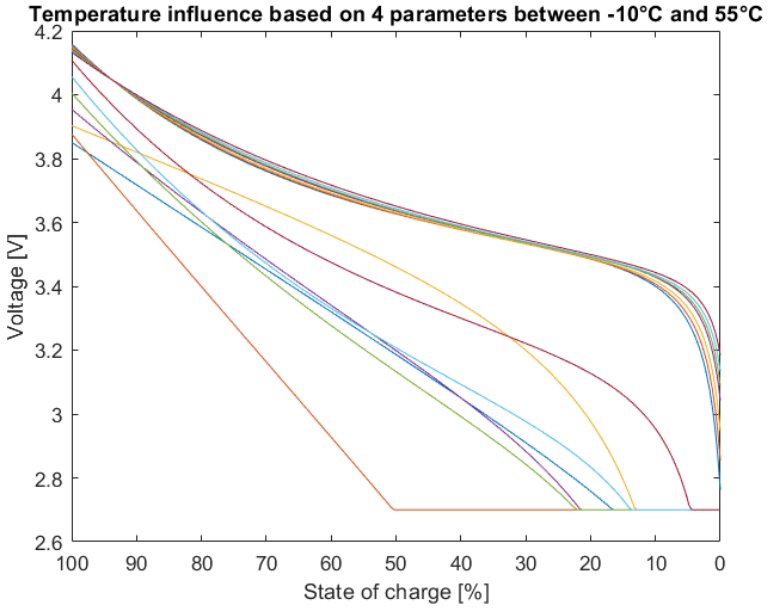

Figure C.5: Temperature influence based on 4 parameters between -10°C and 55°C

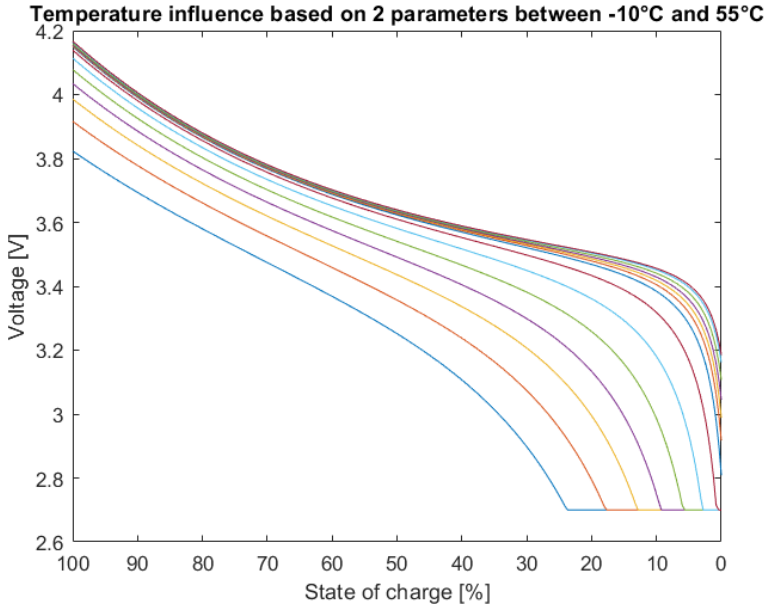

Figure C.6: Temperature influence based on 2 parameters between -10°C and 55°C

D

Simulink implementation

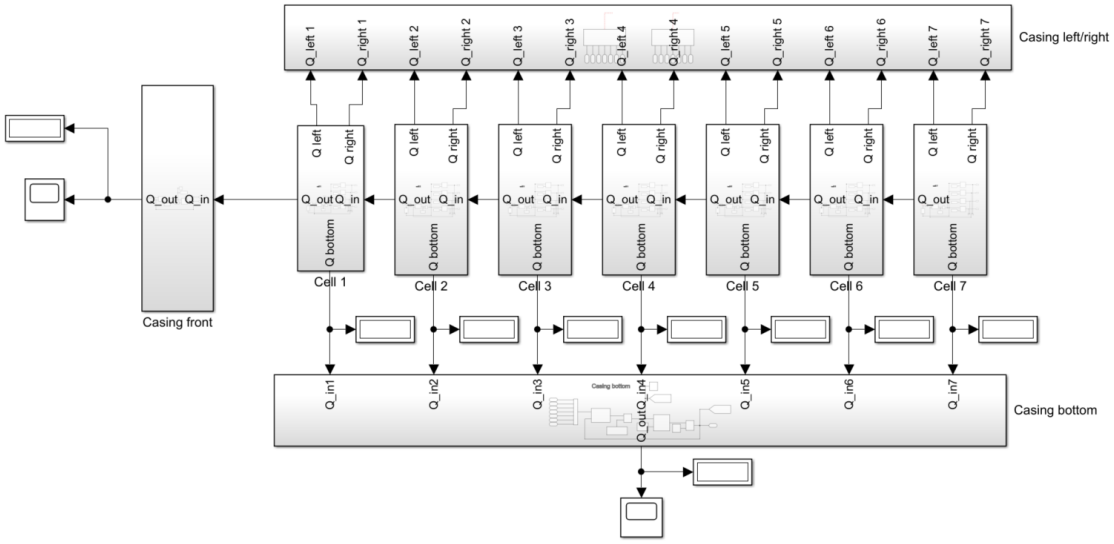

Figure D.1: Simulink implementation of the module

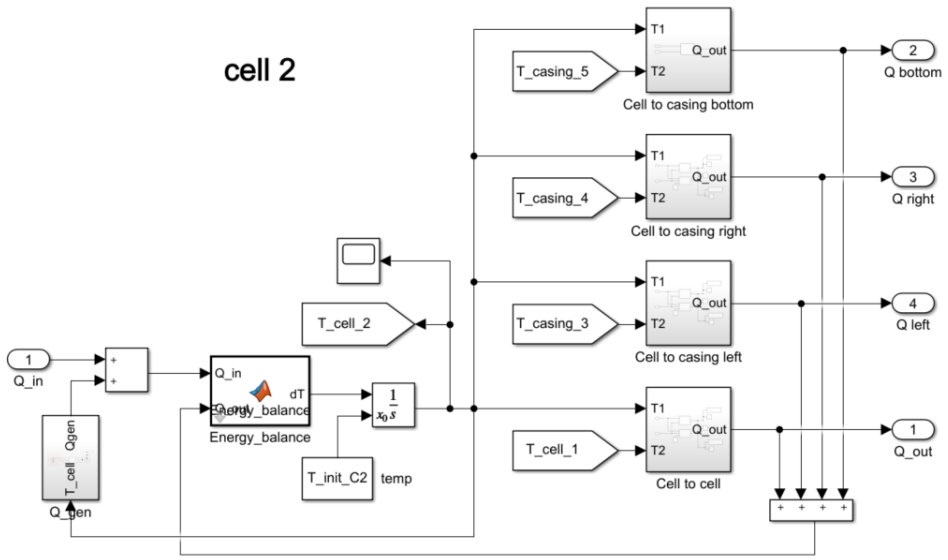

Figure D.2: Simulink implementation of a battery cell

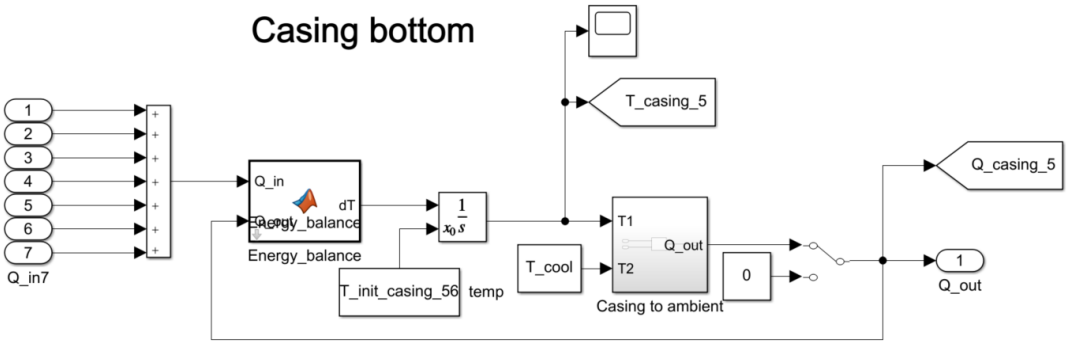

Figure D.3: Simulink implementation of the bottom casing

Submarines face an ongoing (technical) battle to improve the operational effectiveness by increasing the submerged endurance and range. Installing lithium-ion batteries on new or refitted diesel-electric submarines has become increasingly interesting based on their relatively high energy density and specific energy. However, lithium-ion batteries can develop a thermal runaway: a process which exponentially generates heat, leading to the risk of an explosion and fire. The objective of this research is therefore to investigate the implications on preliminary submarine system design based on the thermal behaviour of lithium-ion batteries and to quantify the thermal behaviour and design implications.

TU Delft

Defensie Materieel Organisatie
Ministerie van Defensie